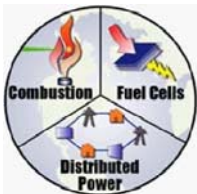


**Public Interest Energy Research (PIER) Program  
FINAL PROJECT REPORT**

**Experimental Study of the Effects of  
Elevated Pressure and Temperature on  
Jet Mixing and Emissions in an RQL  
Combustor for Stable, Efficient and  
Low Emissions Gas Turbine  
Applications**

Prepared for: California Energy Commission

Prepared by:  
Advanced Power and Energy Program  
University of California, Irvine  
131 Engineering Laboratory Facility Irvine,  
California 92697-3550



JANUARY 2012

CEC-500-2012-001

***Prepared by:***

***Primary Author(s):***

V. Jermakian,  
V.G. McDonell  
G.S.Samuelsen,

Advanced Power and Energy Program  
University of California, Irvine  
131 Engineering Laboratory  
Facility Irvine, California  
92697-3550

***Contract Number: 500-00-025***

***Prepared for:***

**California Energy Commission**

Arthur J. Soinski, Ph.D.  
***Contract Manager***

Laurie ten Hope  
***Deputy Director***  
**RESEARCH AND DEVELOPMENT DIVISION**

Robert P. Oglesby  
***Executive Director***

**DISCLAIMER**

This report was prepared as the result of work sponsored by the California Energy Commission. It does not necessarily represent the views of the Energy Commission, its employees or the State of California. The Energy Commission, the State of California, its employees, contractors and subcontractors make no warrant, express or implied, and assume no legal liability for the information in this report; nor does any party represent that the uses of this information will not infringe upon privately owned rights. This report has not been approved or disapproved by the California Energy Commission nor has the California Energy Commission passed upon the accuracy or adequacy of the information in this report.

## Preface

The California Energy Commission's Public Interest Energy Research (PIER) Program supports public interest energy research and development that will help improve the quality of life in California by bringing environmentally safe, affordable, and reliable energy services and products to the marketplace.

The PIER Program conducts public interest research, development, and demonstration (RD&D) projects to benefit California.

The PIER Program strives to conduct the most promising public interest energy research by partnering with RD&D entities, including individuals, businesses, utilities, and public or private research institutions.

- PIER funding efforts are focused on the following RD&D program areas:
- Buildings End-Use Energy Efficiency
- Energy Innovations Small Grants
- Energy-Related Environmental Research
- Energy Systems Integration
- Environmentally Preferred Advanced Generation
- Industrial/Agricultural/Water End-Use Energy Efficiency
- Renewable Energy Technologies
- Transportation

*Experimental Study of the Effects of Elevated Pressure and Temperature on Jet Mixing and Emissions in an RQL Combustor for Stable, Efficient and Low Emissions Gas Turbine Applications* is the final report for the Experimental Study of Jet Mixing in Rich-Quench-Lean Combustors project (contract number 500-00-025) conducted by UC Irvine. The information from this project contributes to PIER's Environmentally Preferred Advanced Generation Program.

For more information about the PIER Program, please visit the Energy Commission's website at [www.energy.ca.gov/research/](http://www.energy.ca.gov/research/) or contact the Energy Commission at 916-654-4878.

## ABSTRACT

Rich burn, quick-mix, lean burn (RQL) combustion is a growing technology in aerospace gas turbines and is a candidate to support fuel flexible stationary power generation. The ability of RQL to minimize the formation of nitrous oxide ( $\text{NO}_x$ ) is heavily dependent on the jet mixing in the quick-mix section. While studies at atmospheric pressure have revealed strategies to minimize  $\text{NO}_x$ , elevated pressure research is required to outline the full set of options. In this study, an experimental test rig was designed and built to facilitate characterization of the mixing of the jets in non-reacting and reacting conditions at high pressure. The test rig demonstrated stable reaction at elevated pressures up to six atmospheres and delivered uniform rich products to the quick-mix section. Quick-mix modules with 12 and 18 round hole orifice configurations were evaluated to characterize mixing in non-reacting and reacting experiments at jet-to-mainstream momentum-flux ratios of 80 and 57, respectively, and a mass-flow ratio of 2.5.  $\text{NO}_x$ , carbon monoxide, oxygen, and carbon dioxide emissions measurements were obtained at these conditions. The non-reacting mixing results demonstrated that the quick-mix design method is applicable to elevated pressure. The reacting experiments with propane successfully verified the repeatability of jet mixing experiments. Additionally, the natural gas experiments resulted in lower  $\text{NO}_x$  and carbon monoxide than propane and verified that the main air preheat temperature is a major factor in  $\text{NO}_x$  production.

**Keywords:** Rich-burn, RQL combustion, aerospace gas turbines, fuel flexible, power generation, quick-mix modules, high pressure experiments, non-reacting mixing,  $\text{NO}_x$  reduction.

Please use the following citation for this report:

Jermakian, V., McDonell, V.G., and Samuelson, G.S., Advanced Power and Energy Program, University of California, Irvine. 2006 *Experimental Study of the Effects of Elevated Pressure and Temperature on Jet Mixing and Emissions in an RQL Combustor for Stable, Efficient and Low Emissions Gas Turbine Applications*. California Energy Commission. Publication number: CEC-500-2012-001.

# TABLE OF CONTENTS

<b>ABSTRACT .....</b>	<b>ii</b>
<b>EXECUTIVE SUMMARY .....</b>	<b>8</b>
<b>CHAPTER 1: Introduction.....</b>	<b>11</b>
1.1 Background and Overview.....	11
1.1.1 Project Goal.....	11
1.1.2 RQL and Jet Mixing Studies .....	12
1.1.3 RQL Concept.....	13
1.2 Project Objectives .....	16
<b>CHAPTER 2: Project Approach.....</b>	<b>18</b>
2.1 Hardware Design and Test Plan Task 2.1.....	18
2.1.1 RQL Test Hardware.....	18
2.1.2 Rich Product Generator.....	21
2.1.3 Rich Burn Section .....	24
2.1.4 QM Modules .....	25
2.1.5 Sampling Probes.....	26
2.2 Fabrication and Facility Modifications Task 2.2 .....	27
2.2.1 Atmospheric Facility.....	28
2.2.2 High Pressure Facility .....	31
2.3. Parametric Jet Mixing Tests Task 2.3.....	36
2.3.1 Phase I Testing.....	36
2.3.2 Phase II Testing .....	37
<b>3 CHAPTER 3 Project Outcomes.....</b>	<b>39</b>
3.1 Phase I Testing.....	39
3.1.1 Rich Product Generator Performance Testing .....	39
3.1.2 Atmospheric Reacting Mixing Tests.....	46
3.1.3 RQL Kinetics Model.....	59
3.2 Phase II .....	65
3.2.1 Elevated Pressure Non-Reacting Mixing Tests.....	65
3.2.2 Elevated Pressure Reacting Mixing Experiment .....	71

3.2.3 Elevated Pressure Parametric Test Matrix Development.....	73
3.3 Summary .....	75
<b>CHAPTER 4: Conclusions and Recommendations .....</b>	<b>78</b>
4.1 Conclusions.....	78
4.2 Recommendations.....	79
4.3 Benefits to California .....	79
<b>CHAPTER 5: Glossary.....</b>	<b>80</b>
<b>CHAPTER 6: References.....</b>	<b>81</b>
<b>APPENDIX A: .....</b>	<b>85</b>
Non-Reacting Jet In Crossflow Experiments.....	85
Non-Reacting Jet In Crossflow Modeling.....	86
Reacting Jet In Crossflow Models.....	87
Reacting Jet In Crossflow Experiments.....	89

## TABLE OF FIGURES

Figure 1 Representation of the Desired NO <sub>x</sub> Route in RQL Combustors .....	13
Figure 2 Single Jet in Crossflow .....	14
Figure 3 Optimum Number of Jet Holes Using Different the NASA and Cranfield Design Methods for the Quick-Mix Section. ....	16
Figure 4 RQL Test Hardware Used in the UCICL High Pressure Test Rig. ....	19
Figure 5 Visual Experimental Representation of the Reaction in the Quick-Mix Section .....	19
Figure 6 Schematic of the Previous RQL Atmospheric Facility .....	20
Figure 7 RQL Pre-Mixing Section a) Hardware Set-Up and b) Vortab Mixer .....	21
Figure 8 Velocity (m/s) Distribution in the CFD Model of the RQL Experimental Combustor .....	23
Figure 9 Schematic of the Bluff body with Internal Components.....	24
Figure 10 Rich Burn Section a) Outer Diameter Liner Cooling and Ports b) Ceramic Liner .....	25
Figure 11 Dimensions of the Quick-Mix Modules.....	26
Figure 12 Emissions Probe Design and Measurement Points.....	27
Figure 13 Figure 4.10 Test stand in atmospheric facility a) premixing section b) rich product generator. ....	28
Figure 14 RQL High-Pressure Test Rig.....	32
Figure 15 Snapshot of the Experimental Labview Data Acquisition Interface.....	34
Figure 16 A) Planes of Measurement in the Quick-Mix Section and B) Data Grid o Each Plane.....	35
Figure 17 Comparison of Measured and Predicted Values of Fuel Lean Stability Limits Using Experimental Data and Ballal and Lefebvre Correlation.....	40
Figure 18 Measured Fuel Lean and Rich Stability Limits of the Rich Product Generator .....	41
Figure 19 Time Averaged Flow Field of the Recirculation Zone of the Rich Product Generator Using DPIV Data .....	42
Figure 20 Instantaneous Flow Field in the Recirculation Zone of the Rich Product Generator Using DPIV.....	43
Figure 21 High Speed Video Images a) Undisturbed Reacting Flow b) Burst from Face of Bluff Body .....	44
Figure 22 Measured Temperature Entering the Quick-Mix Section at a Preheat Temperature of 500°F (533 K) and 1 atm.....	45
Figure 23 Measured Temperature Entering the Quick-Mix Section at a Preheat Temperature of 850°F (727 K) and 1 atm.....	46

Figure 24 Experimental Results of the Fuel Rich Products on Plane 1 ( $x/R=-1$ ) for the Atmospheric Propane Test. ....	47
Figure 25 Rich Products Entering the Quick-Mix Section from Vardakas, et al. (1999) at plane 1 ( $x/R=-1$ ). ....	48
Figure 26 Repeated Measurements of Data on Plane 1 ( $x/R=-1$ ) During Atmospheric Natural Gas Tests .....	48
Figure 27 $NO_x$ Levels at Plane 4 ( $x/R=1$ ) for a) Prior and b) Current Experiments at a J of 57 and MR of 2.5. ....	50
Figure 28 $O_2$ Levels at Plane 4 ( $x/R=1$ ) for a) Prior and b) Current Experiments at a J of 57 and MR of 2.5. ....	51
Figure 29 $CO$ Levels at Plane 4 ( $x/R=1$ ) for a) Prior and b) Current Experiments .....	53
Figure 30 Plane 4 ( $x/R=1$ ) Contour Plot for the Natural Gas Atmospheric Tests at a J of 57 and MR of 2.5. ....	54
Figure 31 Plane 4 ( $x/R=1$ ) Contour Plot for the Natural Gas Atmospheric Tests.....	55
Figure 32 Plane 5 ( $x/R=2$ ) $NO_x$ Data from the Atmospheric Natural Gas Tests at Different Main Air Preheat Temperatures a) 500°F (533 K) and b) 850°F (727 K). ....	57
Figure 33 Plane 5 ( $x/R=2$ ) $CO$ Data from the Atmospheric Natural Gas Tests at Different Main Air Preheat Temperatures a) 500°F (533 K) and b) 850°F (727 K). ....	58
Figure 34 Schematic of Kinetics Modeling Approach.....	60
Figure 35 TFN Species in Each PSR for the RQL Kinetics Model as a Function of Equivalence Ratio. ....	60
Figure 36 TFN Output Versus Jet Mixing PSR Residence Times.....	62
Figure 37 Effects of Elevated Pressure on $NO_x$ and TFN in the Fuel Rich PSRs. ....	63
Figure 38 Preheat Temperature Effects in the RQL Kinetics Model.....	64
Figure 39 Plane 1 ( $x/R=-0.3$ ) Non-Reacting Temperature Data .....	67
Figure 40 Plane 3 ( $x/R=0.275$ for 12 Hole, $x/R=0.225$ for 18 Hole Modules) Temperature Data .....	68
Figure 41 Plane 4 ( $x/R=1$ ) Non-Reacting Temperature Data.....	69
Figure 42 Plane 5 ( $x/R=2$ ) Non-Reacting Temperature Data.....	70
Figure 43 Plane 5 ( $x/R=2$ ) $NO_x$ Data From the Natural Gas Tests at Different Pressures a) Six Atmospheres and b) One Atmosphere. ....	72

## TABLE OF TABLES

Table 1 CFD Modeling Conditions Used to Simulate The Effect of the Bluff Body Radius on Pressure Drop.....	22
Table 2 Effective Range of Analyzers By Volume .....	35
Table 3 Operating Conditions for Atmospheric Reacting Mixing Tests. ....	37
Table 4 Planar Area Averaged Values from the Atmospheric Propane Test at J of 57 and MR of 2.5.....	54
Table 5 Planar Area Averaged Values from the Atmospheric Natural Gas Test at a J of 57 and MR of 2.5.....	55
Table 6 Planar area averaged values for the atmospheric natural gas test with elevated main air preheat temperature. ....	59
Table 7 Rich Burn Residence Time Effect on Overall TFN and NO <sub>x</sub> .....	61
Table 8 Species concentration at atmospheric and elevated pressures for an equivalence ratio of 1.66. ....	62
Table 9 Normalized Axial Length Of Each Plane For The Non-Reacting Mixing Tests.....	66
Table 10 Proposed Parameter Ranges .....	73
Table 11 Fractional Test Matrix .....	75

## EXECUTIVE SUMMARY

The rich burn, quick-mix, lean burn (RQL) staged combustor is a low nitrous oxide ( $\text{NO}_x$ ) combustion concept that has the potential to provide better combustion stability than lean premixed combustion systems while achieving low emissions. The low oxygen concentration in the fuel rich stage creates an environment that diminishes the ability of fuel bound nitrogen to react with oxygen radicals and form  $\text{NO}_x$ . Also in this stage, the  $\text{NO}_x$  formation mechanism that dominates is the prompt  $\text{NO}_x$  mechanism, which produces large amounts of hydrogen cyanide and ammonia. The major products in the fuel rich section are carbon monoxide (CO), hydrogen gas, and nitrogen gas. The second stage of the combustor uses jets injected into the crossflow to avoid high temperatures, which enables high  $\text{NO}_x$  formation through the thermal  $\text{NO}_x$  formation mechanism. Rapid and uniform jet mixing is needed to avoid near-stoichiometric pockets where high temperatures occur. The completion of the mixing brings the combustor to its final fuel lean and low  $\text{NO}_x$  operating condition.

The RQL combustion concept is advantageous for aerospace gas turbines because of the highly stable rich reaction and low  $\text{NO}_x$  potential. Pratt & Whitney has commercial gas turbines which utilize RQL. The RQL combustion strategy also has the ability to reduce  $\text{NO}_x$  formation caused by fuel bound nitrogen, which can be found in fuels derived from bio-mass and coal gasification. These fuels are applicable to stationary gas turbines using RQL technology, including systems using natural gas and liquid fuels. Elliott is another company that uses RQL combustion in its stationary micro gas turbines. Other entities interested in the RQL combustion concept are NETL (National Energy Technology Laboratory), which uses RQL in a trapped vortex system and Precision Combustion Inc., which uses RQL with a catalyst bed. NASA Glenn Research Center and UTRC (United Technologies Research Center) have also been heavily involved in RQL research and development.

The main focus of previous RQL research at the UCI Combustion Laboratory has been on the establishing the relationship between the jet mixing in the quick-mix section and the overall emissions performance of the combustor. The jet mixing is the key to the low  $\text{NO}_x$  capability of the RQL combustor. The research involved reacting and non-reacting experiments at elevated inlet temperatures and pressures coupled with modeling. In contrast to earlier atmospheric studies, the high pressure non-reacting and reacting experiments carried out under the current project reflect a significant step in acquiring information on jet mixing at conditions more representative of those found in practical systems. As a result, this study contributes a significant step in the overall research into the jet mixing phenomenon in RQL combustors. The previous reacting research did not investigate the effect of pressure on jet mixing and  $\text{NO}_x$  emissions at elevated pressures and temperatures.

This project fills a gap in the research and provides insight to gas turbine manufacturers in both the aerospace and power generation industries. The research conducted through the current study also verifies past conclusions regarding the design methods used to optimize the mixing and provide insight regarding the reduction of  $\text{NO}_x$  and CO emissions in RQL combustors.

The overall technical goal of the research project is to determine the role of jet mixing in the quick-mix section in the formation of pollutants and products of inefficient combustion under elevated pressures and temperatures.

The economic goals support the PIER goal of improving the energy cost and value of

California's electricity by providing insight into a robust combustion strategy that avoids combustion instability and, in principle, enables power generation in accordance with the strictest air quality standards in the nation.

The purpose of this project is to characterize the effects of pressure on mixing and the formation of emissions in the RQL combustion concept with propane (to simulate aerospace applications and natural gas (to simulate stationary applications) at elevated pressures and temperatures. The objectives of the project were to:

- Characterize the temperature and emissions fields within the jet mixing section.
- Understand the means by which such species as  $\text{NO}_x$  and CO are produced in the mixing section and relate this insight to the overall performance of the quick-mix mixer.

As part of this project, a high pressure test rig was developed and commissioned to provide the environment necessary to carry out the experiments of interest. The mixing and emissions characteristics for a variety of configurations were quantified for a number of conditions. Non-reacting and reacting mixing experiments were conducted during the project using the RQL high pressure test rig. Temperature measurements were used to characterize the quick-mix section in the non-reacting experiments. Emissions measurements were successfully gathered to characterize the quick-mix section in the reacting experiments. The experiments were complimented by the chemical kinetics modeling to help understand the means by which emissions are formed in the RQL combustor. Conclusions drawn from the measurements are:

- In the non-reacting experiments, elevated pressures did not change the level of jet penetration and overall mixing. As a result, the NASA design method, used to optimize the number of jet holes for a given jet-to-mainstream momentum flux-ratio in a cylindrical duct, is valid as a tool under elevated pressure conditions for the design of the quick-mix section.
- The reacting experimental results showed that an increase in the air temperature entering the rich reactor increases the production and emission of  $\text{NO}_x$ , and thereby validates prior reports that the rich reactor air preheat temperature is a major driver for overall  $\text{NO}_x$  production in RQL combustion. The natural gas atmospheric tests produced lower  $\text{NO}_x$  and CO levels compared to the propane tests, suggesting that stationary and aerospace gas turbines that utilize the RQL combustion concept can achieve lower  $\text{NO}_x$  and CO when using natural gas as a fuel instead of propane. The elevated pressure natural gas experiments showed that pressure creases the  $\text{NO}_x$  produced in the quick-mix section of the RQL combustor due to the increase in thermal  $\text{NO}_x$  formed in the jet wakes near the wall of the combustor.
- Based on chemical kinetics modeling of the RQL combustion concept, an increase in pressure decreases the production of  $\text{NO}_x$  and TFN (total fixed nitrogen) in the fuel thermal and prompt mechanisms. In the same model residence time was varied and the results showed a decrease in overall  $\text{NO}_x$  production but did not show an effect on the initial fuel rich reactor  $\text{NO}_x$  output. Also, an increase in jet and main air preheat temperatures increased  $\text{NO}_x$  in each case modeled.

As part of the project a parametric test matrix was developed to answer questions regarding jet mixing effects on  $\text{NO}_x$  production at elevated pressure. Although these tests were not carried out during the current effort, it is recommended that they be completed to provide a more systematic assessment of the jet mixing and emission behavior in the RQL system. The knowledge gained regarding system operating conditions, design of the quick-mix section, and the development of a chemical kinetics model can all be used to aid designers of RQL combustion systems. Also, the high pressure RQL test rig can be used to repeat experiments conducted by industry to verify their findings.

# CHAPTER 1: Introduction

## 1.1 Background and Overview

The rich burn, quick-mix, lean burn (RQL) staged combustor is a low  $\text{NO}_x$  combustion concept that has been studied for many years under reacting and non-reacting conditions with both models and experiments. The main focus of the research has been on the effects of the quick-mix section on the overall performance of the combustor. The fundamentals of jet mixing in a crossflow govern the quick-mix section of the combustor. Therefore, the minimization of the overall  $\text{NO}_x$  production of the RQL combustor is likely coupled to the jet mixing taking place in the quick-mix section.

Jet mixing in a crossflow has been used in the gas turbine combustor design for many years. This can be seen in the primary, secondary, and dilution jets of the combustor where the jets are used to manage the stoichiometry and mixing in the combustor. In the RQL combustor, the jets are used to abruptly change the fuel rich conditions in the first stage of the combustor to fuel lean conditions. The goal is to (1) achieve an overall lean stoichiometry, and (2) avoid high temperature stoichiometric conditions that cause high  $\text{NO}_x$  producing conditions.

The jet mixing is the key to the low  $\text{NO}_x$  capability of the RQL combustor (Oeschle and Holdeman, 1995). The jet mixing must be rapid and uniform to avoid prolonged residence times at near-stoichiometric conditions during the transition from the fuel rich to fuel lean conditions. In addition, optimizing the performance of the quick-mix section lowers the residence time of high temperature pockets. Optimizing the jet mixing relies on the orifice configuration (Talpalikar, et al. 1991). The orifice configuration controls the level of jet penetration. In addition, the preheat temperatures and equivalence ratio of the fuel rich stage have been identified as contributors to  $\text{NO}_x$  emissions in the RQL combustor (Vardakas, et al. 1999). It is expected that the combustor operating pressure has an effect as well. This has yet, however, to be systematically established.

With a few notable exceptions, previous RQL combustion research has been conducted at atmospheric pressure (for example, Leong, Samuelsen, and Holdeman (1999), and Vardakas, et al. 1999). Meisl, et al. (1994) conducted reacting elevated pressure experiments but did not concentrate on mixing and, in fact, proposed that mixing research at elevated pressure is needed to complement their tests. Elevated pressure research was also conducted at United Technologies Research Center to evaluate the  $\text{NO}_x$  emissions of RQL for aerospace engines, but again without evaluating the role of jet mixing (Rosfjord and Padget, 2001).

### 1.1.1 Project Goal

The previous research conducted at elevated pressure by Meisl, et al. (1994) and Rosfjord and Padget (2001) did not study the effect of pressure on jet mixing and  $\text{NO}_x$  emissions. A systematic evaluation is necessary to establish the relationship between those two factors and elevated pressures. The development of a high pressure test facility for RQL mixing studies was a critical step in the project. In addition, the verification of equations used to design the mixing section, specifically the NASA design method, needs to be assessed at elevated pressures. The

approach adopted is to extend the research of (1) Leong, et al. (1999), which consisted of atmospheric reacting tests with different orifice configurations using propane, and (2) Vardakas, et al. (1999), which evaluated the effect of preheat temperature of the main and jet air on NO<sub>x</sub> emissions using propane as well.

The overall technical goal of the research project is to determine the role of jet mixing in the quick-mix section in the formation of pollutants and products of inefficient combustion under elevated pressures and temperatures.

The economic goals support the PIER goal of improving the energy cost and value of California's electricity by developing a robust combustor that avoids combustion instability that will enable power generation in accordance with the strictest air quality standards in the nation.

### **1.1.2 RQL and Jet Mixing Studies**

The main focus of rich burn, quick-mix, lean burn combustion (RQL) research has been on optimizing the jet mixing section. The research has involved non-reacting experiments coupled with modeling. In addition to non-reacting experiments, there have been limited reacting experiments and even scarcer are high-pressure non-reacting and reacting experiments. High pressure non-reacting and reacting experiments are much more indicative of behavior in practical systems than non-reacting experiments and modeling (numerical and computational fluid dynamic, CFD). Therefore, they are a significant part of the overall research into the jet mixing phenomenon in RQL combustors.

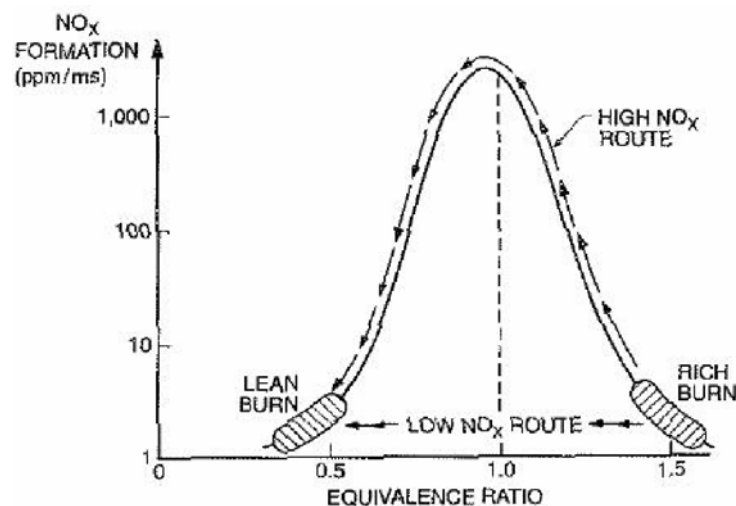
In the early 1990's RQL research advanced because of the NASA High Speed Research (HSR) program, which had the goal of designing a passenger jet for high speed civil transport (HSCT). The HSR program was terminated in February 1999 because of high fuel costs and loss of support from Boeing. Reducing NO<sub>x</sub> was the focus of the research due to ozone destruction in the stratosphere. NO<sub>x</sub> emissions released in the stratosphere directly attack and destroy the ozone layer that protects the earth from ultraviolet radiation in the stratosphere. Along with NO<sub>x</sub> reduction characteristics, RQL is still appealing to the aerospace industry because of its high stability and low affinity to burnout in the initial rich stage. The V/STOL aircraft is another aerospace application that utilizes jets in crossflow mixing during the hover to cruise transition. Also, Pratt & Whitney has incorporated RQL into its jet engines.

RQL combustion is a growing technology in aerospace gas turbines and could be of potential benefit to ratepayers in California if it can be used in stationary power generation. The research conducted through the current study will verify past conclusions regarding the design methods used to optimize the mixing and provide insight regarding the reduction of NO<sub>x</sub> and CO emissions in RQL combustors. The success of RQL in a market flooded with Lean Premixed Prevaporized (LPP), Dry Low NO<sub>x</sub> (DLN), or Lean Direct Injection (LDI) systems is based on potential opportunity to further reduce the emission of NO<sub>x</sub>.

### 1.1.3 RQL Concept

The RQL combustor has three stages. The initial fuel rich stage is stable and produces reaction temperatures lower than near stoichiometric conditions. The low oxygen concentration in the fuel rich stage creates an environment that diminishes the ability of fuel bound nitrogen to react with oxygen radicals and form  $\text{NO}_x$ . Also in this stage, the  $\text{NO}_x$  formation mechanism that dominates is the prompt  $\text{NO}_x$  mechanism, which produces large amounts of HCN and  $\text{NH}_3$ . The major products in the fuel rich section are CO,  $\text{H}_2$ , and  $\text{N}_2$ . The second stage of the combustor uses jets injected into the crossflow to avoid high temperatures, which enables high  $\text{NO}_x$  formation through the thermal  $\text{NO}_x$  formation mechanism. Rapid and uniform jet mixing is needed to avoid near-stoichiometric pockets where high temperatures occur. The completion of the mixing brings the combustor to its final fuel lean and low  $\text{NO}_x$  operating condition. A representation of the  $\text{NO}_x$  path of the RQL combustor is shown in Figure 1. An alternative to injecting jets in a crossflow exists and has been a focus of research recently. The alternative method is called a (TVC) trapped vortex combustor.

Figure 1 Representation of the Desired  $\text{NO}_x$  Route in RQL Combustors



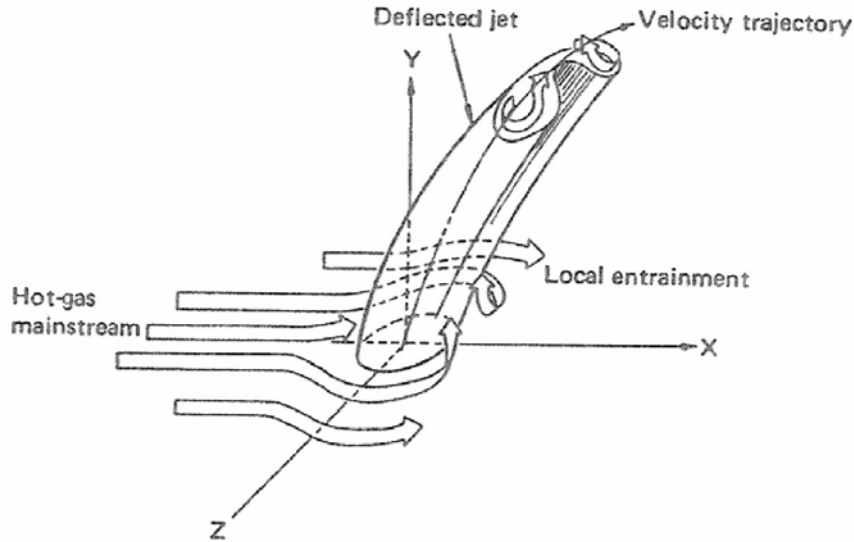
Source: Lefebvre, 1999.

#### *Jet in Crossflow Background*

The RQL approach is comprised of a series of jets injected into a crossflow from a wall. Fundamental examination of this "building block" in the mixer can provide great insight yet remain tractable as an experiment. As a result, the jet in a crossflow approach has been the main focus of RQL research. To understand the jet in a crossflow approach, the fundamentals of a single jet in a crossflow should be understood. A three dimensional image of a single round jet in a crossflow is presented in Figure 2. The single jet entering a crossflow produces a high pressure on the upstream side of the jet structure by blocking the mainstream flow. The integrity of the jet is maintained as it enters the crossflow but eventually the jet starts to bend due to the pressure difference across it. A kidney shaped form develops at the tip of the jet as it mixes with the mainstream flow. The pressure difference also induces vortex systems that

promote mixing. These vortex systems or “wakes” created by jet mixing in a crossflow may generate pockets of near stoichiometric mixtures, which could contribute to NO<sub>x</sub> formation in RQL combustors.

**Figure 2 Single Jet in Crossflow.**



Source: Lefebvre, 1999.

Using experimental data Norster found that a single jet’s maximum penetration was defined by:

$$Y_{\max} = 1.15d_j J^{0.5} \sin \alpha \quad (\text{Lefebvre, 1999}) \quad (3.1).$$

The sine function is used when the jet enters the crossflow at an angle less than 90°. The level of jet penetration is important because it is coupled with mixing. The use of multiple jets in a crossflow is typical of practical combustors. For multiple jets in a tubular duct the correlation changed because of blockage effects to:

$$Y_{\max} = 1.15d_j J^{0.5} MR \quad (\text{Lefebvre, 1999}) \quad (3.2).$$

### *Mixing and Jet Penetration*

The penetration of jets into a crossflow is one key factor that influences the mixing performance of the quick-mix section. Jet penetration is influenced by many parameters: orifice type, number of orifices, mass-flow ratio, and jet to main air momentum-flux ratio. The parameter jet -to-mainstream momentum-flux ratio includes the effects of density and mass flow rate. Since temperature and pressure are used to derive the density they also affect the momentum-flux ratio. There are two equations that are used in understanding momentum-flux-ratio. The first equation is based on the simple physical definition of momentum and is:

$$J = \frac{\rho_{jets} V_{jets}^2}{\rho_{main} V_{main}^2} \quad (3.3).$$

The previous equation can be used to derive an equation that describes the operating parameters of the combustor in terms of (note that DR is only equal to  $T_{jets}/T_{main}$  if the molecular weights of

the two streams are equal):

$$J = \frac{T_{jets}}{T_{main}} \left( \frac{A_{main}}{A_{jeteff}} \right)^2 MR^2 \quad (3.4).$$

Additionally, the ratio of areas of the main duct and jets are important parameters to use in designing the quick-mix section. The temperature of mainstream hot gases, the temperature of the jets, and the mass-flow ratio of mainstream air to jet air are critical operating conditions that have to be monitored to evaluate jet penetration.

### *Design of the Quick-Mix Section*

The design of the quick-mix section is critical in achieving the rapid mixing necessary for avoiding the high NO<sub>x</sub> producing conditions that the RQL concept is based on. The NASA design method outlined in Holdeman, et al. (1996) uses a correlation to design the jet mixing section of an RQL combustor. The correlation was found from a study of jet-to-mainstream momentum-flux ratio effects on mixing. The following equation when solved will reveal the number of circular holes needed for optimum mixing:

$$n = \frac{\pi \sqrt{2J}}{C} \quad (3.5);$$

where n equals the optimum number of holes, C is an experimentally derived constant, and J is the jet-to-mainstream momentum-flux ratio (Talpillikar, et al. 1991). Estimation of the expected reaction temperature, desired pressure drop across the duct liner, the desired jet to main mass flow ratio, and discharge coefficient of the hole enables the size of the hole to be finalized. The steps for the implementation of the NASA method and its background research can be found in Holdeman, et al. (1996).

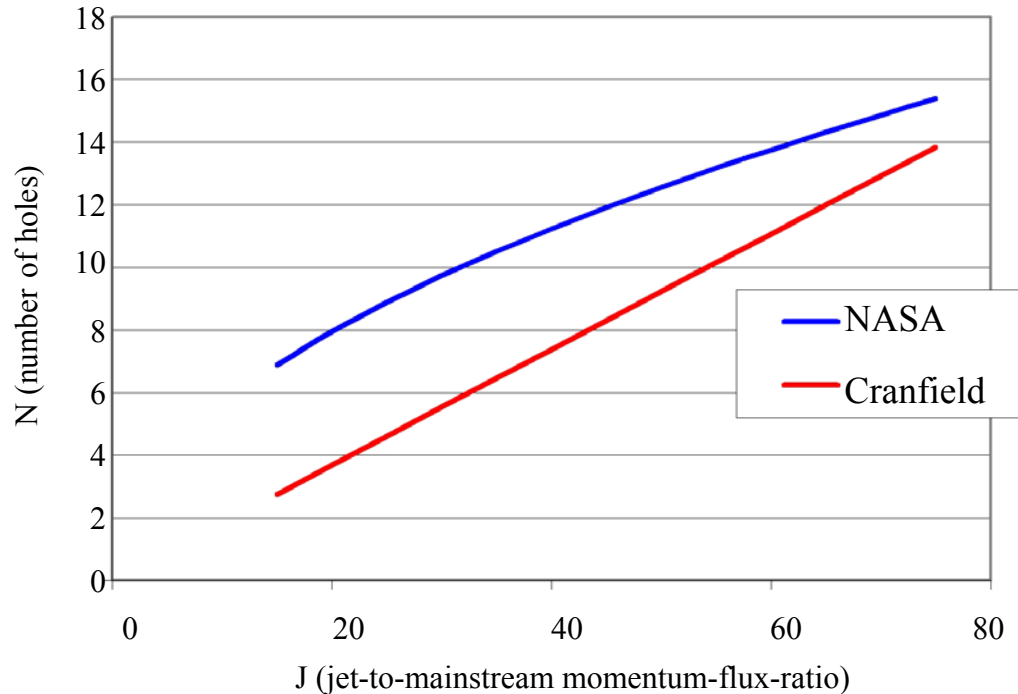
Another method that can be used to design the mixing section was developed at Cranfield University (Lefebvre, 1999). This method uses equation 3.2, the Norster equation for multiple jets (Lefebvre, 1999). The jet penetration,  $Y_{max}$ , is set equal to one third of the duct radius for tubular combustors. The jet hole diameter can then be solved for using the jet-to-mainstream mass-flow ratio. Once again the estimation of reaction temperature, desired pressure drop across the liner, and discharge coefficient of the holes are needed to calculate the optimum number of holes, except in this method the number of holes are calculated after the size of the orifice is set. The equation used to calculate the number of jet holes is:

$$nd_j^2 = 15.25\dot{m}_j (P\Delta P / T)^{-0.5} \quad (3.6).$$

A comparison of the results from both design methods is shown in Figure 3.3. The calculations were made based on a constant total effective jet area. Compared to the NASA method the

Cranfield method predicts that less holes are needed for a given momentum-flux ratio. Over-penetration is expected in the Cranfield design method because of the large C values (calculated from equation 3.5). Additionally, the jet hole size is larger for the Cranfield method.

**Figure 3 Optimum Number of Jet Holes Using Different the NASA and Cranfield Design Methods for the Quick-Mix Section.**



## 1.2 Project Objectives

Research at elevated pressure is needed to characterize the effects of pressure on mixing and the formation of emissions in the RQL combustion concept with both propane (to simulate aerospace applications and natural gas (to simulate stationary applications). This study is directed to providing this opportunity. The objectives of the project that will help meet the overall project goals are to:

- Characterize the temperature and emissions fields within the jet mixing section.
- To understand the means by which such species as  $\text{NO}_x$  and CO are produced in the mixing section and relate this insight to the overall performance of the quick-mix mixer.

The following major tasks are needed to fulfill the objectives of this project (1) the hardware design, fabrication, and assembly of a high pressure test facility for the RQL experimental combustor suitable for operation on both natural gas and propane, (2) the repeat of previously reported atmospheric tests with propane and natural gas to commission the facility, and (3) a systematic, parametric study of mixing at atmospheric and elevated pressure

conditions using state-of-the-art diagnostics and modeling. To explore the application of RQL technology to stationary micro turbine generators and thereby enhance the fuel flexibility in the market, extensive studies were devoted to RQL operation on natural gas.

## **CHAPTER 2: Project Approach**

The project approach undertaken involved many sub-tasks. These tasks were grouped according to the technical tasks outlined in the work statement for this project.

### **2.1 Hardware Design and Test Plan Task 2.1**

The hardware design was focused on the RQL experimental combustor. A high pressure RQL experimental combustor was designed with a bluff body stabilized rich product generator. The rich product generator was designed with a fuel-air premixing section, a bluff body to stabilize the reaction, and an igniter to initiate the reaction. A uniform flow in terms of velocity, concentration, and temperature was provided to the quick-mix section.

The RQL experimental combustor was assembled in the high pressure test rig with additional components including: the rich burn section, quick-mix modules, and the sampling probes. The rich burn section was fabricated with a ceramic lined inner diameter and water cooled outer diameter. The quick-mix section modules were designed with round orifices using the NASA design method developed by Holdeman, et al. (1987), and were sized according to the previous RQL atmospheric tests by Leong (1995).

The test plan was developed and finalized after Phase I and is described in more detail in subsequent sections.

#### **2.1.1 RQL Test Hardware**

To best replicate and extend upon previous RQL atmospheric experiments at UCICL, the RQL test hardware were designed based on existing hardware used by Vardakas, et al. (1999). The objective of the design was to provide a uniform flow of rich products to the quick-mix section. The flow field was designed to be uniform in terms of velocity, concentration, and temperature to isolate the behavior of jet mixing. The hardware was designed with a consistent internal diameter of 80 mm (3.15 inches) after the bluff body. The RQL test hardware is shown in Figure 4. The direction of the air flow, the different sections, and the location of the jet holes and the bluff body are presented.

**Figure 4 RQL Test Hardware Used in the UCICL High Pressure Test Rig.**

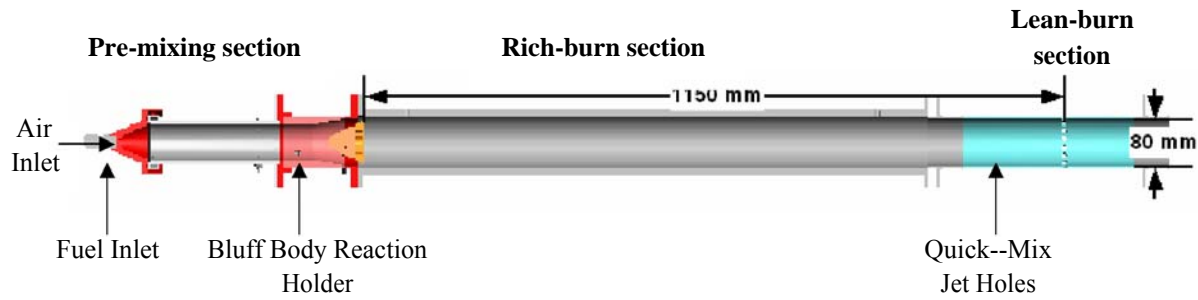
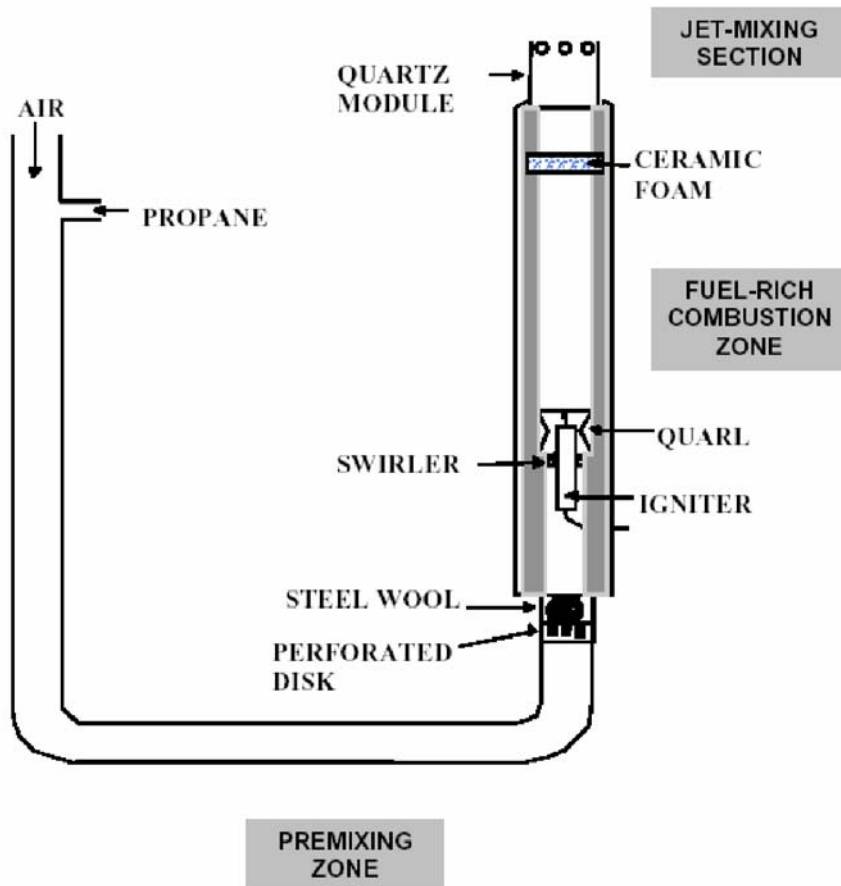


**Figure 5 Visual Experimental Representation of the Reaction in the Quick-Mix Section**



The previous combustor concept, shown in Figure 5, utilized a swirl-stabilized reaction to produce the rich products. The premixed fuel and air were filtered through steel wool and a perforated disk. In addition, a ceramic foam matrix was utilized to create a uniform flow at the entrance of the quick-mix section. The current high pressure RQL experimental combustor design utilized a bluff body to stabilize the reaction and a long rich burn section was used to create the desired uniform flow.

Figure 6 Schematic of the Previous RQL Atmospheric Facility



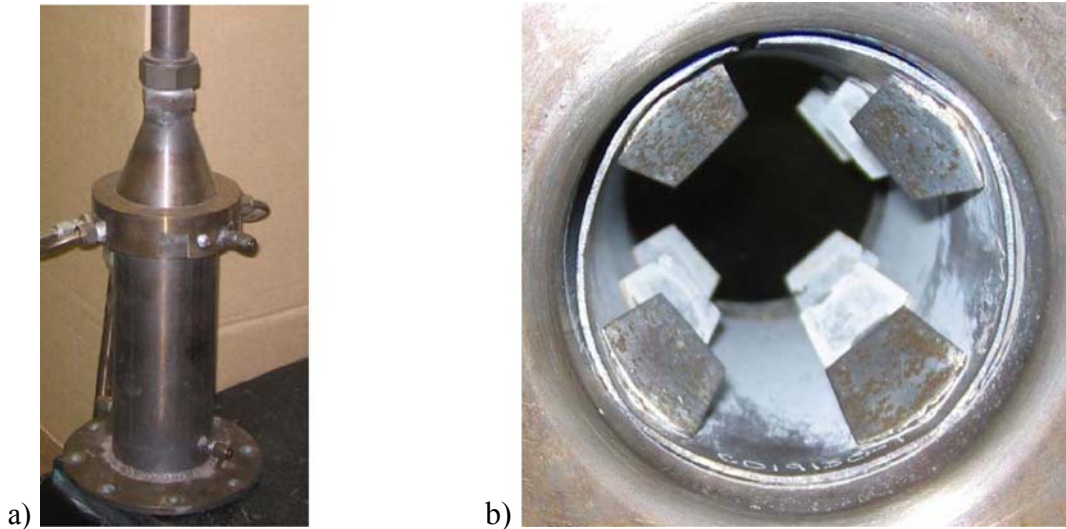
Source: Vardakas, et al. 1999

### *Pre-mixing Section*

The preheated main air enters the RQL experimental combustor through a 1" 25.4 mm (1 in.) tube into the pre-mixing section, the hardware is shown in Figure 7 a). A bellows is inserted in the flow path of the main air for axial thermal expansion in the combustor. The flow area expands with a cap to an ID of 63.5 mm (2.50 in.) where the fuel is injected. The fuel is injected through a circular array of eight equally spaced 3.17 mm (0.125 in) diameter holes by way of a plenum. The eight fuel jets then mix with the air supplied to the combustor.

The fuel and air flow through a 203 mm (8. in.) mixing section before reaching the bluff body section. A static mixer by Vortab™, shown in Figure 7 b), is attached to the ID of the pre-mixing section to enhance mixing before the bluff body. The thermocouple for monitoring the temperature is located at the end of this section. The thermocouple is not used to measure the premixed temperature of the fuel and air streams, but as an indicator for flashback.

**Figure 7 RQL Pre-Mixing Section a) Hardware Set-Up and b) Vortab Mixer**



### **2.1.2 Rich Product Generator**

#### *Concept*

A bluff body was used to stabilize the reaction of the rich product generator. The bluff body stabilizes a reaction by blocking the flow path and induces a pressure drop in the flow. The pressure drop across the bluff body created a recirculation zone where the reaction can stabilize. The pressure drop across the bluff body also is used to generate a velocity greater than the flame speed of the fuel to prevent flashback. If the pressure drop is not high enough the reaction can propagate upstream and destroy the combustor. The bluff body must also be able to survive in high temperature environments and maintain structural integrity. Sensors for monitoring the preheated main air temperature and the pressure of the combustor are included in the bluff body section of the combustor, as well. Finally, the reaction could not begin without an igniter. The bluff body houses an igniter capable of initiating the reaction of the fuel and air mixture by stabilizing a hydrogen pilot.

#### *Design*

The bluff body of the rich product generator, as mentioned above, must provide adequate blockage, which induces a pressure drop, to avoid flashback and insure stable operation. The design parameter that influences the pressure drop is the diameter of the bluff body. The diameter of the bluff body influences the aerodynamic blockage of the 80 mm (3.15 inches) duct of the RQL experimental combustor. The aerodynamic blockage is essentially the effective area created by the bluff body geometric blockage. The geometric blockage is the percentage area of the duct that is blocked by the bluff body. The aerodynamic blockage is larger than the geometric blockage because the flow around the bluff body, when passing between the duct and bluff body, induces added blockage of the flow. The amount of blockage influences the strength of recirculation zone and the velocity profile entering the quick-mix section.

The desired pressure drop across the bluff body (based on the pressure difference between upstream and downstream of the bluff body relative to the upstream pressure) for the expected

airflow for atmospheric testing was 4percent. This would provide velocities high enough to avoid flashback. The minimum main air flow rate that the experimental combustor was designed to operate at was 0.025 kg/sec (45 scfm). The velocities at the bluff body exceed 20 m/s for this main air flow rate, as well as the other operating conditions used in this study. The minimum main air flow rate was based off previous atmospheric tests using an RQL experimental combustor with the same duct diameter (Vardakas, 1999). The flow rate and duct diameter of the experimental combustors were matched to compare atmospheric data from the current RQL facility to the previous facilities. The flame speeds for the fuels used in this study at one atmosphere and 533 K (500°F) main air preheat temperature for methane and propane are 1.9 m/s and 2.1 m/s. At a main air preheat temperature of 727 K (850°F) the flame speeds increase to 4.5 m/s and 4.9 m/s. As long as the velocity at the bluff body is higher than these flame speeds flashback will be avoided. Elevated pressures have a negligible effect on flame speeds in fuel rich reactions.

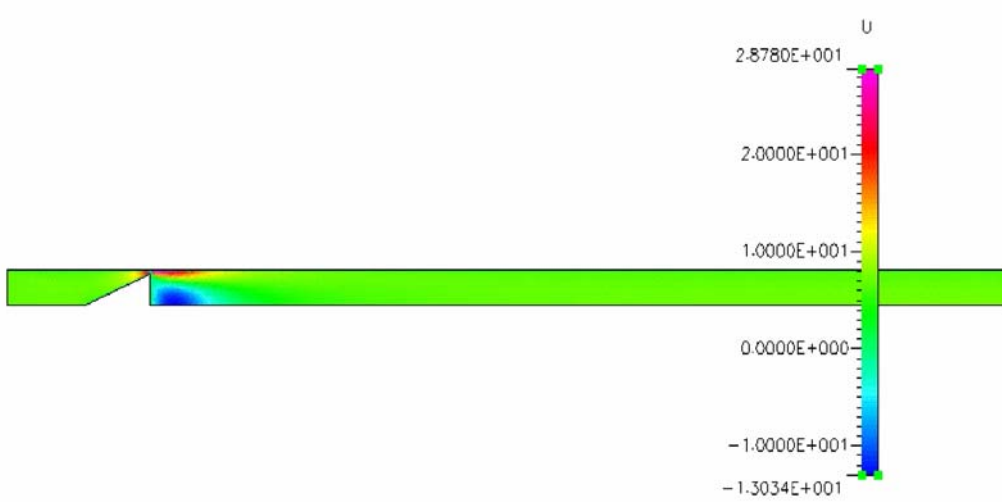
Computational fluid dynamics, CFD, modeling was helpful in identifying the diameter that would be best for stabilizing a reaction. An axis-symmetric 2-D geometry was used in the analysis. The duct diameter was set at 80 mm and three bluff body radii of 30 (1.18), 32.5 (1.28), and 35 mm (1.38 in.) were used in the model. The cone angle of the bluff body was set at 45 degree, which provided a gradual transition in the flow field to the bluff body diameter. The inlet flow was air preheated to 533 K (500°F) and the pressure was 98.1 kPa (0.97 atm). The conditions are summarized in Table 1.

**Table 1 CFD Modeling Conditions Used to Simulate The Effect of the Bluff Body Radius on Pressure Drop.**

Duct diameter, radius (mm)	40
Bluff body radii (mm)	30, 32.5, 35
Bluff body cone angle	45
Temperature, K	533
Pressure, kPa	98.1

The blue region in Figure 8 indicates the location of the recirculation zone. The 35 mm (1.38 in.) bluff body radius provided a pressure drop of 0.30 kPa (0.0030 atm) or 0.31percent. The bluff body radius was changed in the CFD model geometry to a radius of 38 mm (1.50 in.), where a pressure drop of close to 4percent was achieved

**Figure 8 Velocity (m/s) Distribution in the CFD Model of the RQL Experimental Combustor**



The bluff body radius was also calculated with a second method. This method calculated the effective area of the duct from the desired pressure drop across the bluff body. The effective area of the bluff body and the desired pressure drop are coupled. The effective area was calculated using the equation from Holman (1978):

$$\dot{m} = A_{eff} \sqrt{\frac{2g_c P}{RT} \Delta P} \quad (4.1).$$

The known parameters were the desired pressure drop value and the flow conditions expected during testing. A discharge coefficient of 0.6 was used to calculate the geometric area. The area of the bluff body was subtracted from the area of the duct and set equal to the calculated geometric area. This meant the radius of the bluff body needed to be 38 mm (1.50 in.) to induce the desired pressure drop. The geometric blockage and aerodynamic blockage of the bluff body at that radius are 0.90 and 0.94, respectively. The geometric blockage,  $B_g$ , and the aerodynamic blockage,  $B_a$ , are calculated using the following equations from Lefebvre (1983):

$$\text{a) } B_g = \frac{d_{bb}^2}{D^2} \quad (4.2),$$

b)

$$\frac{1}{(1-B_a)^2} - 1 = \varepsilon \frac{B_g}{(1-B_g)^2} \quad (4.3) \quad \text{where}$$

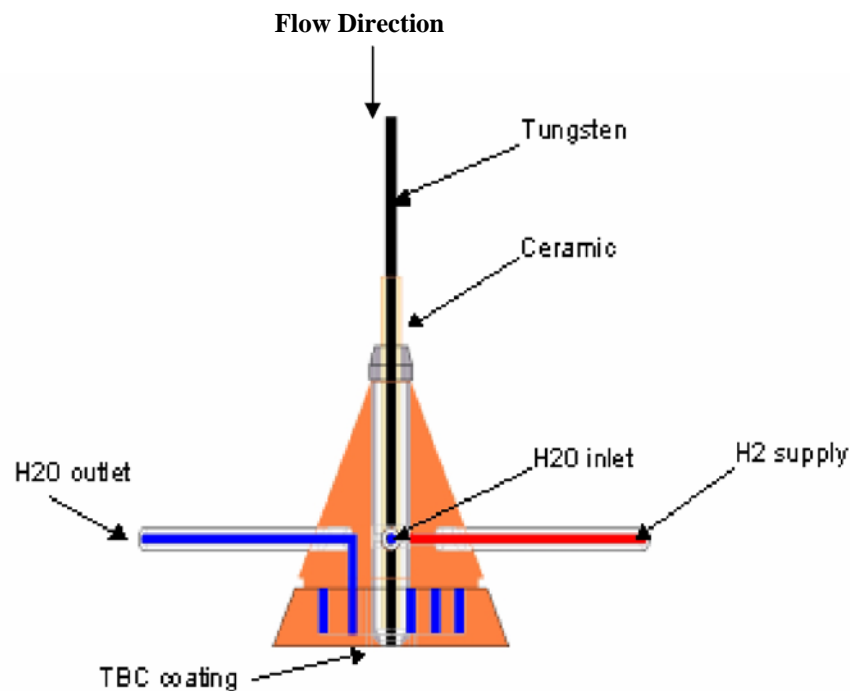
$$\varepsilon = 4.4 \left( \sin \frac{\theta}{2} \right)^{0.5} \quad (4.4).$$

The CFD results and the calculations using equation 4.1 successfully demonstrated that the bluff body would create a stable and safe reaction.

## Ignition and Cooling

The bluff body has the additional capabilities of housing an igniter, delivering hydrogen, and resisting heat. The bluff body was assembled with three 6.35 mm (0.25 in.) tubes. These three protruding tubes were used to provide cooling water and deliver hydrogen to the bluff body. The tubes were welded in the bluff body section walls to help support its weight as well. Two of the tubes were used as the inlet and outlet of the water cooled face of the bluff body. The third tube was used to deliver hydrogen to the center of the bluff body. The components of the bluff body are described in Figure 9. A tungsten rod isolated from the bluff body with a ceramic tube supplied the spark needed to ignite the pilot. In addition, to the water cooled face of the bluff body, a thermal barrier coating was used to protect it from the heat of the reaction. Stainless Steel 316 was used in the fabrication of the bluff body section, and all previously mentioned components.

**Figure 9 Schematic of the Bluff body with Internal Components.**



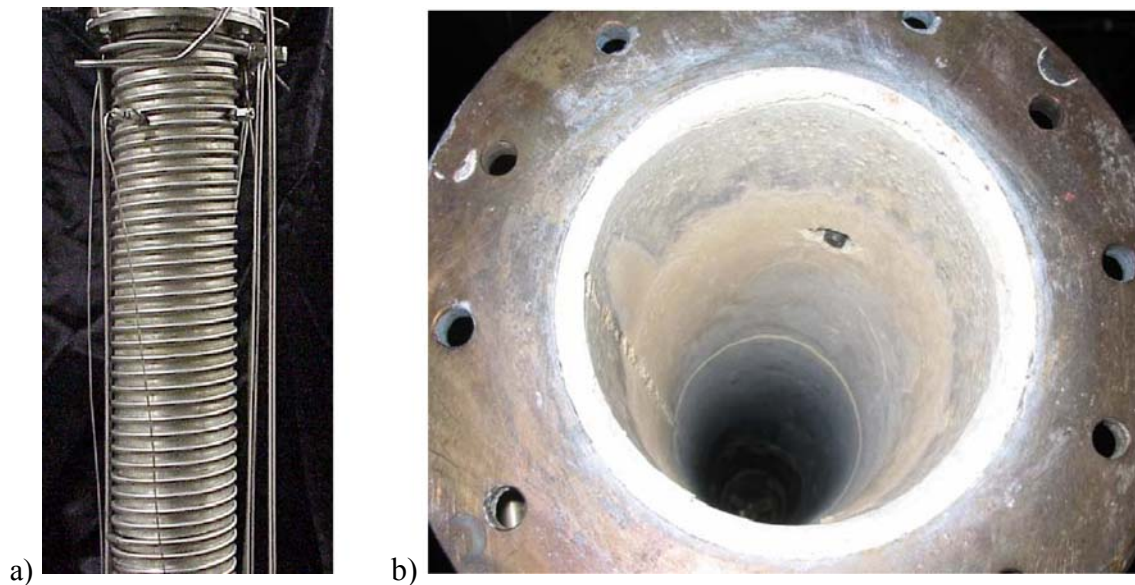
### 2.1.3 Rich Burn Section

The products of the rich combustion emanating from the bluff body stabilized reaction flow through a water cooled, ceramic lined section. The goal of this section is to provide sufficient time for the rich combustion products to reach a thermal and chemical equilibrium, and to provide a uniform gas stream to the quick-mix section. The design placed the jet holes 1150 mm (45.3 in.) away from the face of the bluff body. The rich burn section of the combustor was 914 mm (36 in.) in length and was made from SS 316. The remaining distance to the jet holes is part of the quick-mix module. CFD results of the flow in Figure 8 show a uniform color scheme at 1150 mm (45.3 in.) from the face of the bluff body. This suggests that this distance was sufficient

to provide uniform velocity entering the quick-mix section. The results in the non-reacting mixing tests and rich products in the reacting atmospheric tests proved that temperature and species concentration were uniform, as well.

The water-cooled liner of the rich burn section was fabricated using two helices. The helices were made from 6.35 mm (0.25 in.) tubes. The tubes were wrapped around the liner in machined grooves and were brazed into place. The effectiveness of the water cooling of the liner in maintaining the integrity of the rich burn section was monitored at 30 (1.18), 457 (18.0 in.), and 884 mm (34.8 in.) away from the face of the bluff body with thermocouples. The high temperatures expected in the rich burn section, even with the ceramic inner liner, gave high priority to monitoring the liner temperature. The pressure was measured with a port located at 884 mm in the rich burn section and was then used to calculate the pressure drop across the bluff body. The reaction temperature entering the quick-mix section is measured with a high temperature exotic type C thermocouple.

**Figure 10 Rich Burn Section a) Outer Diameter Liner Cooling and Ports b) Ceramic Liner**



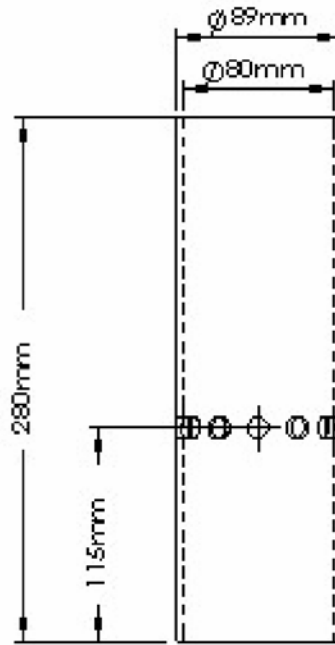
### 2.1.4 QM Modules

The quick-mix section was designed to facilitate changing the modules without having to disassemble the experimental combustor or the high-pressure vessel. The dimensions of the quick-mix modules are shown in Figure 11. The quick-mix modules were fabricated using Kanthal APM extruded tubes. Kanthal APM can safely be used in high temperature environments up 1973 K (3092°F).

The hole number and size are different for each module. The NASA method was used to design the quick-mix modules. Previous studies by Leong and Samuelsen (1996) identified that at a J of 57 the best mixing was achieved with a 12 hole module. Quick-mix modules with 8, 12, and 18 holes were fabricated with hole diameters of 13.5 (0.531), 11.0 (0.433), and 8.99 mm (0.354 in.), respectively. The fabricated modules were designed to maintain an effective jet area of 860 mm<sup>2</sup>

(1.25 in.<sup>2</sup>) and were assumed to have discharge coefficient of 0.7. The geometric jet area was 1143 mm<sup>2</sup>. In addition, the quartz modules from previous experiments were available for use.

**Figure 11 Dimensions of the Quick-Mix Modules**

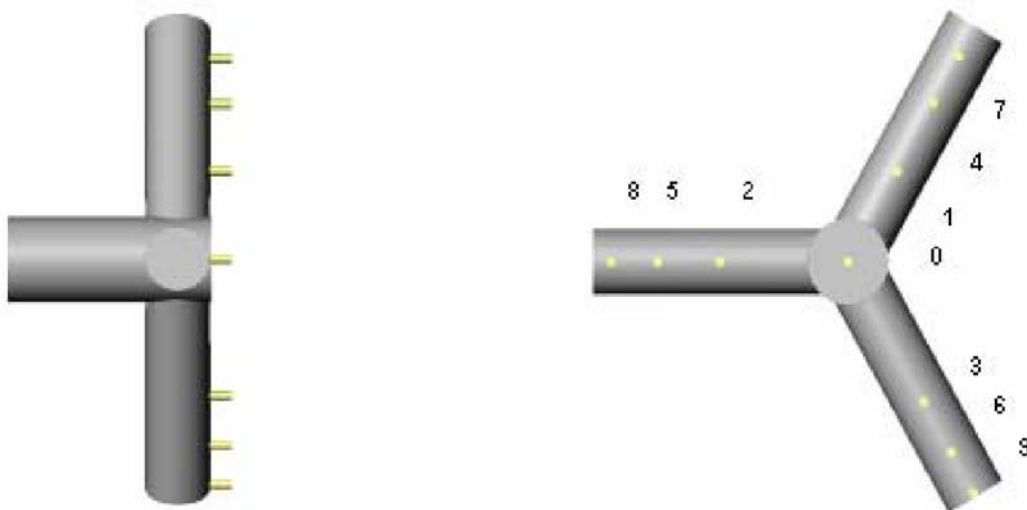


### 2.1.5 Sampling Probes

The probe was designed as a multi-port rake with ten measurement points with the ability to traverse axially and rotate. The probe was oriented co-axially with the RQL hardware and mounted through the exhaust section of the test rig. The position of the probes was changed with a system of motors and gears. Also, the position of the probe was monitored with axial and radial transducers. The pressure seal packing design of the probe allowed for axial and rotational movement. This capability allowed measurements at planes above and below the jet holes. In addition, the rotational movement allowed the probe to be swept across each plane to cover the centerline of two jet holes.

The probe, shown in Figure 12, was designed with sample locations centered on equal area annuli (recall that the experimental hardware has an 80 mm inside diameter). The diameter of the probe is 79 mm. The number of sample locations was nine plus one on the centerline, for a total of ten sample points. The holes were numbered with increasing radius starting from zero ending with nine and their locations are as follows: 0, 15.3, 19.9, 23.6, 26.8, 29.6, 32.2, 34.6, 36.9, and 38.9 mm. The sampling holes were located 3.2 mm above the surface of the spokes to minimize the disruption of the flow when sampling. To survive the high temperature environment, the sample tubes were made of Inconel 600 tubing with 1.6 mm outside diameter and 0.13 mm wall thickness. A Hastelloy C conical transition provides some stiffness and mounting surface for the sample tube/probe spoke interface. This design was used for both the temperature and emissions measurements.

**Figure 12 Emissions Probe Design and Measurement Points.**



To survive the high temperature environment, the probe was water cooled through a total loss cooling circuit. That is, water is pumped through the probe and then ejected through passages on the backside of the spokes (opposite the sample points) directed with the flow. A water tank and pump supplied clean, de-mineralized cooling water for the probe as well as the rich burn section. De-mineralized water is used to prevent mineral build-up in the probe and inside of the combustor.

Sampling probes were designed and used to characterize the emissions and temperature profiles in the quick-mix section. The emissions and the temperature sampling probes enter the high pressure test rig through the exhaust section. To have this ability the exhaust section of the pressure vessel was designed with a flanged Tee section. The emissions probe was designed for use during reacting tests. The temperature probe was designed for use in elevated pressure non-reacting mixing tests.

## **2.2 Fabrication and Facility Modifications Task 2.2**

The main experimental facility used in the testing of the RQL experimental combustor was the high pressure facility. In addition, an atmospheric test facility (a different one than the Vardakas, et al. 1999 and Leong, 1995 experiments) was used during the developmental stage of the RQL experimental combustor. After atmospheric performance of the rich product generator was characterized, the RQL experimental combustor was assembled in a pressure vessel in UCICL's high pressure facility.

Numerous performance tests were conducted with the rich product generator of the RQL experimental combustor that would bring confidence, experience, and reliability for future experiments using the high pressure test rig. These tests were conducted in the atmospheric and high pressure testing facilities. The flame stability limits at fuel lean and rich conditions were established in these tests. Also, the pressure drop across the bluff body of the rich product generator was monitored to ensure flashback would not occur at the experimental conditions expected in the high pressure test rig. DPIV (Digital Particle Image Velocimetry) and high-

speed video were also used to characterize the recirculation zone of the rich product generator. These tests were important in verifying the stability of the flow field created by the bluff body. The results of these tests are described in detail in section 5.1

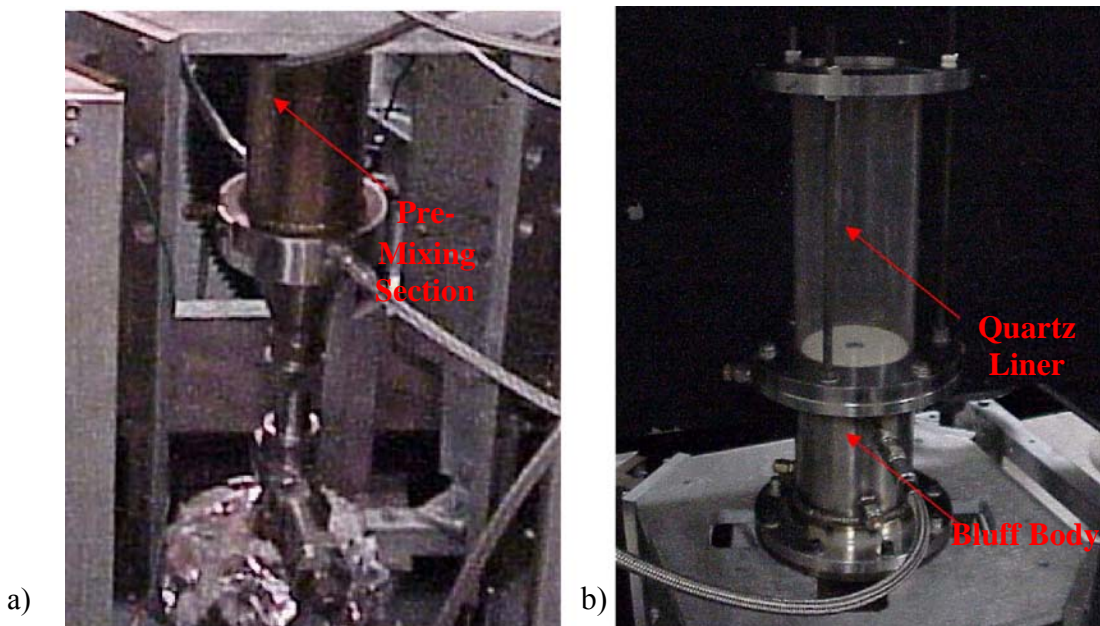
### 2.2.1 Atmospheric Facility

The atmospheric facility could deliver up to 0.034 kg/sec (0.075 lb/sec or 60 scfm) of air and preheat the air up to 505 K (450°F) using a heater upstream of the test stand. The airflow was delivered to the system through a 4.57 mm (0.18 in.) sonic venturi controlled with the upstream pressure. The system was calibrated using a LFE, laminar flow element, rated up to 0.025 kg/sec (45 scfm). In addition, a second calibration was done with another LFE rated up to 0.090 kg/sec (160 scfm) to verify the system calibration curve for operation above 0.025 kg/sec (45 scfm).

The fuel used to study the performance of the RQL experimental combustor in the atmospheric facility was natural gas. The fuel flow rate was monitored using a rotometer and was calibrated with two different LFEs. In addition to natural gas, hydrogen was used as the pilot fuel to start the reaction of the premixed fuel and air. The pilot fuel was shut off after the reaction was stabilized during experiments.

The up-fired test stand, shown in Figure 13, in the atmospheric facility was used in the performance testing of the rich product generator. The pre-mixing and bluff body sections were used in the assembly of the test stand. The recirculation zone of the bluff body was observed through a quartz liner with an 80 mm inner diameter and 203.2 mm (8 in.) in length. The pressure drop across the bluff body was measured with a water manometer. The quartz section made it possible to take data using digital particle image velocimetry, DPIV and high-speed video.

**Figure 13 Figure 4.10 Test stand in atmospheric facility a) premixing section b) rich product generator.**



The atmospheric testing of the rich product generator was critical in developing the standard operating procedure, SOP, of the experiment. The goal of the SOP was to avoid operation at or near stoichiometric conditions. A manual switching mechanism provided the ability to flow the fuel either into the pre-mixing section or to bypass it into the exhaust. To begin a reaction the fuel was initially set in the bypass direction and adjusted to meet the desired fuel to air ratio. After the pilot reaction was started the fuel flow direction was switched to the premixing section. This method was utilized during stability testing and was an overall integral part of ensuring safe and prolonged operation of the rich product generator.

The atmospheric reaction stability tests were conducted at various main air preheat temperatures and main air flow rates. The flow rate and preheat temperature both influence the pressure drop across the bluff body. A bluff body pressure drop starting at 8 inches of H<sub>2</sub>O (1.99 kPa or 0.289 psi) was used as a minimum during stability tests. This value corresponded to the lowest pressure drop allowable (2percent) to maintain safe operation of the rich product generator. The air flow rate was increased at increments of 2 inches of H<sub>2</sub>O (0.497 kPa or 0.722 psi) until the facility limits were reached.

A non-reacting flow seeded with Alumina particles was used in the PIV experiment. The flow rate of air was 45 scfm and the air was not preheated. The high speed video tests were conducted at lean and rich operating conditions with the same air flow rate with no preheat. The lean and rich equivalence ratios were 0.6 and 1.66, respectively.

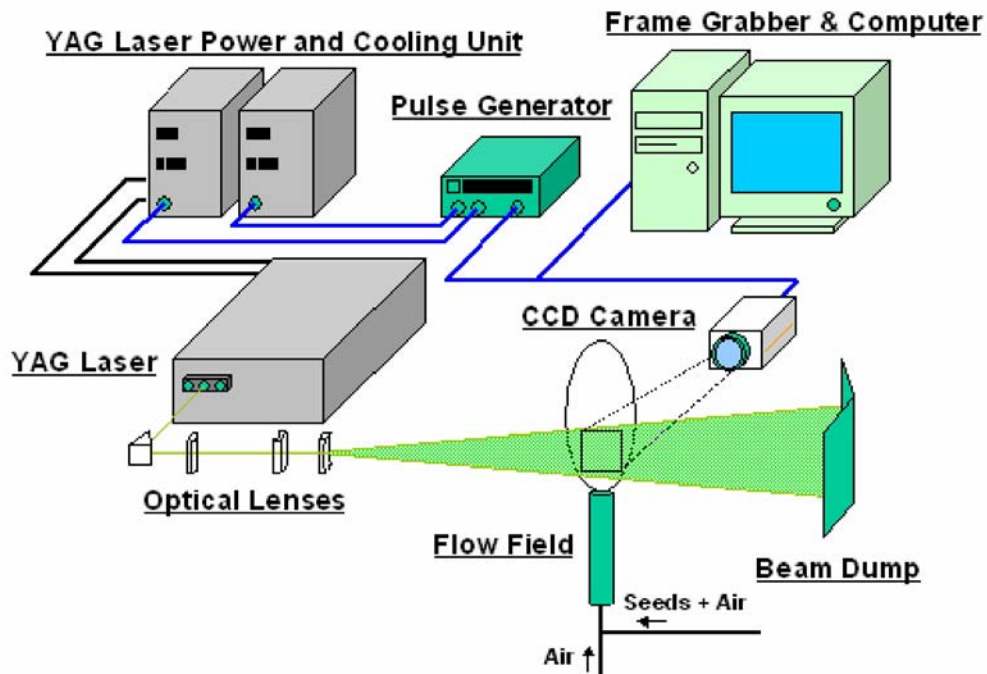
**Table 4.2 Fuel Lean and Rich Reaction Stability Operating Conditions.**

Temperature °F (K)	DP BB inches H <sub>2</sub> O (kPa)
72 (295)	8 - 12 (1.99 - 2.98)
150 (339)	8 - 14 (1.99 - 3.48)
300 (422)	8 -18 (1.99 - 4.47)

### *Digital Particle Image Velocimetry*

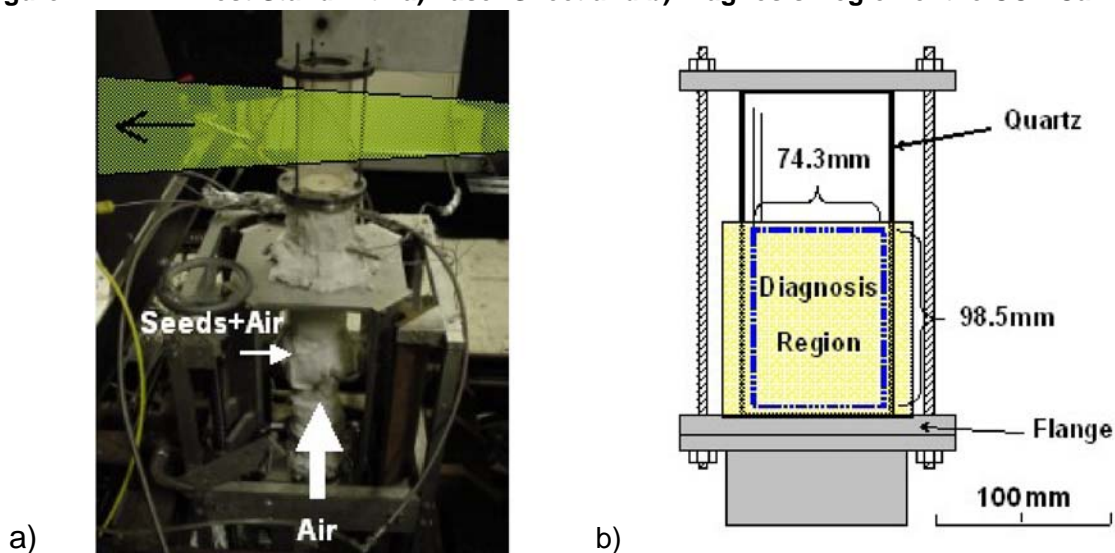
DPIV, digital particle image velocimetry, was used to analyze the recirculation of the rich product generator. DPIV is a non-intrusive technique used to measure the instantaneous and time averaged velocity flow fields in a 2-D plane by capturing two images. The displacements of marked particles were analyzed to determine the velocity and direction of the flow field. The DPIV set up is shown in Figure 4.11. The DPIV experimental set up is complicated and requires great attention to detail to gather reliable and repeatable data.

Figure 4.11 Experimental Set-Up DPIV System



The set-up consists of a laser, a CCD camera, and a pulse generator. The pulse generator controls the frame grabber, the Nd Yag laser, and the CCD Camera. The DPIV system utilized incorporated an Nd Yag Laser made by Continuum. The model Surelite III outputs visible green light at wavelength of 532nm. The laser is rated as Class 4 meaning it can cause severe damage when looked at directly, even if it is scattered. The laser pulses at a frequency of 10 Hz and emits 350 mJ per pulse. A CCD camera, Kodak Model ES 1.0, is used to capture the image of the flow field. The camera was set in the double exposure mode. The resolution of the images was over one million pixels, 1008 by 1018 pixels. A pulse generator, Stanford Research Systems DG 535, was used to control the timing of the laser, camera, and the computer.

Figure 4.12 DPIV Test Stand with a) Laser Sheet and b) Diagnosis Region of the CCD Camera



Software by Insight was used to decipher the displacement, velocity, and direction vectors of the particles in the images captured by the CCD camera. To generate images with scattered light the flow was seeded with Alumina,  $\text{Al}_2\text{O}_3$  powder nominally 2.0  $\mu\text{m}$  in size from MicroAbrasives GB500. The set up of the experiment is shown in Figure 4.12. The laser beam illuminates the seeded particles in the flow. The laser beam is initially a round beam approximately 10 mm in diameter. A series of optics are used to create a laser sheet from the beam to illuminate the seeded particles in the flow and allow the images to be captured with the CCD camera. A non-gloss black paper was carefully positioned on one side of quartz to mask any surface reflections from entering the camera. The software cannot determine the differences between particles scattering and surface reflections.

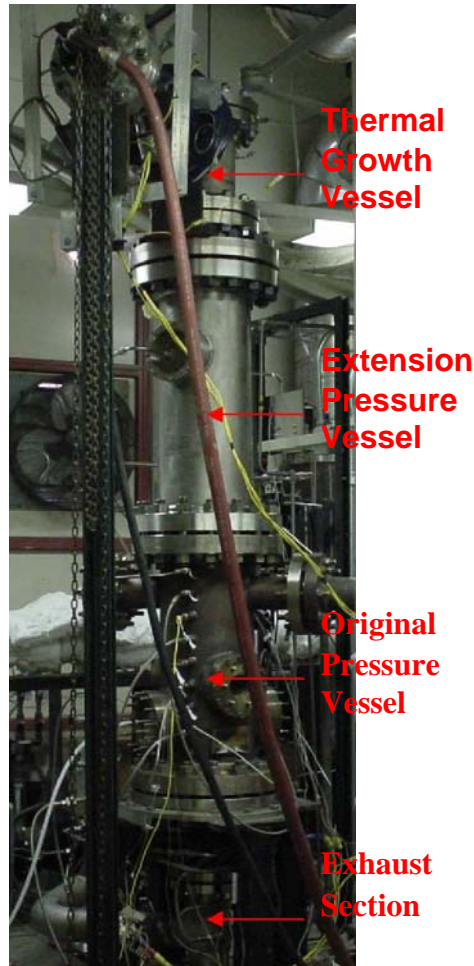
### *High Speed Video*

The high speed video was recorded with an Ultima APX FASTCAM. The camera could record up to 200,000 frames per second (fps). The camera was set at 4000 fps to be able to record an area encompassing the bluff body and the quartz module. The recorded images were analyzed using Photron High Speed Motion Analysis software. The high speed visualization is useful in providing visual data about the region where the reaction anchors and turbulent characteristics of the recirculation zone. The turbulent characteristics may also provide information useful in large eddy simulations, LES.

### **2.2.2 High Pressure Facility**

The RQL test rig was integrated into a complex system in the high pressure test facility at the UCICL. The RQL test rig was mounted in a down-fired position inside a pressure vessel. The combustor was comprised of five distinct sections: a premixing section, a bluff body, a rich burn section, a quick-mix section, and a lean burnout section. The total length of the RQL test hardware was 1.8 m (5.94 ft). The original high-pressure vessel could not handle the length of the RQL test hardware. For this reason, an extension vessel was built. In addition, a thermal growth vessel was built to accommodate the increase in length of the combustor during reacting experiments. The thermal growth vessel, exhaust section, original pressure vessel, and the new pressure vessel, all together stand over 3.04 m (10 ft) above the floor of the facility. The assembled test rig with all its components is shown in Figure 4.13.

Figure 14 RQL High-Pressure Test Rig



Two air circuits were used to supply the main and jet air to the RQL experimental combustor. The facility could provide jet air flow up to 1.81 kg/sec (4 lb/sec or 3236 scfm) with air preheat temperatures up to 811 K (1000°F). The main air flow could be as high as 0.168 kg/sec (0.37 lb/sec or 300 scfm) with air preheat temperatures up to 866 K (1100°F) preheat. The flow rates of each circuit were controlled electronically and were regulated using flow meters. The supply of dried and filtered air was delivered with a system of compressors. A 72 kW heater was added to the facility for preheating the main air to the required operating temperatures. A second existing set of heaters, rated at 550 kW, was used to preheat the plenum air needed for the jets in the quick-mix section. The jet and main air are in different independent circuits which allows more flexibility and control during experiments.

The fuels used in the high pressure facility were both natural gas and propane. The natural gas was supplied with a compressor with a delivery pressure as high as 500 psig at 200 scfm (3545 kPa at 0.061 kg/sec). The flow rate of natural gas was regulated with a sonic orifice. The system had the capability of using different sizes of sonic orifices depending on the desired flow rate and operating pressure of the experiment. The propane was supplied by a 25 gallon (94.6 L) tank of liquefied propane and was delivered at low pressure. The tank was submerged in a

heated water bath to insure that a constant fuel flow rate was maintained as the liquefied propane evaporated. The 25 gallon (94.6 L) tank can be used in experiments lasting up to 5 hours. A Coriolis flow meter was used to measure the propane mass flow rate.

The facility has a self-contained water quench system that is used to reduce gas temperatures before entering the backpressure valve, which is used to create the backpressure. The system pressure limit is 120 psig (9.2 atm or 974 kPa). The airflow rate, preheat temperature, and system operating pressure are all interrelated. The maximum conditions cannot be achieved for all three parameters simultaneously.

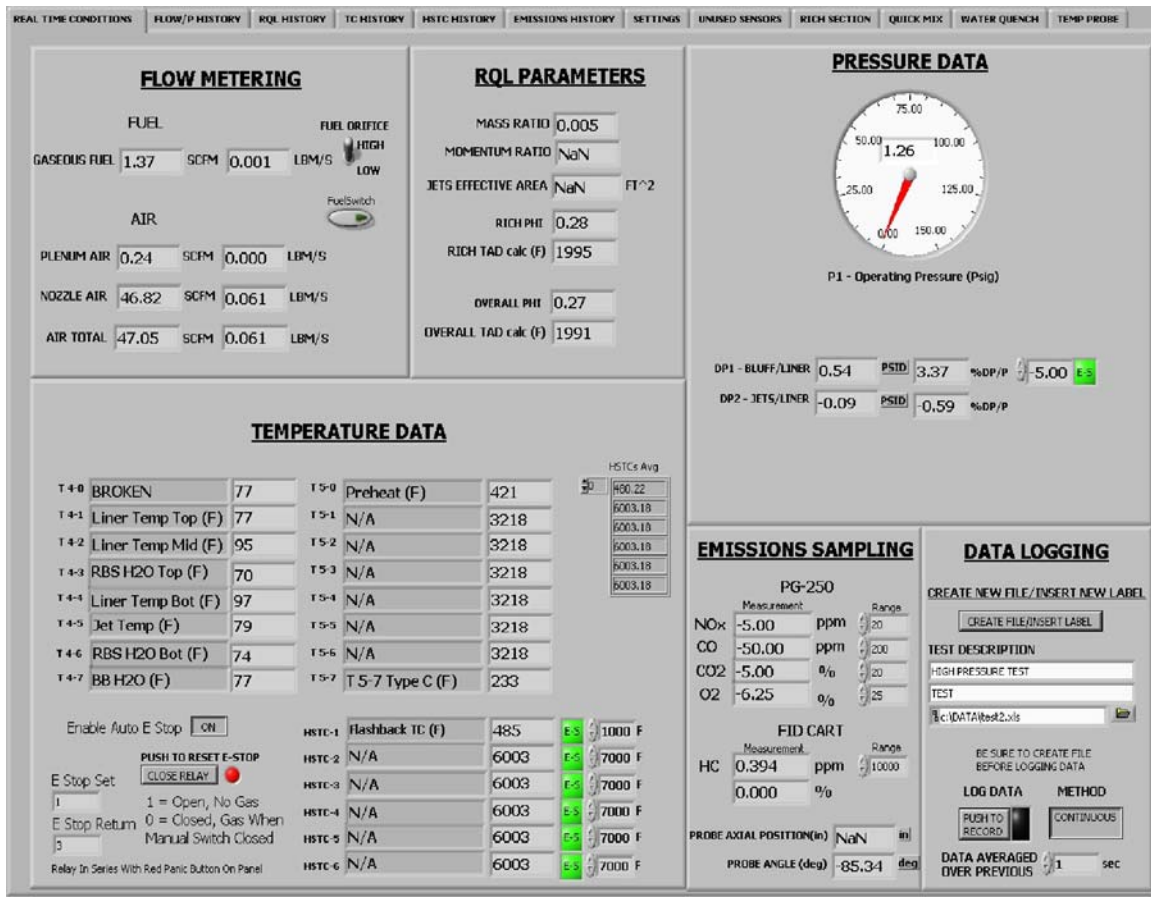
The facility had a distinct operational characteristic to insure flexibility and control of experiments. This characteristic was the ability to independently control the main air and the jet air. The main air and the jet air each have independent heaters to achieve the desired temperatures. The main air enters the vessel through the thermal growth section, while the quick-mix air is fed from the existing vessel and fills the plenum. The temperature of the jet air is used to increase the momentum-flux-ratio of the combustor during experiments (see equation 2.4). Previous research has shown that jet preheat temperatures up to 533 K (500°F) have a minimal effect on NO<sub>x</sub> emissions (Vardakas, et al. 1999). The pressure drop across the jet holes and the jet temperature are needed to calculate the momentum-flux ratio. The pressure drop is measured with a port in the pressure vessel and the aforementioned rich burn section pressure port. The test rig thermocouples and pressure ports provide the information needed to make instantaneous calculations of  $J$ . The end result is that the MR, densities of the jet and main air,  $A_{eff}$ , and  $A_m$  are known and equation 2.3 and 2.4 can be solved for  $J$ .

### *Data Acquisition*

The high-pressure facility has a full complement of instrumentation for the monitoring of flows, temperatures, and pressures. Mass flow sensors measure the air flow in the three existing air circuits in the facility. The fuel circuits are measured by a combination of critical flow orifices, Coriolis mass flow sensors, and pressure transducers.

The signals from all the sensors and measurement devices are sent to a data acquisition console. The data are processed and displayed using LabView. The LabView interface, shown in Figure 15, displayed all temperature, flow rates, pressure, pressure drop, RQL related parameters, and emissions measurements during testing and included an emergency fuel shut off system. The data provided by the interface were saved into a Microsoft Excel file.

Figure 15 Snapshot of the Experimental Labview Data Acquisition Interface.



Emissions were monitored with a continuous emissions monitoring system. CO, O<sub>2</sub>, CO<sub>2</sub>, and NO<sub>x</sub> were measured using a Horiba PG-250. NO could also be measured with this analyzer. Hydrocarbons were to be measured using a Horiba FIA-236 (Flame Ionization Analyzer). The FIA has the ability to measure from 0-100,000 ppm of C. The rich products were expected to have 10-12 percent CO in the stream, which is above the measurement capabilities of the PG-250. As a result, another Horiba instrument, model AIA-210 for measuring CO with an infrared analyzer and a range of 20percent (200,000 ppm) was identified for use in measuring the rich product stream. Table 2 summarizes the measurement capabilities of the analyzers in the continuous emissions monitoring system. The emissions analyzing system used during experiments consisted of a water drop out section, which resulted in “dry” values for NO<sub>x</sub>, CO, CO<sub>2</sub>, and O<sub>2</sub>.

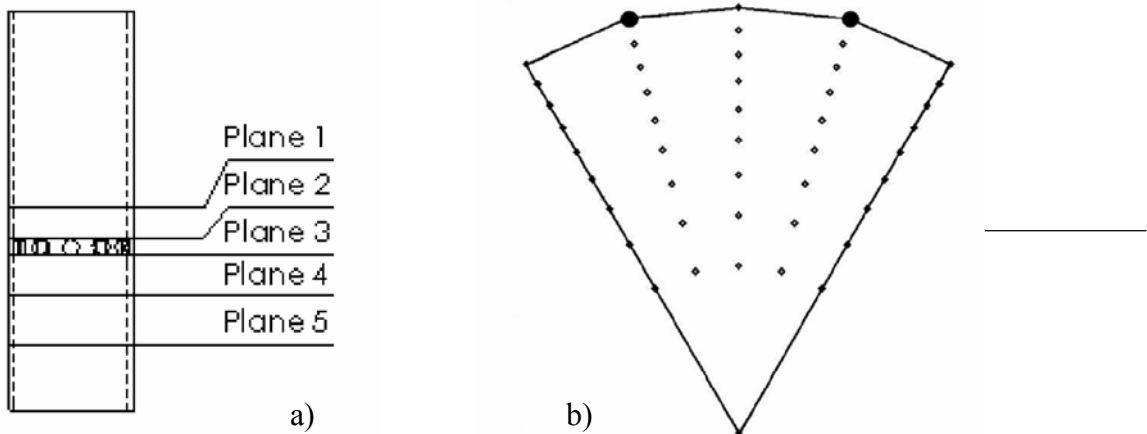
During testing, the individual gas streams from each data point were directed to a sample selection board. This board permits each gas stream to be individually selected. The sample stream is then directed to the continuous emission monitoring system. The continuous emission monitoring system is integrated with the same high-pressure data acquisition system as the facility instrumentation.

**Table 2 Effective Range of Analyzers By Volume**

Species	PG-250	FIA-236	AIA-210
NO <sub>x</sub>	0-2500 ppm	--	--
CO	0-5000 ppm	--	0-25%
CO <sub>2</sub>	0-20%	--	--
O <sub>2</sub>	0-25%	--	--
HCs	--	0-10%	--

Data were taken on five different planes. ZZZZ is a representation of the measured planes. Planes 1, 2, 3, 4 and 5 correspond to the planes above, on the leading edge, the trailing edge, one duct radius downstream, and two duct radii downstream of the leading edge of the holes, respectively. Note that the axial sampling planes were calculated by dividing the axial distance from the leading edge of the jet mixing holes divided by the radius of the combustor. Positive values denote planes downstream of the jet mixing holes and the negative value means the plane above the holes. The probe is swept across two jet hole centerlines to provide the data points necessary to generate a representation of each plane. The total angle swept for the 12 hole configuration is 60°. For the 8 hole and 18 hole modules, a 90° and 40° sector is necessary to cover the two jet hole centerlines, respectively. The grid created by the data obtained is also shown in Figure 4.15. The two dark holes in the grid represent the angles that coincide with jet hole centerlines. This method was used in both temperature and emissions measurements. Temperature measurements were taken on each plane and emissions measurements were only taken on planes 1, 4, and 5. The results from the temperature and emissions measurements on plane 1 showed that the flow entering the quick-mix section is uniform and symmetric. The results from plane 1 are described in detail in section 3.3 and 3.5.

Figure 16 A) Planes of Measurement in the Quick-Mix Section and B) Data Grid o Each Plane



In a previous atmospheric study published in Vardakas, et al. (1999), the emissions data were analyzed at plane 4 of the quick-mix section. Also, on each plane the data grid consisted of only three different duct radii measurement points for each angle, not including the point on the centerline. The three radii were  $R/3$ ,  $2R/3$ , and  $R$ . The measurement points on the current emissions probe that near the same locations as the three radii are: 1, 4, and 9. Comparing planar area weighted averages from these points with a similar analysis provided a closer comparison of the two data sets.

## **2.3. Parametric Jet Mixing Tests Task 2.3**

The testing conducted on this project was to be carried out in three phases. Phase I was designed to verify the operation of the test facility, test hardware, and instrumentation and to essentially demonstrate consistency with previous studies. The Phase I studies also define the operational limits of the test facility and hardware and form the basis of Phase II test plan.

### **2.3.1 Phase I Testing**

#### *Rich Product Generator Performance Testing*

The reaction stability experiment was conducted to test the rich blow out limit of the combustor. The two levels of preheat for the main air was 533 K (500°F) and 727 K (850°F). The combustor was operated at these preheat temperatures with the operating pressure of one, three, and six atmospheres. The temperature entering the rich burn section was recorded for the atmospheric tests. The main air flow rate of 0.025 kg/sec (45 scfm) was maintained for the entire atmospheric tests conducted in the high pressure facility. The fuel used during these tests was natural gas.

#### *Atmospheric Reacting Mixing Experiments*

The performance of the RQL experimental combustor in the high pressure test rig was tested to assure that the system would meet the desired operating conditions for reacting tests. The stability of the combustor and the capabilities of the emissions probe were used in the development of a statistically designed experiment. The successful operation of the data acquisition and safety systems was tested. The temperature of the rich product was characterized at varying equivalence ratios for use in calculating instantaneous jet-to-main momentum-flux ratio. The expected flame temperature of the mainstream rich products entering the quick-mix section was 1500 K (2240°F). The details regarding this task are found in section 2.2.

The atmospheric reacting mixing tests were conducted with both propane and natural gas. The propane was used to repeat the experiments conducted by Vardakas, et al. (1999). The operating conditions for the atmospheric reacting mixing tests are listed in Table 4.4. The same conditions were used when testing with natural gas. A higher preheat of 727 K (850°F) condition, more indicative of the temperature entering the combustor of a stationary gas turbine, was added as well. Vardakas, et al, (1999) also studied the effects of jet air preheat temperature and concluded that the jet air preheat temperature did not affect NO<sub>x</sub> emissions. The maximum operating jet

air preheat temperature in the Vardakas, et al. (1999) study was 533 K (500°F). In the repeated atmospheric reacting mixing tests, the jet air preheat temperature was always below 533 K (500°F). The actual jet air preheat temperature during these tests was on average 383 K (230°F). Only the plane upstream of the jet holes, one duct radii downstream, and two duct radii downstream were measured. The NO<sub>x</sub> and CO results were compared with contour plots and planar area averaged data.

The ability to successfully demonstrate the repeatability of previous work was a major step in commissioning the facility in terms of its capabilities, specifically in its ability to be used in jet mixing research.

**Table 3 Operating Conditions for Atmospheric Reacting Mixing Tests.**

<b>Parameter</b>	<b>Value</b>
P (kPa)	101.3
rich $\Phi$	1.66
overall $\Phi$	0.45
T <sub>main</sub> (K)	1500
T <sub>jet</sub> (K)	380
Momentum-flux ratio J	57
Mass-flow ratio MR	2.5

### *Chemical Kinetics Modeling*

In addition, a chemical kinetics model for the RQL combustor was developed using Chemkin 4.0. The fuel rich products were modeled using a PSR (perfectly stirred reactor), plug flow reactor, and equilibrium products. The quick-mixing section was modeled with eight PSRs with different operating equivalence ratios. The analysis and results from this model will provide insight results from the kinetics model showed the effects of pressure, preheat temperatures, and residence time on NO<sub>x</sub> and CO formation. This task is described in detail in section 3.4.

### **2.3.2 Phase II Testing**

Phase II included a series of systematic, parametric tests incorporating the effect of pressure on the emissions production and jet mixing performance. Phase III was to include additional tests selected strategically to address questions that arise from the Phase II effort.

#### *Non-reacting Elevated Pressure Mixing Experiment*

Non-reacting cold and hot flow mixing were studied at elevated pressure in the high pressure test rig during Phase II. The main and jet flows were operated at different temperatures. The jet mixing was evaluated using measurements collected by the temperature sampling probe. This non-reacting study was used to evaluate the effect of elevated pressures on jet penetration and mixing performance.

The non-reacting mixing experiment was conducted in the high pressure facility. During the experiment, the main air was preheated to 727 K (850°F) and mixed with non-preheated jet air. The temperature entering the quick-mix section was much lower than 727 K (850°F) because of the heat loss through the combustor. The system was tested at two operating pressures, one and six atmospheres, with 12 hole quick-mix module. Six atmospheres was chosen as the operating pressure during experiments because it would simulate the pressure of a micro turbine generator. The jet-to-main mass flow ratio was maintained at 2.5. This operating condition was used in the previous atmospheric tests conducted at UCICL (Vardakas, 1999). The jet-to-main momentum-flux ratio was on average 80. A J of 57 could not be reached due to facility limitations in the level of main air preheat temperature. Nonetheless, this experiment gave insight into jet mixing at elevated pressure and was not conducted for jet mixing optimization purposes.

### *Elevated Pressure Reacting Mixing Experiment*

An elevated pressure reacting mixing experiment was conducted at the same conditions used in the atmospheric reacting mixing experiments in Phase I to gain insight regarding the effects of pressure on NO<sub>x</sub> emissions. The fuel used in this test was natural gas and the operating pressure was set at 6 atm. This pressure reflects the operating pressure of the combustor used in a typical micro turbine generator for stationary power generation. The test conditions were at a J of 57, MR of 2.5, main air preheat temperature of 533 K (500°F), rich  $\Phi$  of 1.66, overall  $\Phi$  of 0.45, and a jet preheat temperature of 380 K (225°F). The temperature of the main crossflow in the elevated pressure reaction was higher than the atmospheric reacting experiments. The temperature of the fuel rich products entering the QM section was measured at 1602 K (2425°F). Data was measured on plane 5, two duct radii downstream of the leading edge of the jet holes, at  $x/R=-2$ . In these tests three emission analyzers were used including the Horiba PG-250. The Horiba FIA-236 was used to measure hydrocarbons and the AIA-210 was used to measure high CO values.

### **Test Plan for Full Set of Experiments**

The equilibrium calculations for fuel rich conditions at different preheat temperatures and pressures complimented the analysis the data from the reacting mixing tests in Phase I and II in developing the test plan for a Design of Experiments parametric study of the RQL experimental combustor. The equilibrium results were obtained using Chemkin v3.7 and the GRI Mech 3.0 mechanism for both propane and natural gas cases. The results, along with the shakedown and experimental results were used in the development of the test matrix for high pressure reacting mixing tests.

# 3 CHAPTER 3

## Project Outcomes

### 3.1 Phase I Testing

#### 3.1.1 Rich Product Generator Performance Testing

The bluff body was assembled in an atmospheric testing facility to verify the design and operation. The bluff body was designed to prevent flashback and to stabilize rich reactions. During these tests, the pressure drop was measured above 2 percent across the bluff body at the minimum expected main air flow rate and was deemed sufficient to prevent flashback. High pressure reaction stability tests were conducted in the high pressure facility to define the rich stability limits of the rich product generator at the conditions expected in reacting mixing tests. The recirculation zone created by the bluff body was characterized using DPIV (digital particle image velocimetry) in non-reacting tests and high-speed video during reacting tests.

The tests demonstrated the reliability of the igniter and pilot for initiating the reaction and maintaining consistent stable operation during fuel rich reactions. These performance tests insured safety, verified the design, and provided valuable experience in using the bluff body as the rich product generator for the RQL experimental combustor.

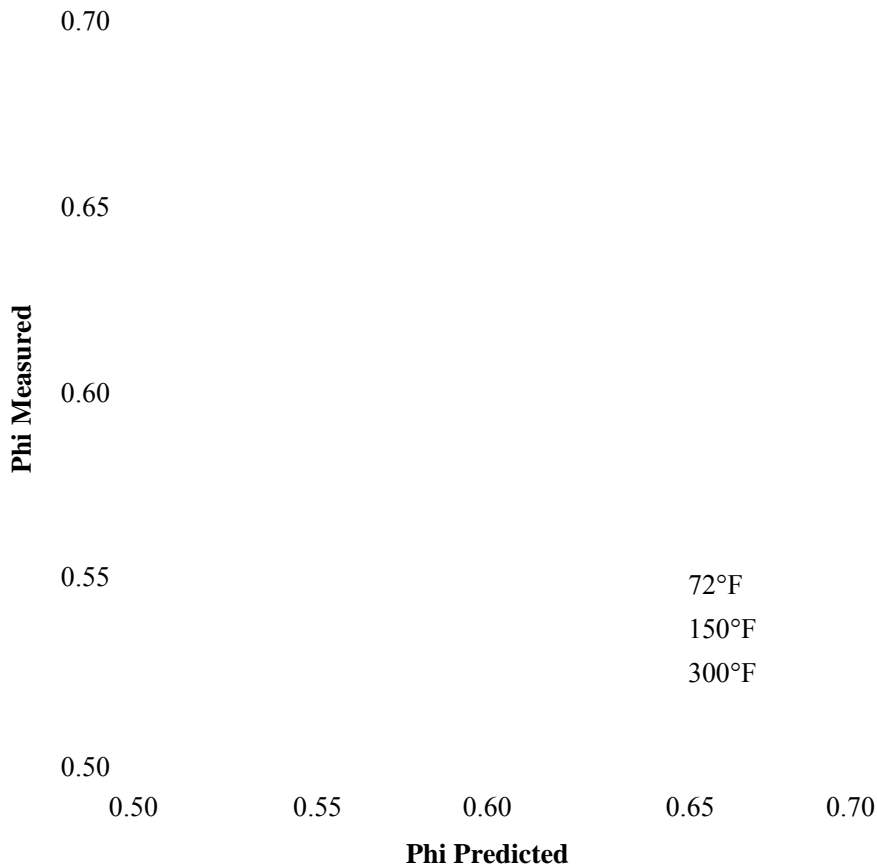
#### Atmospheric Reaction Stability

Atmospheric reaction stability tests defining the lean and rich extinction limits of the rich product generator, with natural gas as the fuel, were conducted at various pressure drops and preheat temperatures. The measured lean extinction limits were compared to the predicted lean extinction limits using the correlation by Ballal and Lefebvre (1979), which was derived for bluff body stabilized reactions.

The equation used for the correlation is presented in Figure 17.

**Figure 17 Comparison of Measured and Predicted Values of Fuel Lean Stability Limits Using Experimental Data and Ballal and Lefebvre Correlation.**

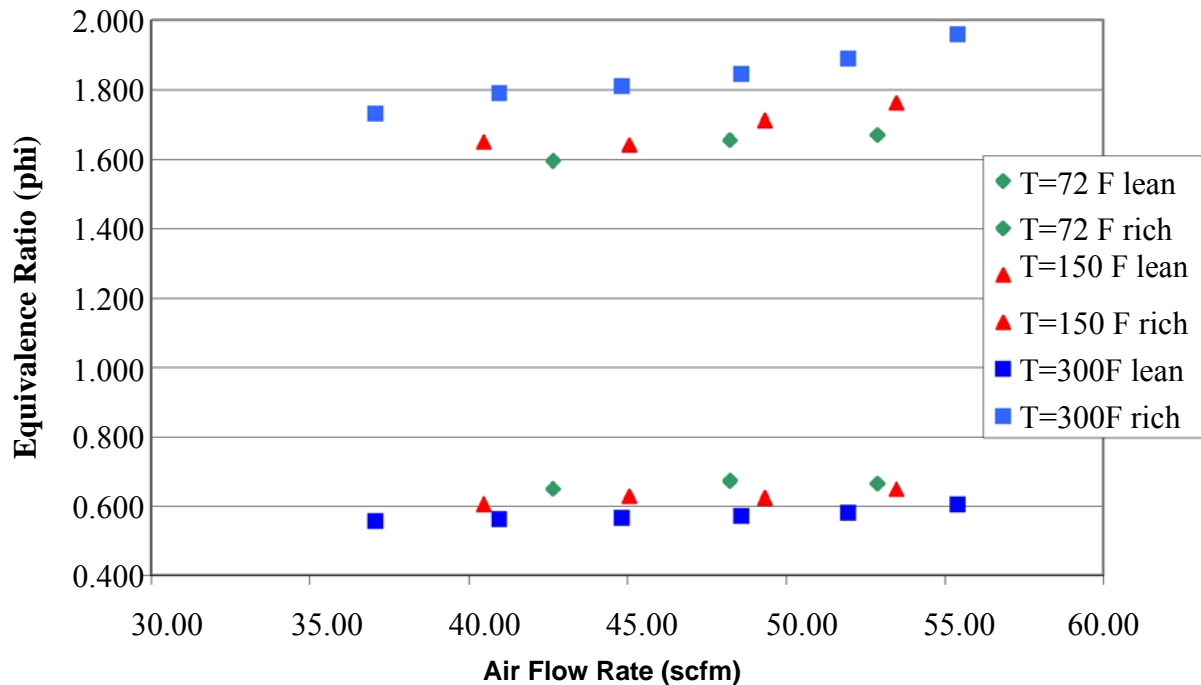
$$\phi_{WE} = k \left[ \frac{U}{P^{0.25} T_0 \exp\left(\frac{T_0}{150}\right) D(1 - B_g)} \right]^{0.16} \quad (5.1).$$



The weak extinction limits observed for the current system were well predicted with the correlation as shown in Figure 17. The constant of proportionality,  $k$ , in the above equation is 4.25 for the bluff body used in the RQL experimental combustor. The range of mass flow rates of air did not provide enough data to show the full stability range of the rich product generator. Increasing the preheat temperature extended the rich and lean stability limits, as was expected. The highest rich blow out limit was measured at an equivalence ratio 1.96 for a preheated main air temperature of 300 °F and a pressure drop of 18 inches of H<sub>2</sub>O across the bluff body. The measured fuel rich and fuel lean stability limits are plotted in Figure 18.

The rich stability limits measured gave confidence that stable rich conditions could be achieved under elevated pressures and higher main air preheat scenarios.

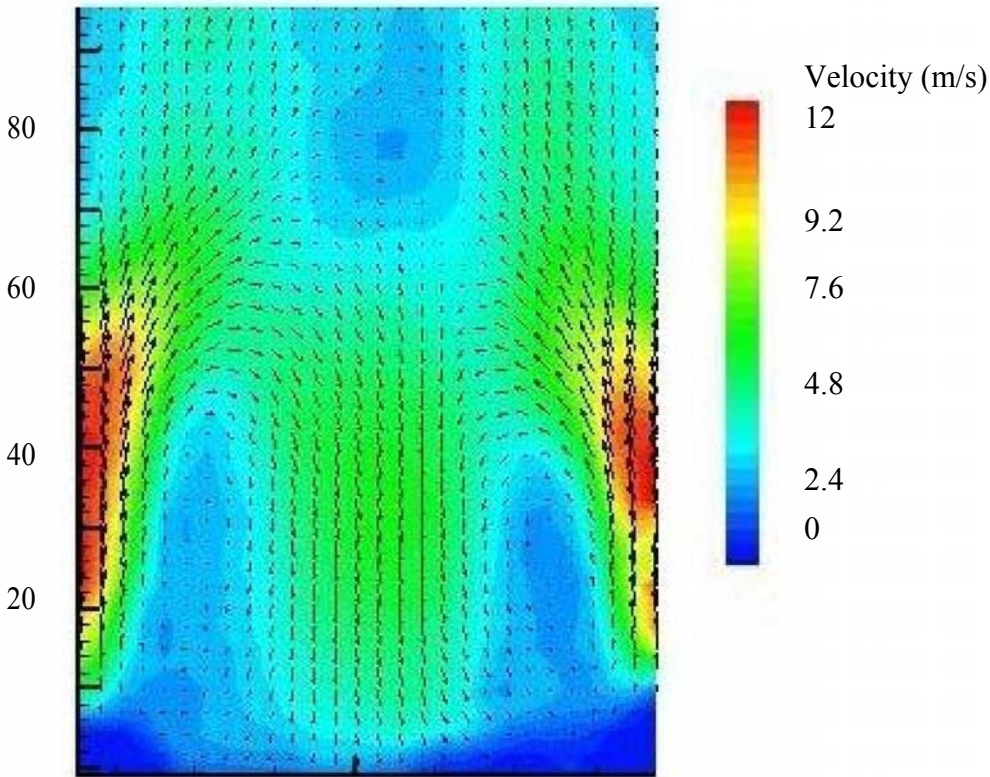
**Figure 18 Measured Fuel Lean and Rich Stability Limits of the Rich Product Generator**



#### *DPIV and HSV*

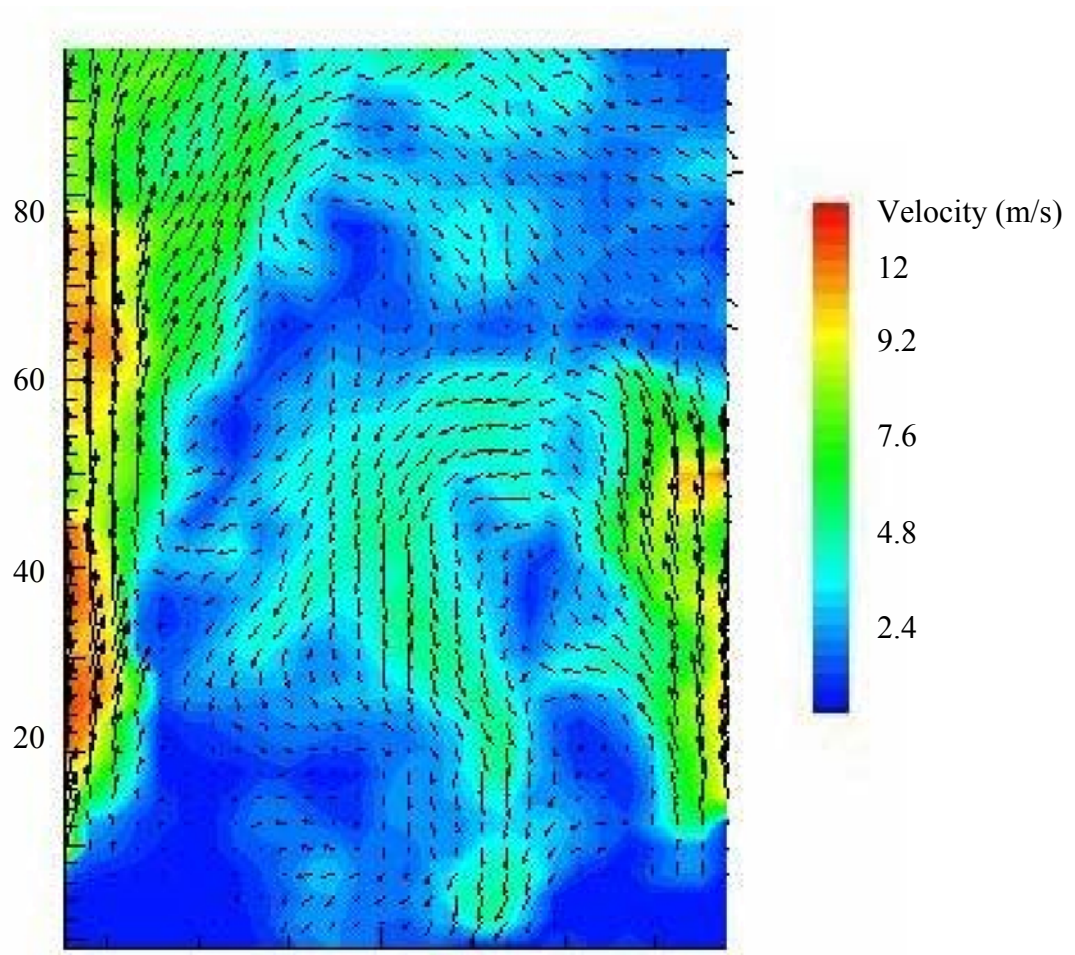
The recirculation zone of the rich product generator was characterized with a non-reacting flow field. The flow field was analyzed in both instantaneous and a time averaged cases. Tecplot v. 8.0 was utilized to conveniently manipulate and average the DPIV vector fields. The time averaged flow field in the combustor, shown in Figure 19, was a result of averaging 100 images taken at a rate of 1 Hz. The highest velocities were seen near the walls and were a result of the blockage of the bluff body. The results reveal an axis-symmetric flow with strong recirculation. The length of the recirculation zone was approximately one duct diameter. This is evident in the low velocity seen at  $x = 35$  mm and  $y = 80$  mm. Information about the flow close to the walls and the bluff body was lost due to the limitations caused by reflection and noise in the images. The limitations are evident near the lower region of Figure 19 where most of the velocities are close to zero.

**Figure 19 Time Averaged Flow Field of the Recirculation Zone of the Rich Product Generator Using DPIV Data**



The instantaneous flow field in Figure 20 shows the fluctuations in the flow. The flow velocity near the right wall of the duct at  $x$  of zero, dominates the recirculation zone compared to the left side of the duct at  $x = 75$ . The velocity vectors show that the right side flows from the right to the left wall and forces the air entering down and into the middle of the flow field. In contrast to the symmetric and well-behaved time averaged flow field, the instantaneous behavior features considerable irregularities.

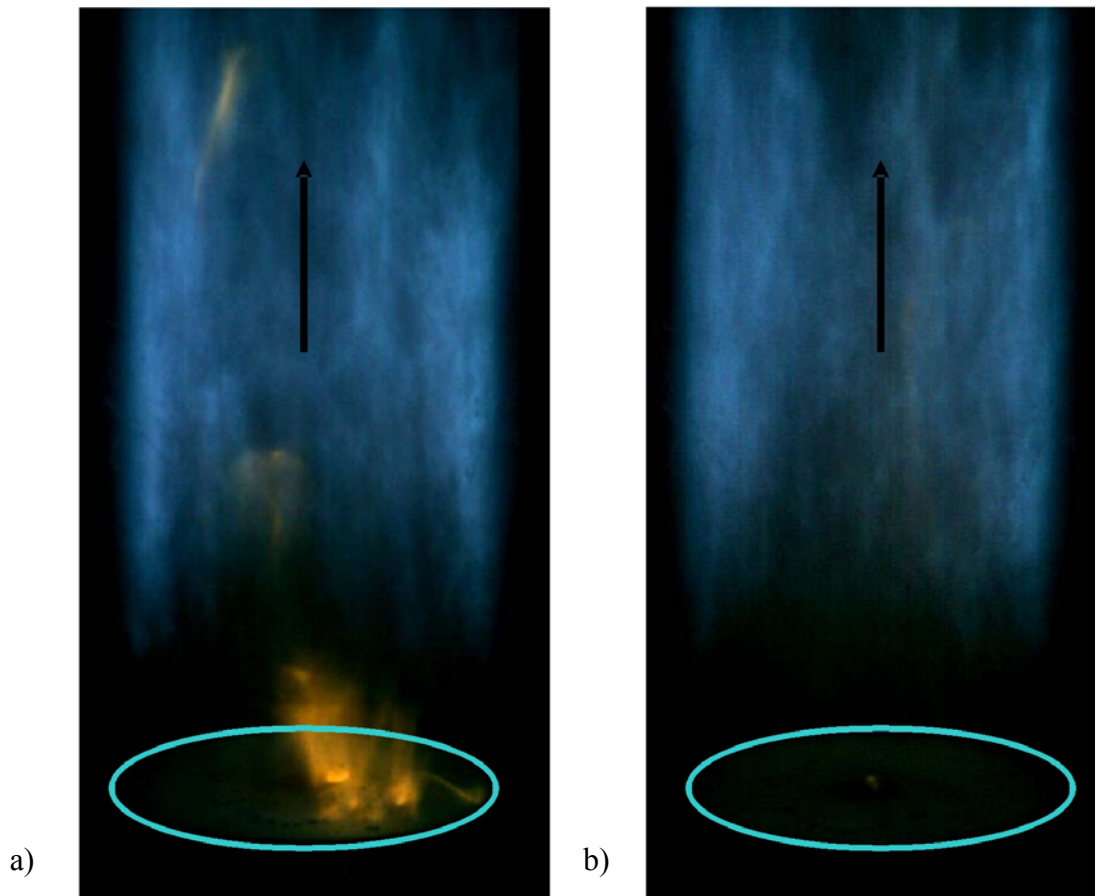
Figure 20 Instantaneous Flow Field in the Recirculation Zone of the Rich Product Generator Using DPIV



High speed (4000 fps) video images of the recirculation zone were recorded for an equivalence ratio of 1.66, which provided further insight into the flow field dynamics. The images showed that every 6-8 ms, disturbances in the reaction would occur. An example of the disturbances in the reacting flow field is shown in part a) and the undisturbed flow field is shown in part b) of Figure 21.

The disturbances were visualized as orange bursts and originated from the recirculation zone. The color blue denotes the flow of the rich products of combustion out of the recirculation zone. The burst created by turbulence and instantaneous variations in the flow field could be a result of a buildup of highly rich fuel pockets creating soot. The disturbances were much less prominent in the fuel lean case.

**Figure 21 High Speed Video Images a) Undisturbed Reacting Flow b) Burst from Face of Bluff Body**



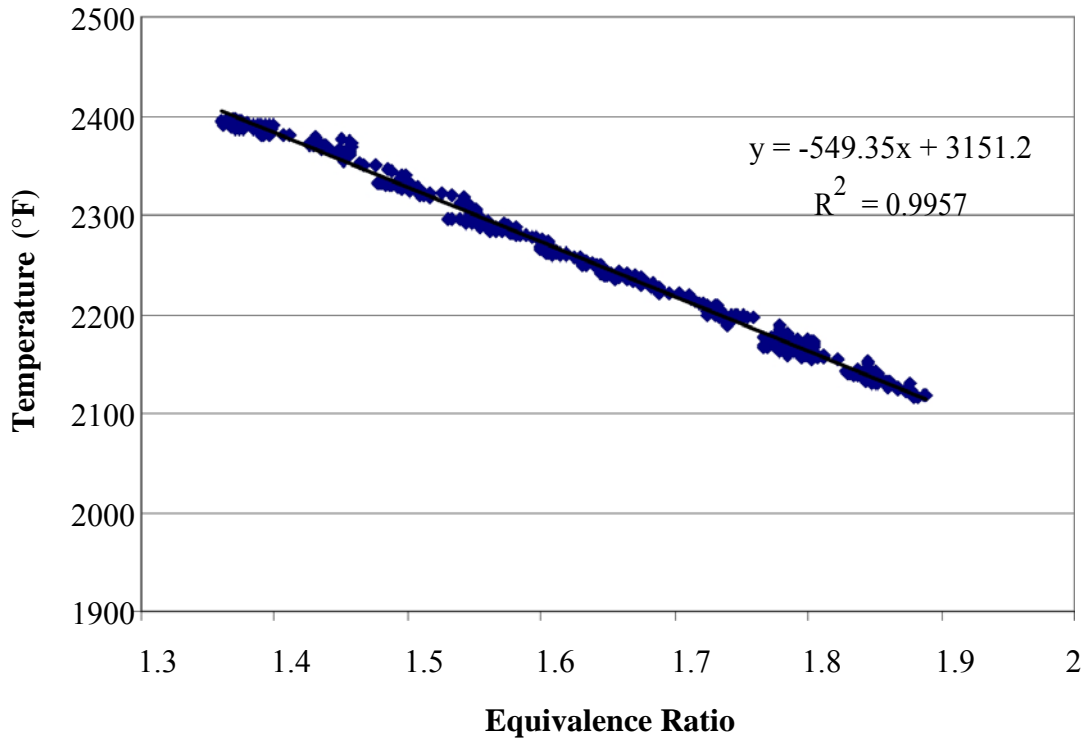
### *High Pressure Reaction Stability*

The reaction stability tests revealed that the combustor was stable at all expected test conditions. The higher preheat temperatures of the main air and the operating pressures of the combustor increased the stability limits of the combustor compared to atmospheric stability tests. Stability was verified up to an equivalence ratio of 2.3 for six different cases. Blow out of the rich reaction was beyond the fuel rich conditions reached during operation. The combustor was operated at the pressure of 1,3, and 6 atmospheres at main air pre-heat temperatures of 500°F (533 K) and 850°F (727 K). The fuel lean stability limits were not important in this phase of testing.

During the stability tests the reaction temperature was measured at the exit of the rich burn section with varying rich burn equivalence ratio. The two cases studied used natural gas as the fuel and varied the main air pre-heat temperature at a pressure of one atmosphere. For both cases the measured temperatures of the rich products entering the quick-mix section were more than 500°F (533 K) below the calculated adiabatic flame temperature for natural gas at the test conditions. For example, the temperature at an equivalence ratio of 1.66 and main air preheat of 500°F (533 K) is 3048°F (1676 K) and 3309°F (2094 K) at a preheat temperature of 850°F (727K). The temperatures measured at these same conditions were 2239°F (1499 K) and 2307°F (1537 K),

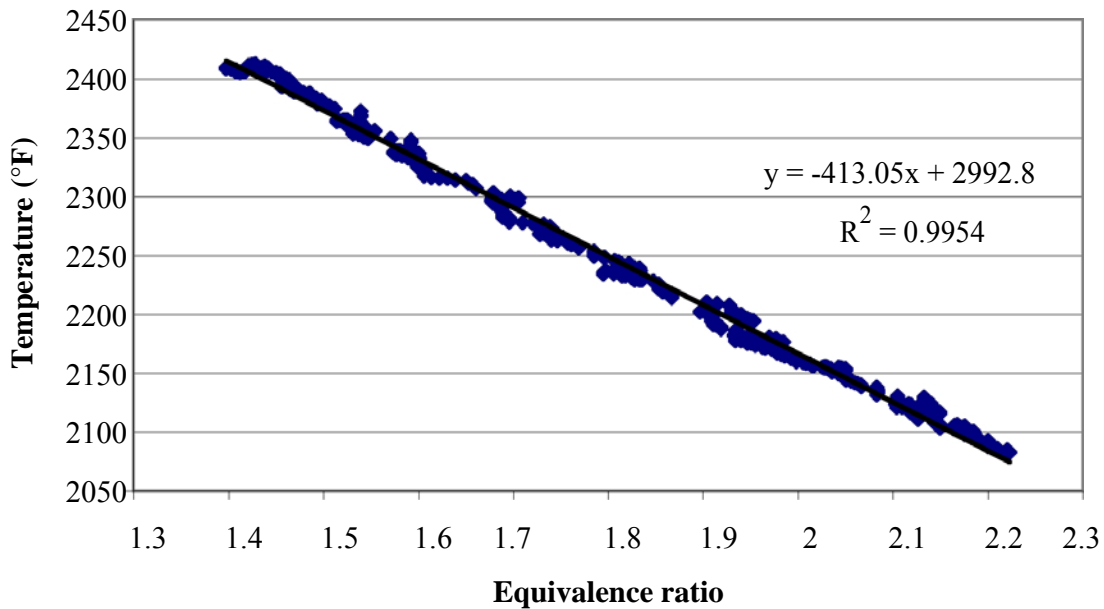
respectively. Substantial heat loss from the rich burn section to the water cooled walls could explain these temperatures, but it should be noted that adiabatic flame temperatures can only be achieved in ideal conditions that are difficult to simulate.

**Figure 22 Measured Temperature Entering the Quick-Mix Section at a Preheat Temperature of 500°F (533 K) and 1 atm.**



The temperature data from these tests were used during reacting mixing tests when the exotic molybdenum coated, high temperature, type C thermocouple used to monitor flame temperature did not function. The collected data have been plotted in Figure 22 and Figure 23. The results show a linear relationship between equivalence ratio and the measured temperature. Linear regression was used to acquire an equation to express the relationship. This equation was used during atmospheric mixing tests. The temperature entering the quick-mix section is needed in the instantaneous calculation of the jet-to-main momentum-flux ratio,  $J$ , which is calculated using equation 3.4. The temperature of the flow entering the combustor, the mass-flow ratio, and the effective area are the experimental operating conditions that can be varied to achieve a desired  $J$ . The rich burn equivalence ratio controls the temperature entering the quick-mix section and directly affects the  $J$  calculation. The jet air was not preheated during any of the reaction stability experiment. The mass-flow ratio and the effective area are coupled by equation 4.1. An increase in mass-flow ratio results in a higher flow rate entering the quick-mix section, which then increases the pressure drop across the jet holes.

Figure 23 Measured Temperature Entering the Quick-Mix Section at a Preheat Temperature of 850°F (727 K) and 1 atm.



### 3.1.2 Atmospheric Reacting Mixing Tests

The atmospheric reacting mixing tests were a significant milestone for the current high pressure RQL test facility. The results showed that the uniform and axis-symmetric species concentration is provided to the quick-mixing section. Emissions measurements were successfully gathered to characterize the quick-mix section. The results confirmed the observations of Vardakas (1999) in relation to main air preheat temperature effects on  $\text{NO}_x$ . The tests with natural gas produced lower  $\text{NO}_x$  and CO compared to propane.

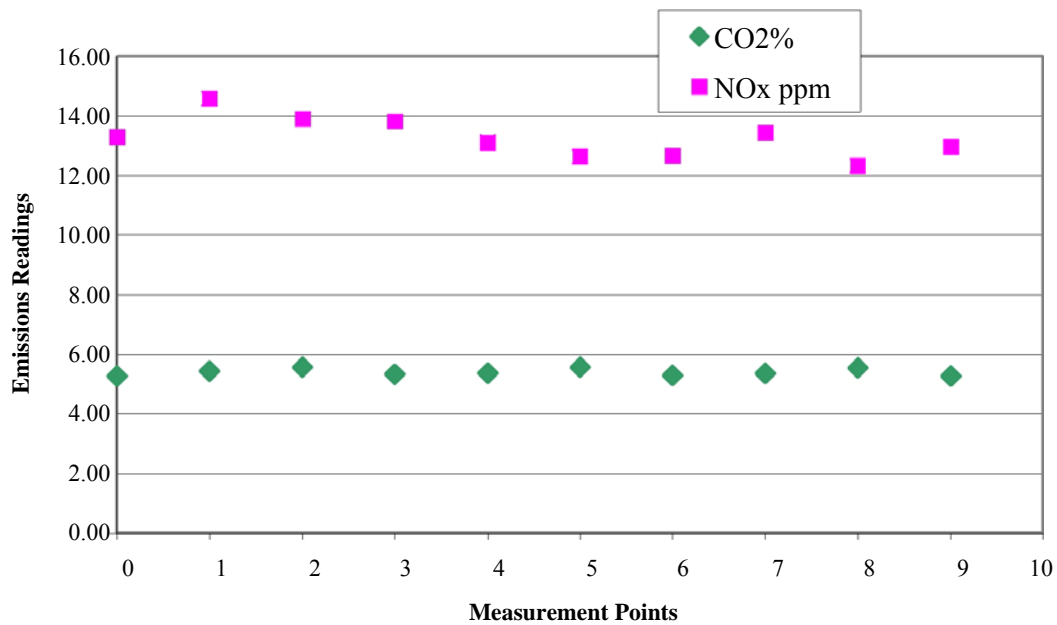
The results from the emissions measurements during the reacting mixing tests were used to compare 1) results from the high pressure facility to those obtained previously in the atmospheric facility, 2) natural gas and propane emission production, and 3) the effect of main air preheat on natural gas. The test conditions were the same as for Vardakas, et al. (1999): propane as the fuel, 500°F (533 K) main air preheat, one atmosphere, momentum-flux ratio of 57, and a 12 hole configuration for the quick-mix section. The same conditions were used in tests with natural gas, except a higher main air preheat case, 850°F (727 K), was included as well. The emissions recorded during tests were:  $\text{O}_2$ ,  $\text{CO}_2$ , CO, and  $\text{NO}_x$ . The operating conditions are summarized in Table 4.4.

#### *Experimental data of the rich products*

The data from the repeated atmospheric tests of Vardakas, et al. (1999) with propane were used not only for comparison, but to validate the characteristics of rich products entering the quick-mix section. The  $\text{NO}_x$  emissions in plane 1 were found to be axis-symmetric and uniform entering the quick-mix section in the propane and natural gas tests. The  $\text{CO}_2$  levels were uniform and axis-symmetric as well. The measured values for  $\text{NO}_x$  and  $\text{CO}_2$  in plane 1 for tests using propane are shown in Figure 24. The  $\text{CO}_2$  measured values were also uniform across the

plane and had a standard deviation across the plane of 2.2percent of the average measured value of CO<sub>2</sub>.

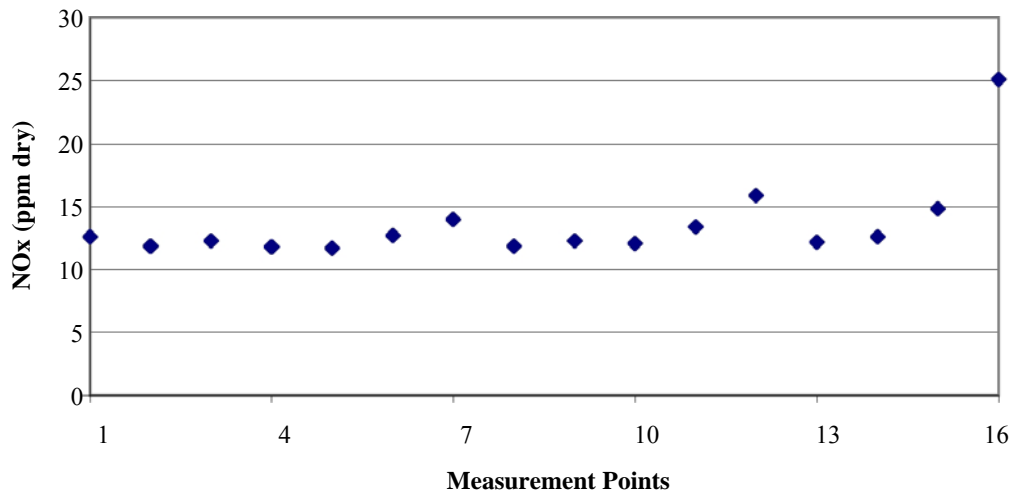
**Figure 24 Experimental Results of the Fuel Rich Products on Plane 1 (x/R=-1) for the Atmospheric Propane Test.**



The measured CO<sub>2</sub> and NO<sub>x</sub> data were corrected because the average O<sub>2</sub> level measured across the plane was 2.7percent, which, after further investigation was determined to be due to an insufficient flow through the sample line for the atmospheric test condition. The entrainment of air into the sample was because of the plumbing arrangement of the emissions analyzer. The O<sub>2</sub> level for rich conditions should be zero percent according to equilibrium calculations (Chemkin Equil) using GRI Mech 3.0, which show an expected concentration of 0.070 ppm. To use the data for their intended purpose, the CO<sub>2</sub> levels plotted were corrected to zero percent O<sub>2</sub>. Equilibrium calculations (Chemkin Equil) were used with the GRI Mech. 3.0 mechanism to compare CO<sub>2</sub> values. The corrected CO<sub>2</sub> value (4.88percent on a dry basis) was almost identical to the CO<sub>2</sub> values expected at the operating conditions of the experiment (4.89percent on a dry basis). Based on this analysis, the presence of dilution in the sampling system was affirmed and was corrected for and it showed that data could be still be used to evaluate the emissions readings and trends in the combustor.

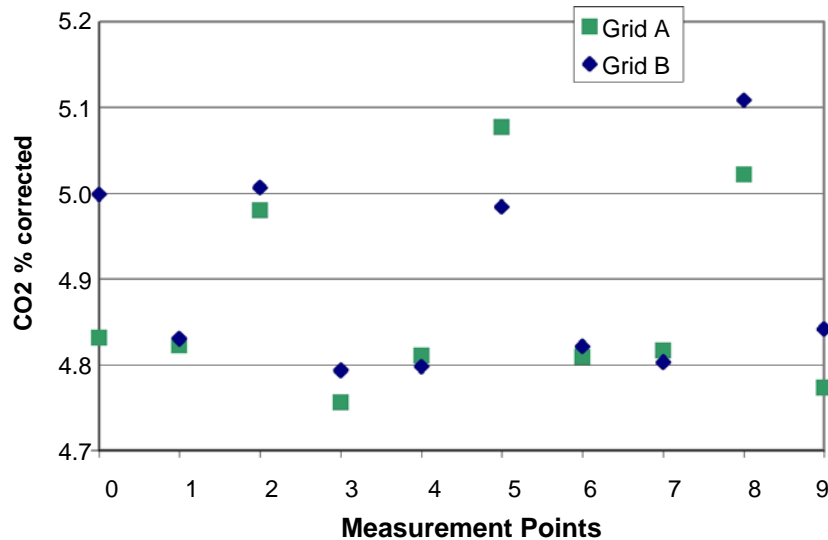
In terms of NO<sub>x</sub>, the NO<sub>x</sub> entering the quick-mix section were also similar in the current and previous atmospheric propane tests. The previous experimental data shown in Figure 25 had an average level of 13.28 ppm while the current experimental data had an average of 13.58 ppm, shown in Figure 24.

**Figure 25 Rich Products Entering the Quick-Mix Section from Vardakas, et al. (1999) at plane 1 ( $x/R=-1$ ).**



In addition to the propane data, data were obtained on plane 1 for tests at the same conditions but using natural gas as the fuel. The data in Figure 26 show very good repeatability. The data once again have a low standard deviation of 2.3percent across the plane.

**Figure 26 Repeated Measurements of Data on Plane 1 ( $x/R=-1$ ) During Atmospheric Natural Gas Tests**



These results coupled with the fact that the emissions probe's spokes by themselves allow an axis-symmetric comparison of data because they are 120 degrees apart, validates that the rich burn products are uniform and axis-symmetric before entering the quick-mix section of the rich burn products. The NO<sub>x</sub> data from the current study in the rich products have an uncertainty of 6percent at each point. The data were taken for over 60 seconds at each point. The CO, CO<sub>2</sub>, and O<sub>2</sub> had an average uncertainty of less than 1percent.

### *Mixing experiments with propane*

Planar measurements of NO<sub>x</sub> for the present and prior study of Vardakas, et al. (1999) are shown in Figure 27. The low regions of NO<sub>x</sub> correspond to the region that jets have penetrated into and started to mix. Although the effect of jet penetration is much more evident at the trailing edge of the jet holes, the plane one duct radii (plane 4,  $x/R=1$ ) can show overall mixing trends. The influence of the jet wakes near the walls is evident in plane 4 for both sets of data, starting at 30 mm radius. The high residence times and equivalence ratios in the wakes increases NO<sub>x</sub> production. The low NO<sub>x</sub> levels seen at 25 mm radius correspond with the jet penetration region. Near optimum penetration is evident for a J of 57 with 12 holes. This validated by calculating constant C in equation 3.5. The calculated value was between 2.7 and 2.8 for this test, 2.5 being the optimum value. The jet penetration regions in the previous and current experiments were different. The jet penetration region started at  $2/3R$  (27 mm) duct radius from the centerline compared to the current experiment, at 25 mm. The significant difference was that the previous data had a narrow low NO<sub>x</sub> band from 20-27 mm, where as the low NO<sub>x</sub> band in the current data extends from the centerline to about 25 mm radius. In addition, the centerline of the previous data shows a decrease in NO<sub>x</sub>, meaning the jets have not mixed to the core of the combustor. The difference in jet penetration and overall mixing could be shown by the difference in mixing closer to the core of the combustor, the lower level of NO<sub>x</sub> near the  $1/3R$  (13mm) duct radius, and the additional data points.

The area averaged planar NO<sub>x</sub> emission from plane 4 of the previous atmospheric RQL experimental combustor was 24.9 ppm (dry basis). The NO<sub>x</sub> emissions for the current experiment were 19.2 ppm (dry uncorrected) using the points 0, 1, 4, and 9. As mentioned previously, the current measurement locations include 9 radii compared to three radial locations used in the past experiment. The area- weighted average using the nine radial measurement locations was 17.7 ppm, 8percent lower than the measurements based on only three radii. The two methods do not differ drastically in planar averages and can be used in analyzing trends in the data. Yet, having more measurements did provide higher accuracy in the results, much greater resolution, and more information for developing planar contour plots. This is evident in the added resolution in the current data between the radii of 10 and 30 mm. In the previous data from Vardakas, et al. (1999) there is a lot of information lost in the same region, which could help explain the high CO and NO<sub>x</sub> near the core of the combustor.

The contour plots were made with Golden Software Surfer 8. Surfer 8 is a program that can be used to make 2-D and 3-D contour plots. The contour plots were generated from a data grid using the Kriging method (Golden Software, 2002). The uncertainty in J and MR were less than 5percent and were mostly due to fluctuations in the air flow rates caused by the facility's air compressors. The NO<sub>x</sub> data standard deviation was less than 5percent and the CO standard deviation was 1percent, while the O<sub>2</sub> and CO<sub>2</sub> standard deviation were less than 2percent.

Figure 27 NO<sub>x</sub> Levels at Plane 4 (x/R=1) for a) Prior and b) Current Experiments at a J of 57 and MR of 2.5.

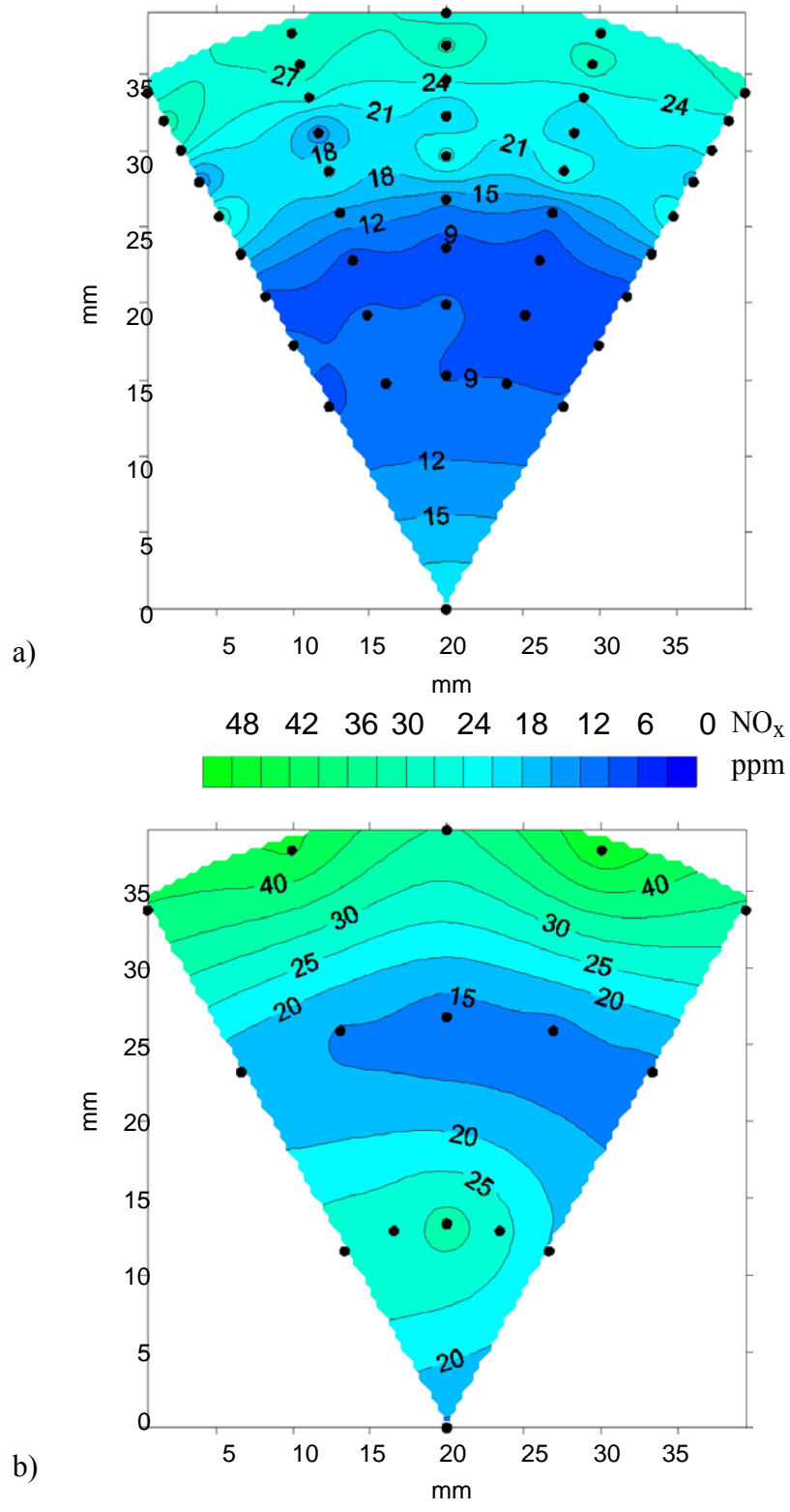
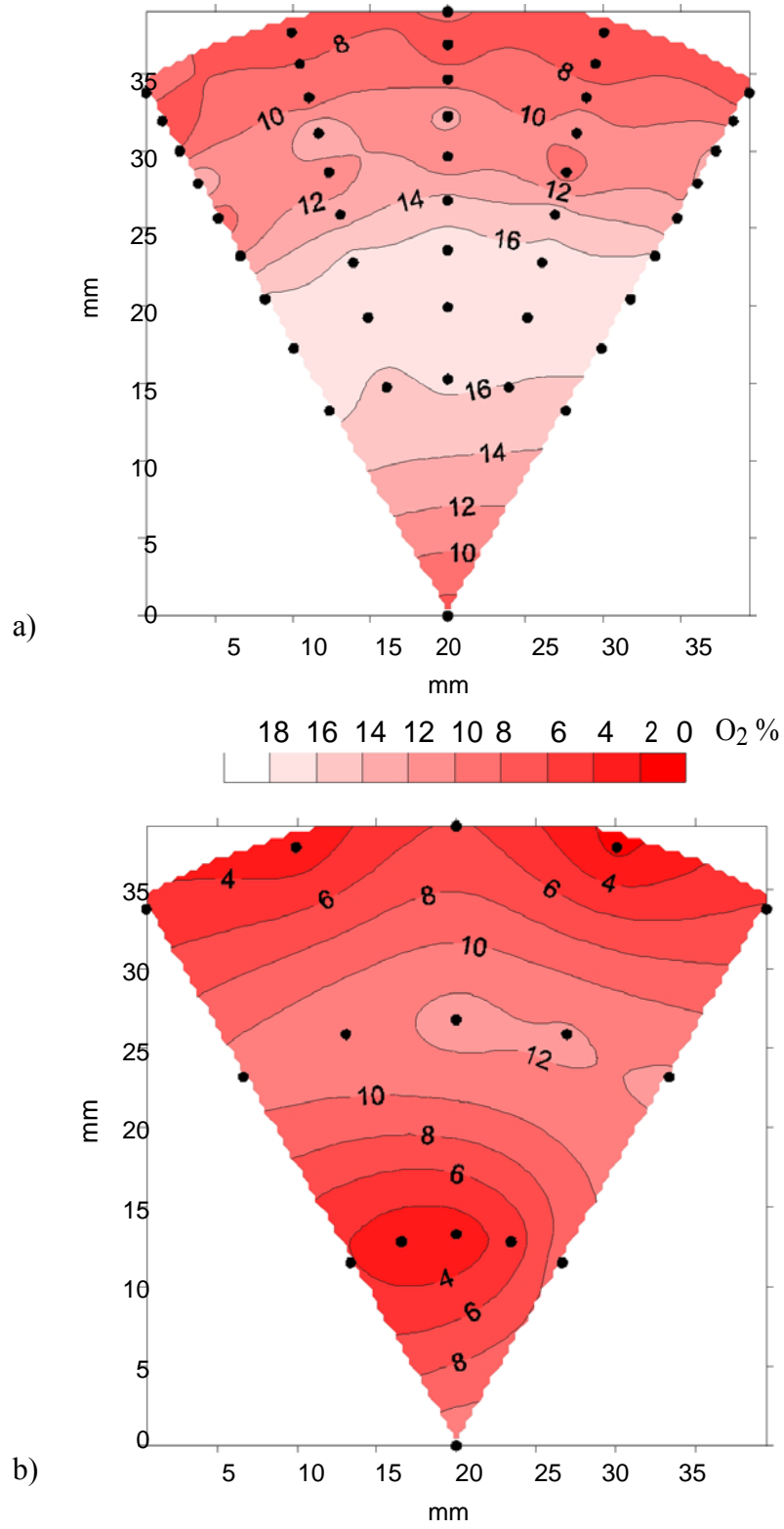


Figure 28 O<sub>2</sub> Levels at Plane 4 (x/R=1) for a) Prior and b) Current Experiments at a J of 57 and MR of 2.5.



The O<sub>2</sub> percent data showed similar trends in both the current and previous contour plots in Figure 28. In the current data the high O<sub>2</sub> band corresponds to the same region, 10 to 30 mm duct radii. The jet streams have dispersed throughout the plane, as was evident in the NO<sub>x</sub> data. The walls and the core exhibit the lowest levels of O<sub>2</sub>, also similar to the NO<sub>x</sub> data. The previous O<sub>2</sub> contour plot also shows similar jet mixing trends. A major point of difference again is the extremely low level of O<sub>2</sub> at 1/3R radius. At this same point, there is a corresponding high level of NO<sub>x</sub>. This suggests that the O<sub>2</sub> from the jet is creating a highly reactive boundary with the rich products at the core of the combustor. The high levels of NO<sub>x</sub> are attributed to thermal NO<sub>x</sub> formation from the high temperature produced in by the reaction of the rich product and the jet air. The average O<sub>2</sub> percent in Vardakas, et al. (1999) data was 8.02 and 12.1 in the current experiment. This difference could be a result of having additional data points in each plane.

The area-weighted averaged CO from the past atmospheric study was 20,000 ppm (2.00 percent) compared to 4774 ppm for the present work (Vardakas, 1999). The highest CO readings in the prior data were at the centerline and the R/3 radial measurement locations; this can be seen in Figure 29. This suggests that by plane 4 the jet had not reached the core of the combustor. High gradients and the white regions of low CO show that the jet penetration levels can still be discerned. In the current study, the jet mixing reached close to the centerline by plane 4, as suggested by the discussions of Figure 27 and Figure 28, and were more evenly distributed from the walls to a radius of 15 mm, near the core of the combustor. The more reactive quick-mix section can explain the substantial difference in CO. The reaction was closer to completion since NO<sub>x</sub> levels were similar but the level of mixing to core was different. The rich products entering the quick-mix section are expected to have CO levels above 100,000 ppm. The 75,000 ppm level revealed in Figure 29 supports the claim that the jets had not fully mixed near the core of the combustor since 75 percent of the CO had not yet been oxidized. The high level of CO supports the conclusion a highly reactive, near-stoichiometric region is present with high levels NO<sub>x</sub> and low levels of O<sub>2</sub> where the rich products are initially mixing and reacting with the jet air. Additionally, more data points would have provided valuable information for a better understanding and comparison of the repeated experiments.

The NO<sub>x</sub> data in the mixing tests were corrected to account for a leak in the sampling system. The method for correcting the data in planes 4 and 5 were based on the O<sub>2</sub> percent measured in the plane 1 data. The percentage of the sample that was from the entrained air was calculated by assuming the amount sampled by the emissions monitoring systems was constant. An O<sub>2</sub> mass balance for plane 1 (fuel rich case) provided enough information to calculate the amount of air added to the sample. The mass balance showed that on average 14 percent of the total sample was from entrained air. This information was used to correct the data in planes 4 and 5. Every measured point was corrected with a species mass balance. The corrected NO<sub>x</sub>, CO, CO<sub>2</sub>, and O<sub>2</sub> data from each plane are shown in Table 4.

Figure 29 CO Levels at Plane 4 ( $x/R=1$ ) for a) Prior and b) Current Experiments

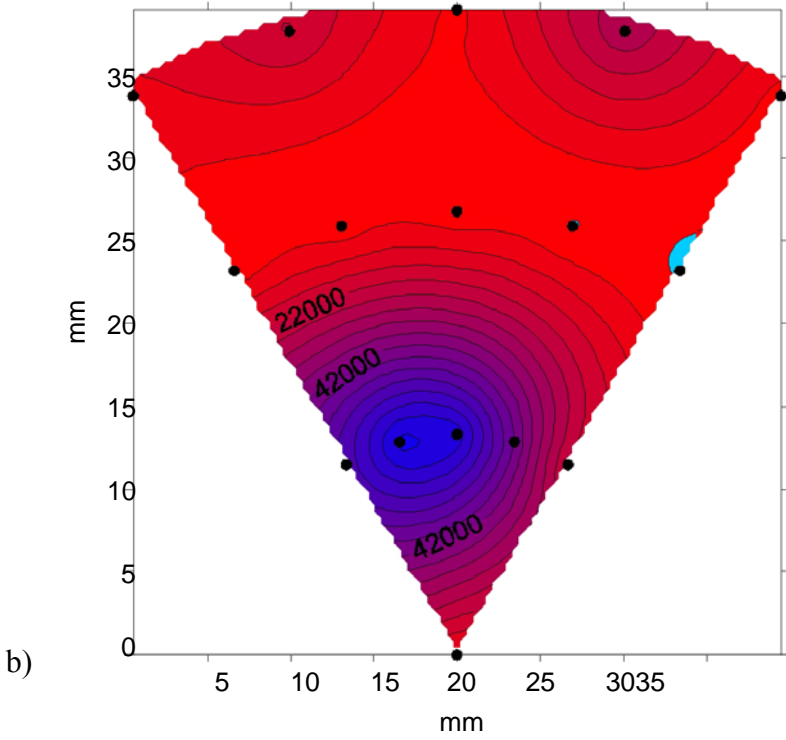
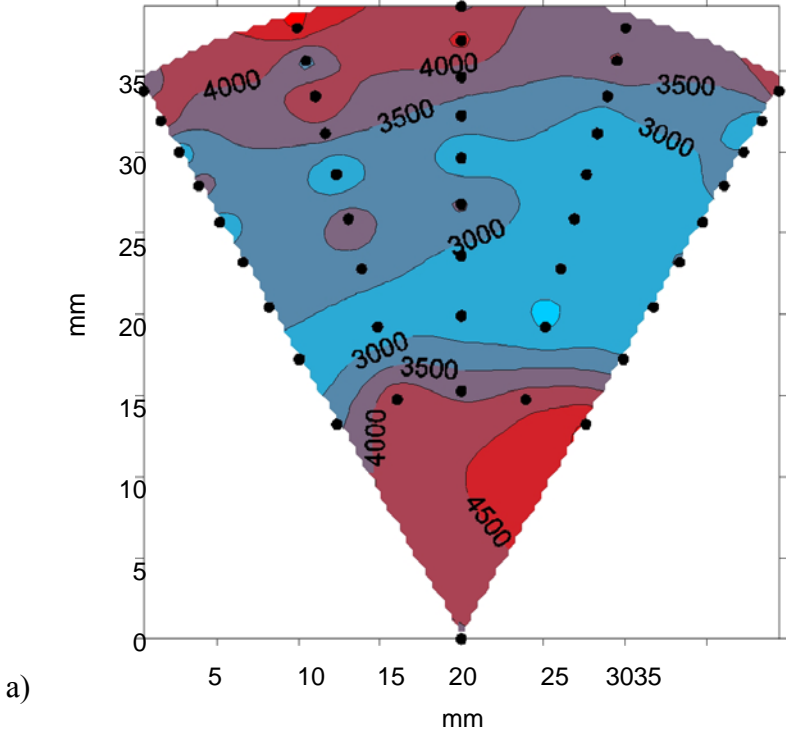


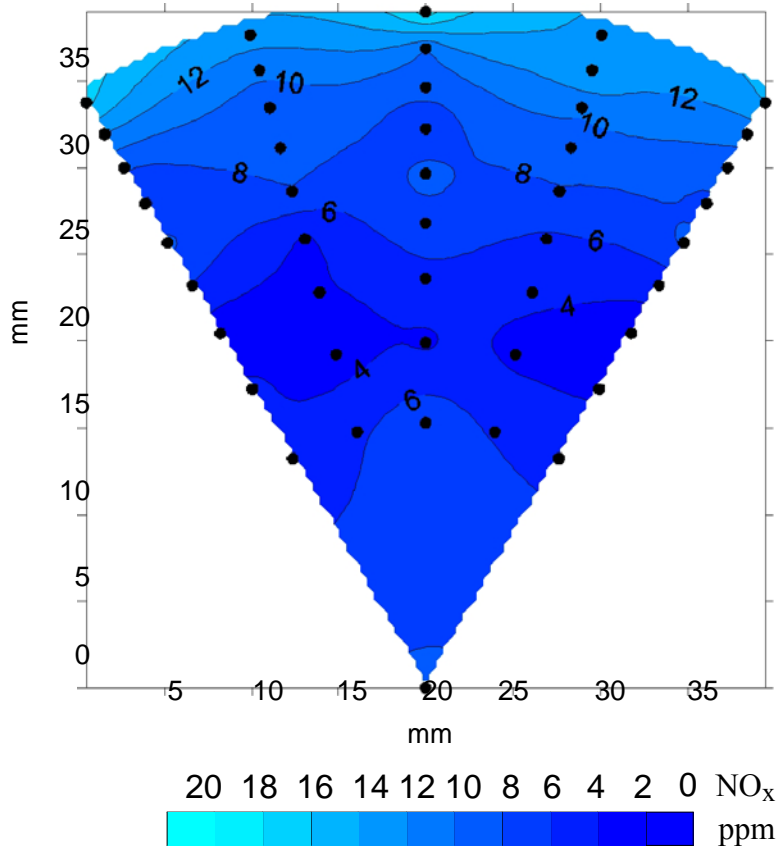
**Table 4 Planar Area Averaged Values from the Atmospheric Propane Test at J of 57 and MR of 2.5.**

Plane	NO <sub>x</sub> (ppm)	CO (ppm)	O <sub>2</sub> %	CO <sub>2</sub> %
1	13.3	-	0.0	5.41
4	17.7	4094	12.1	5.02
5	18.7	2871	12.1	5.20

*Mixing experiments with natural gas*

The atmospheric natural gas tests were completed at the same conditions that were used in the atmospheric propane tests. The mixing behavior was similar but the NO<sub>x</sub> levels with natural gas were much lower as can be seen in Figure 30. The mixture is uniform until a radius of 30 mm when the NO<sub>x</sub> levels rise abruptly. The NO<sub>x</sub> reaches its highest levels near the walls of the quick-mix section again.

**Figure 30 Plane 4 (x/R=1) Contour Plot for the Natural Gas Atmospheric Tests at a J of 57 and MR of 2.5.**



The propane emissions proved to be higher in both the rich and overall NO<sub>x</sub> production. The higher NO<sub>x</sub> was not surprising since equilibrium calculations predict NO<sub>x</sub> to be higher for propane. For RQL based stationary and aerospace engines, the use of natural gas is better option, in terms of NO<sub>x</sub> emissions, than propane. The NO<sub>x</sub> standard deviation was less than 5percent and the CO uncertainty was less than 2percent. In addition the constant C in equation 2.5 was between 2.7 and 2.8 for the natural gas test.

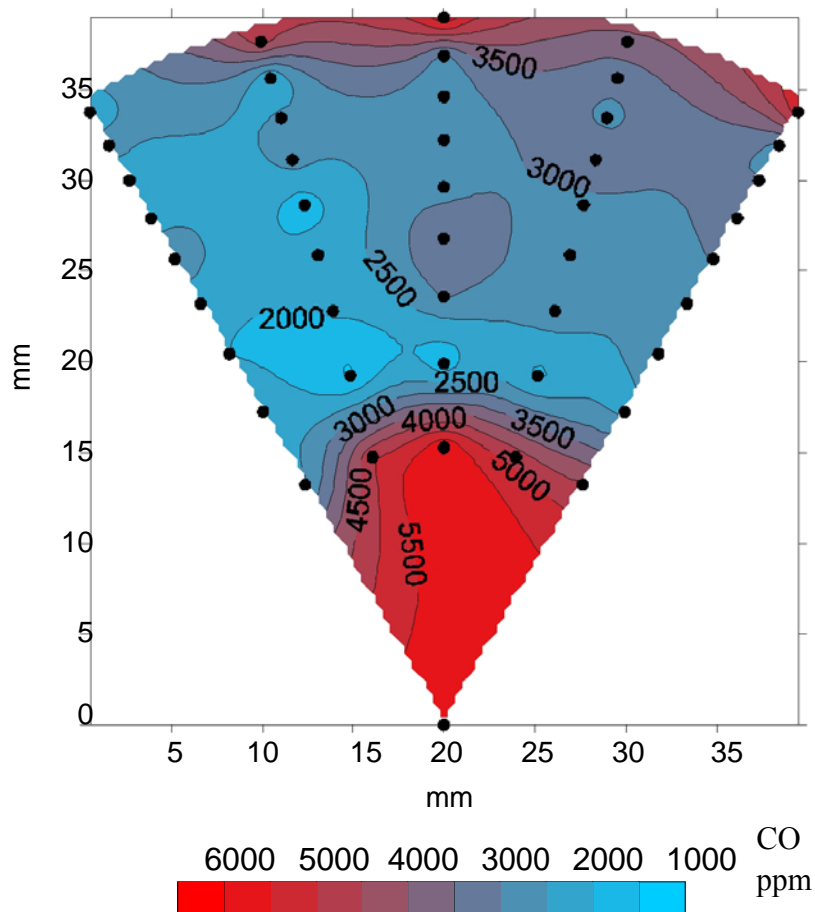
The area averaged  $\text{NO}_x$  measured on plane 1 and 4 were 2.45 ppm and 7.91 ppm, respectively. By plane 5 the  $\text{NO}_x$  increased to 10.4 ppm, proving that taking additional data on this plane is important. The reaction is closer to completion at plane 5 compared to plane 4. Table 5 summarizes the planar area averaged measurements taken during these tests.

**Table 5 Planar Area Averaged Values from the Atmospheric Natural Gas Test at a J of 57 and MR of 2.5.**

Plane	$\text{NO}_x$ (ppm)	CO (ppm)	$\text{O}_2\%$	$\text{CO}_2\%$
1	2.45	-	0.0	4.89
4	7.91	3267	14.7	3.18
5	10.4	2588	12.9	4.31

The CO emissions in the natural gas test were also lower than the propane test. The CO levels in both planes 4 and 5 show evidence of this. The plane 4 area-averaged CO emissions level was 3267 ppm for the natural gas and 4094 ppm for the propane. The contour plot in Figure 31 shows that the centerline to the first data point at 15.3 mm has the highest levels of CO. By plane 5 more of the CO is oxidized as the jet mixing continues to become more uniform.

**Figure 31 Plane 4 (X/R=1) Contour Plot for the Natural Gas Atmospheric Tests**



### *Elevated Temperature Mixing Experiments With Natural Gas*

The experiment with natural gas discussed in the previous section was duplicated but with the main air preheated to 850°F (727 K). As the results in Table 6 show, the main air preheat caused the NO<sub>x</sub> level to increase to 5.40 ppm in the rich products compared to 2.45 ppm in the 500°F (533 K) preheat case. In plane 5, NO<sub>x</sub> levels rose from 10.4 ppm to 16.4 ppm. The results in Figure 32 show that the preheat temperature of the main air did in fact increase the NO<sub>x</sub> output of the combustor. Hence, these results verify the conclusions drawn by Vardakas, et al., (1999). The NO<sub>x</sub> data measured had a standard deviation of less than 5percent and the CO standard deviation was less than 2percent. To maintain the same mixing characteristics, the constant C in equation 2.5 for this experiment was between 2.7 and 2.8 as well.

In terms of CO emissions, the higher main air preheat temperature actually caused a decrease in CO. The plane 5 CO emissions dropped from 2588 to 2431ppm. In the contour plots in Figure 33, the highest levels of CO are near the walls and the core of the combustor. For the 500°F (533 K) preheat case, the high levels of CO found near the core of the combustor in plane 4 have decreased as the reaction continued to oxidize CO to the levels found in plane 5.

Figure 32 Plane 5 ( $x/R=2$ )  $\text{NO}_x$  Data from the Atmospheric Natural Gas Tests at Different Main Air Preheat Temperatures a) 500°F (533 K) and b) 850°F (727 K).

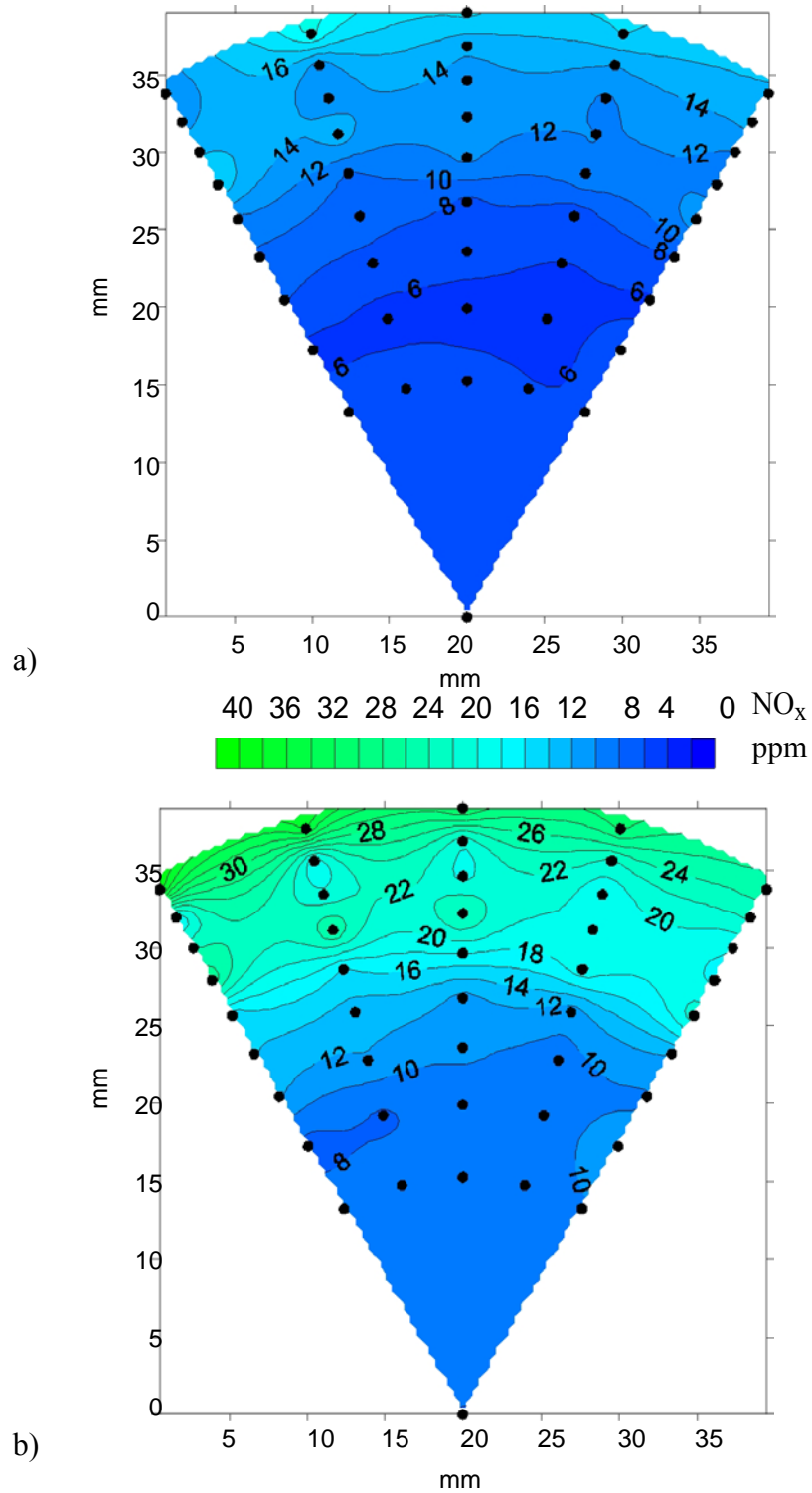
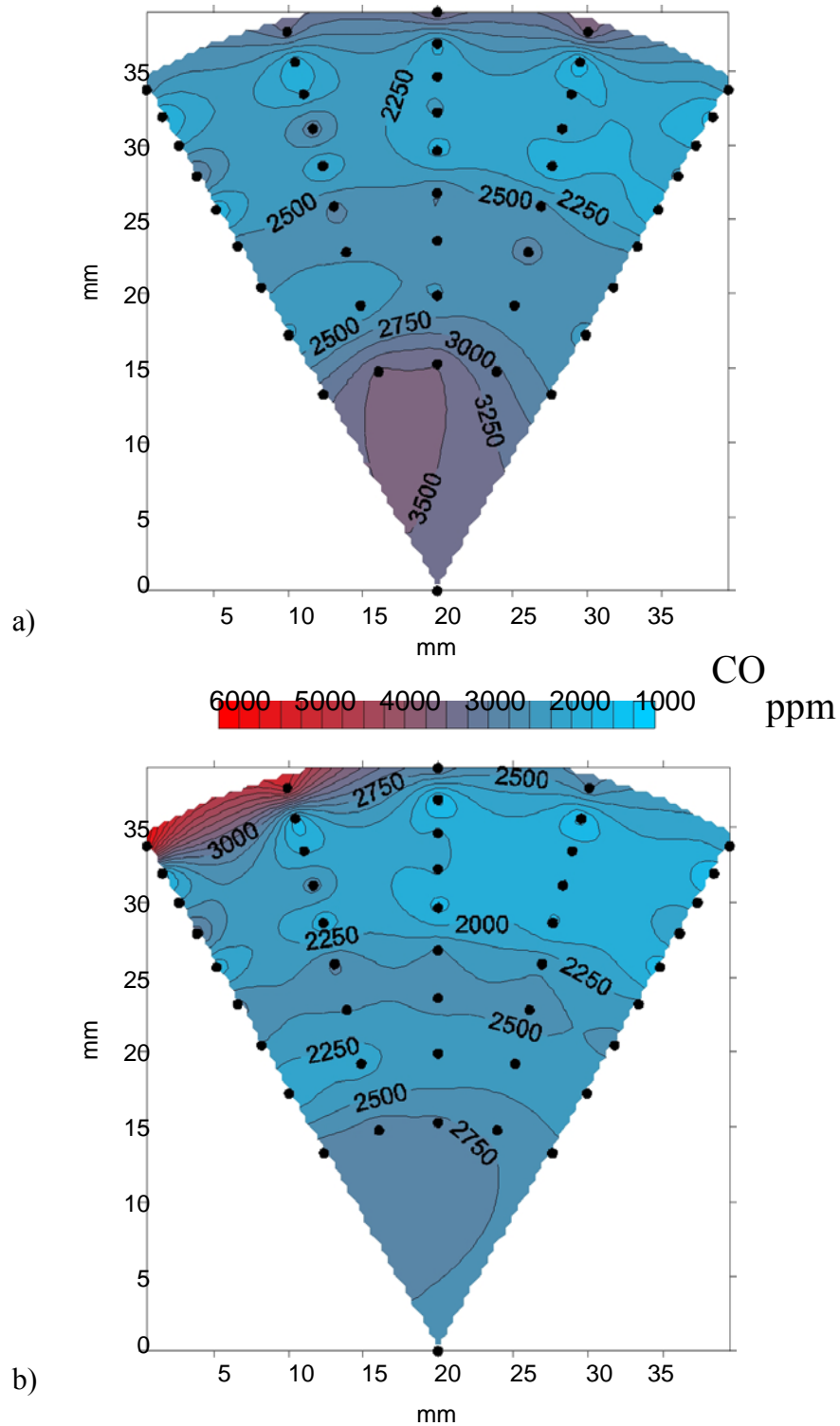


Figure 33 Plane 5 ( $x/R=2$ ) CO Data from the Atmospheric Natural Gas Tests at Different Main Air Preheat Temperatures a) 500°F (533 K) and b) 850°F (727 K).



But the highest levels CO are still found near the core of the combustor. In the 850°F (727 K) case, the higher preheat temperature improved the uniformity of CO by reducing the high CO levels near the core of the combustor. In the 850°F (727 K) case, some residual effects of the jet wakes did cause high levels of CO near the walls.

**Table 6 Planar area averaged values for the atmospheric natural gas test with elevated main air preheat temperature.**

<b>Plane</b>	<b>NO<sub>x</sub> (ppm)</b>	<b>CO (ppm)</b>	<b>O<sub>2</sub>%</b>	<b>CO<sub>2</sub>%</b>
1	5.40	-	0.0	5.40
5	16.4	2431	13.0	4.24

### **3.1.3 RQL Kinetics Model**

A chemical kinetics model of the RQL combustion concept was developed to gain insight into the effects of pressure, residence time, and preheat temperatures on NO<sub>x</sub> and CO. An increase in pressure reduced the level of NO<sub>x</sub> in the fuel rich PSRs. A decrease in residence time decreased overall NO<sub>x</sub> production but did not affect the initial fuel rich PSR. An increase in jet and main air preheat temperature increased NO<sub>x</sub>. The opposite effects were seen with CO.

The chemical kinetics model was developed using Chemkin V. 4.0. The chemical kinetics mechanism used was GRI Mech. 3.0. The reaction was assumed to be at a steady state and constant pressure in a perfectly stirred reactor, PSR. A series of reactors were used to model the rich burn and the subsequent mixing of the quick-mix air. The rich reaction was modeled with one PSR. The jet mixing was modeled with eight PSRs in series that moved the initial rich reaction to the final fuel lean equivalence ratio. A schematic of the modeling approach is presented in Figure 34.

The factors that were varied in the cases modeled were: residence time (both rich and quick-mix reactors), preheat temperatures (both air and fuel in the rich and quick-mix air), pressure, and the number of PSRs. The baseline case for the rich air flow preheated to 533 K (500°F), the fuel to 298 K (77°F), and was run at one atmosphere. The jet air inlets in the baseline case were non-preheated.

**Figure 34 Schematic of Kinetics Modeling Approach.**

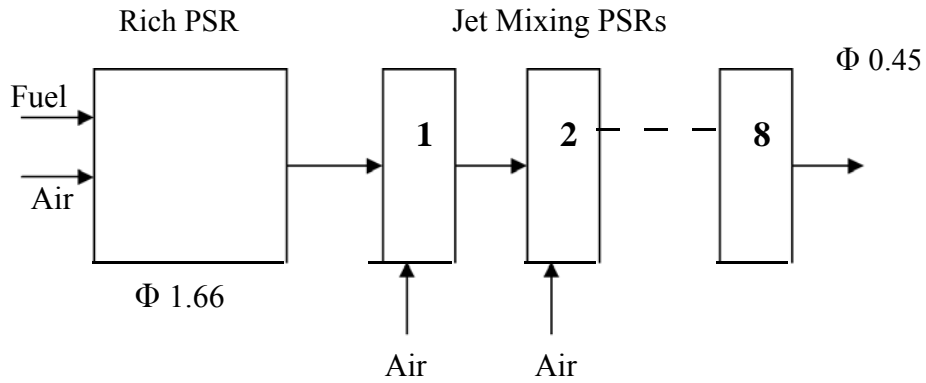
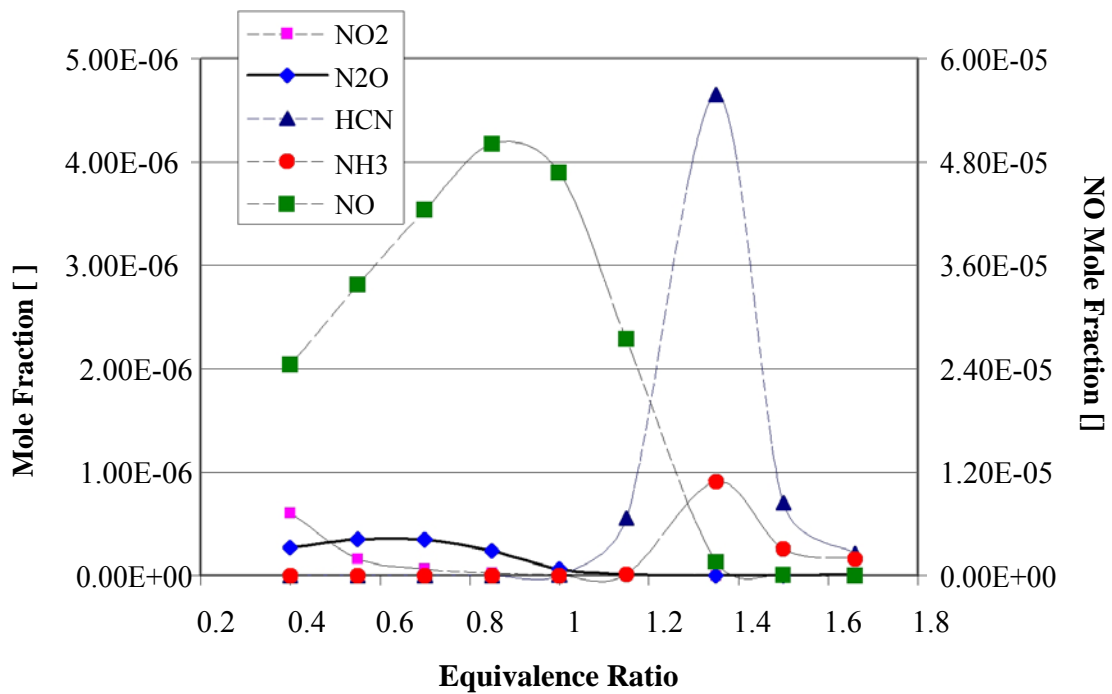


**Figure 35 TFN Species in Each PSR for the RQL Kinetics Model as a Function of Equivalence Ratio.**



and N<sub>2</sub>O increases to levels close to one ppm. By the last PSR, the 9<sup>th</sup> one, the equivalence ratio is 0.40 and the TFN levels are close in each of three cases with varying initial rich reaction residence time. The TFN levels from lowest to highest residence time are: 25.3, 25.6, 25.7 ppm as shown in Table 7. The modeling results were initially outputted as “wet” values, including the H<sub>2</sub>O species, but when comparisons were made to the experimental results, the modeling results were converted to “dry” basis by excluding H<sub>2</sub>O. The following equation describes the conversion method:

$$\frac{[\text{"wet" "concentration"}]}{1 - [\text{H}_2\text{O concentration}]} = [\text{"dry" "concentration"}] \quad (5.2).$$

**Table 7 Rich Burn Residence Time Effect on Overall TFN and NO<sub>x</sub>**

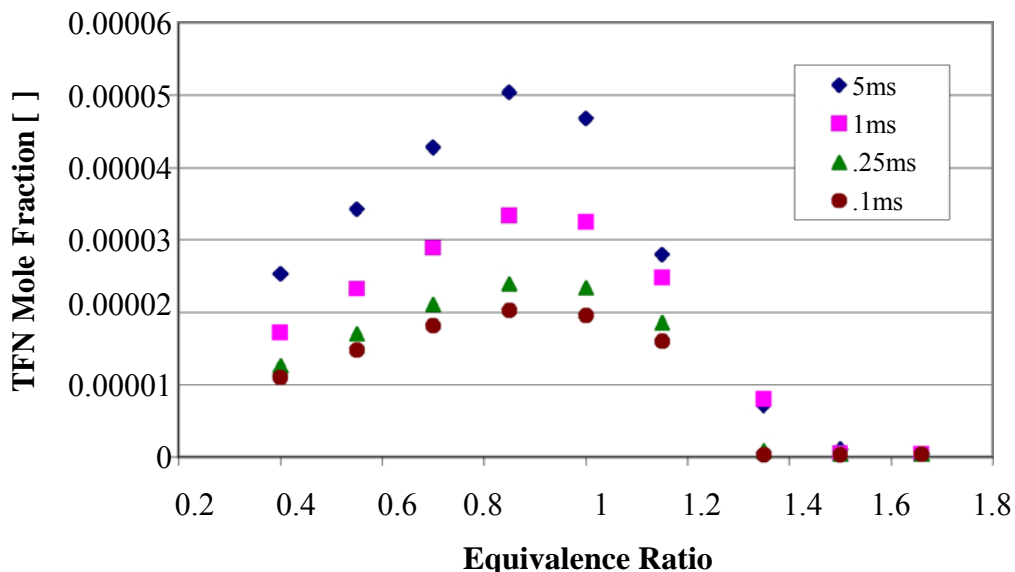
Rich Residence Time (ms)	Overall TFN (ppm)	NO <sub>x</sub> (ppm)
50	25.3	25.0
75	25.6	25.3
100	25.7	25.5

The results show that as long as the initial rich reaction has a large residence time and the equivalence ratio is at or near the TFN minima, the final output of TFN in the RQL combustor is not highly dependent on the rich residence time. If the fuel rich equivalence ratio is at or near a phi of 1.4 then the risk of producing high levels of NO<sub>x</sub> is higher because the large levels of TFN entering the jet mixing section would be converted to NO<sub>x</sub>. Also, the residence time of the rich section is dependent on the length of the rich section. By reducing the length in the rich burn section and maintaining low NO<sub>x</sub> output the cost of manufacturing an RQL combustor could be reduced.

### *Jet Mixing*

The jet air PSRs used to simulate the quick-mixing of the rich burn products from the first PSR were run at 0.1, 0.25, 1, and 5 ms. The sum of the residence time in each of the jet mixing PSRs is the total mixing time for the quick -mix section for each case. In terms of the four different residence times mentioned above, the total mixing times are 0.8, 2, 8, and 40 ms. Based on experimental conditions the estimated quick-mix residence time is on the order of 5 ms. The NO<sub>x</sub> levels seen for the 40 ms and 80 ms are not realistic for practical operations. The cases modeled, presented in Figure 5.20, showed that the quick-mixing residence time is major driver for the final output of TFN. The 2ms case outputs 12.6 ppm of TFN, where as the 8 ms case outputs 17.2 ppm, a 37percent increase. These results are close to the experimental results. The results from these models reiterate the importance of mixing quickly and its significance in meeting emission requirements in a stationary gas turbine application. Also, note that as the residence time is lowered, the model gets closer to an ideal instantaneous mixing case. If only one jet mixing PSR with the same overall mixing residence time was used in the model, the TFN level is 0.74 ppm.

Figure 36 TFN Output Versus Jet Mixing PSR Residence Times



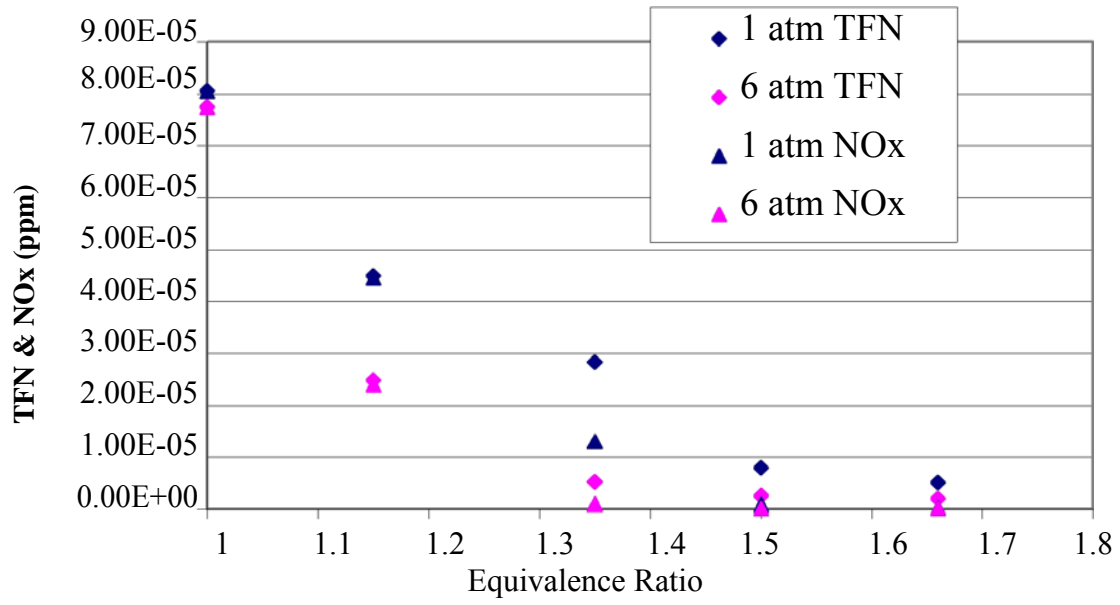
*Pressure Effects*

The same conditions used in the baseline case were run at six atmospheres and using the same method as the atmospheric models. The results in Figure 5.21 show that TFN and NO<sub>x</sub> levels decrease at elevated pressures. High levels of TFN and NO<sub>x</sub> are formed in the fuel rich PSRs at both pressure conditions. The species data in Table 8 show that at elevated pressure the concentrations of H<sub>2</sub>, HCN, NH<sub>3</sub>, and NO decrease and while N<sub>2</sub> rises. The species concentration change suggests that the rate limiting steps of the thermal and prompt NO mechanisms are inhibited at elevated pressures. Elevated pressure emissions measurements and a sensitivity analysis of the results would provide more insight into the reactions occurring in the jet mixing reactions.

**Table 8 Species concentration at atmospheric and elevated pressures for an equivalence ratio of 1.66.**

Pressure	H <sub>2</sub> %	HCN (ppm)	NH <sub>3</sub> (ppm)	NO (ppm)	N <sub>2</sub> %
1 atm	7.42	2.91	1.98	0.191	61.7
6 atm	6.58	0.863	1.09	0.043	62.2

Figure 37 Effects of Elevated Pressure on NO<sub>x</sub> and TFN in the Fuel Rich PSRs.

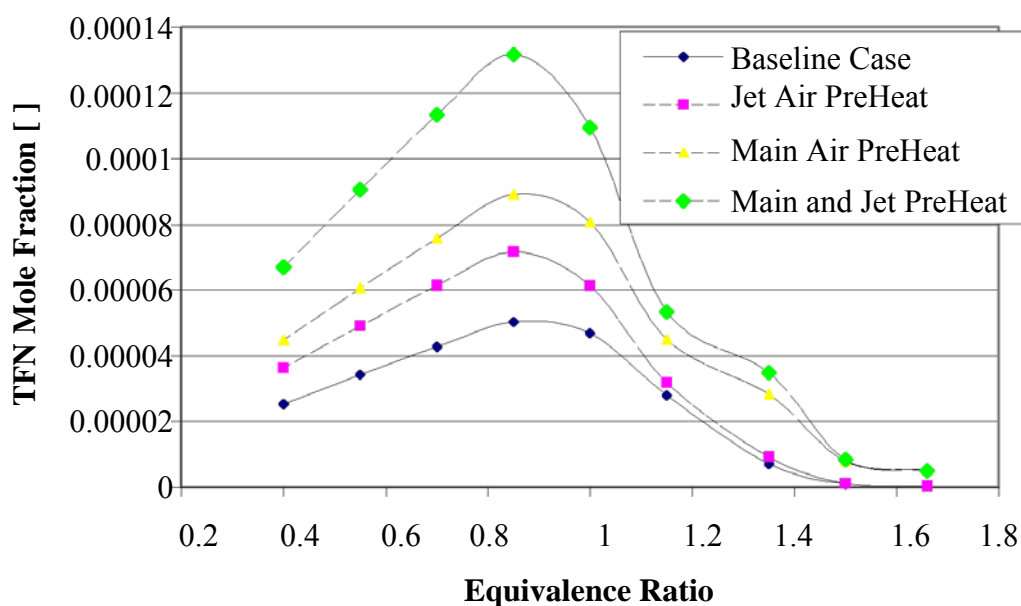


## Preheat Temperature Effects

The preheat temperature effects were also studied in a kinetics model in three different preheating cases, excluding the baseline case described in the kinetics modeling section. The baseline case has the main air preheated to 533 K and the jet air non-preheated. After the rich PSR, a series of eight PSRs were used to model the jet mixing from the initial rich stage to the final fuel stage. The three cases modeled were at a preheat temperature entering the first PSR at 727 K (850°F), preheat of the subsequent jet air in the next eight PSRs at 533 K (500°F), and the combination of both the preheat cases aforementioned. The results in Figure 5.22 showed that the main air preheat temperature had a significant impact on initial and overall TFN (and  $\text{NO}_x$ ) production, as the experimental results also showed. The jet air preheat temperature also increased the TFN production.

These results in terms of jet air preheat temperature are different than the experimental results of Vardakas, et al. (1999). Vardakas concluded that the jet air preheat temperature had minimal effect on overall  $\text{NO}_x$  formation in the RQL experimental combustor. The modeling results in Figure 38 show a large effect by the jet air preheat temperature on  $\text{NO}_x$  and TFN formation.

**Figure 38 Preheat Temperature Effects in the RQL Kinetics Model.**



The difference in Vardakas's results and the results in current study can be explained by the thermal  $\text{NO}$  mechanism. Since Vardakas's experimental results were not dependent on jet preheat temperature the thermal  $\text{NO}$  mechanism must not be as important in the quick-mix section. The kinetics modeling results show that jet air temperature does drive the  $\text{NO}$  and TFN production. The diverging results suggest that the  $\text{NO}_x$  might be formed early in the jet mixing process where the prompt mechanism may be more dominant than thermal  $\text{NO}$ . Further investigation and development of the model should be made to match experimental observations and verify that the modeling approach using a series of PSR is accurate.

## *CO Production*

The parameter changes in the models have the opposite effects for CO compared to NO<sub>x</sub> and TFN. Increases in the preheat temperature of both the main and jet air reduce CO. The reduction of the residence time of the jet PSRs causes an increase CO. The initial rich PSR residence has a negligible effect on the production of CO and elevated pressure conditions reduce CO. This is important in control strategies for stationary gas turbines using an RQL combustor.

## **3.2 Phase II**

### **3.2.1 Elevated Pressure Non-Reacting Mixing Tests**

The non-reacting mixing experiment showed that jet penetration and overall mixing are not affected by an increase in pressure. The design of the quick-mix section was based on the NASA design method. Temperature measurements were made to characterize the quick-mix section.

Non-reacting mixing tests were conducted in the high pressure facility to verify if the jet penetration and mixing correlation are applicable at elevated pressures, which had not been proven experimentally in previous studies. The main air was preheated to 850°F (727 K) and mixed with non-preheated jet air. The temperature entering the quick-mix section was much lower because of the heat loss through the combustor. Two jet hole configurations, 12 and 18, were tested at one and six atmospheres. Six atmospheres was chosen as the operating pressure during experiments because it would simulate the pressure of a stationary gas turbine. The jet-to-main mass flow ratio was maintained at 2.5. The jet-to-main momentum-flux ratio in each case was on average of 80, and was based on the facility limitations.

The planes of interest in this experiment were planes 1, 3, and 5. The penetration of the jets was more pronounced at the trailing edge rather than the leading edge of the jet holes. For this reason the data in Plane 3 are analyzed. In addition, the mixing was closer to equilibrium in plane 5 compared to plane 4 because of the additional mixing farther downstream. The planes of interest and the grid points of the data can be referred to in Figure 16. The temperature measurements of each plane were plotted with Surfer using the Kriging method. The data was collected over a period at least 30 seconds and then averaged for each point. The temperature standard deviation at each point was less than 1percent. The momentum-flux ratio during the same period of time had a standard deviation of 3percent. The data on each plane do not have the initial ten points desired. The probe points 2, 6, 7, and 9 were damaged and worked sporadically during the 18 hole module tests. This resulted in a loss of data points at the radii of 19.9, 32.2, 34.6, and 38.9 mm. Also because of limitations of the probe axial movement plane 1 was only 12.2 mm (0.5 in.) above the jet hole leading edge. Table 9 shows the axial length of each plane for the 12 and 18 hole modules. The 12 hole module is used in the reacting mixing experiments as well, except the plane 1 location was changed to  $x/R=-1$ . This was done to sample farther upstream and avoid interference with the jet holes by the trailing edge of the probe.

**Table 9 Normalized Axial Length Of Each Plane For The Non-Reacting Mixing Tests.**

Plane	12 hole (x/R)	18 hole (x/R)
1	-0.3	-0.3
2	0	0
3	0.275	0.225
4	1	1
5	2	2

#### *Entering the Quick-Mix Section-Plane 1*

The data, excluding the outer diameters, in plane 1 confirm the uniformity of the temperature field entering the quick-mix section. The plane 1 data are presented in Figure 39. The effects of the jets can be seen even though the probe is above the jet holes. This was a result of not traversing a larger distance above the holes and due to probe perturbation. The high pressure data show less temperature variance compared to the atmospheric pressure cases. The locations of the jets entering the mixing section become quite evident by two pockets of low temperature.

#### *Jet Penetration-Plane 3*

In plane 3 the jets penetration can be distinguished clearly in the flow field. This is distinguishable because of the two distinct low temperature regions at a radius of 25 mm. A substantial difference is seen in the distance the jets penetrate into the flow between the 12 and 18 hole configurations. The 18 hole configuration was expected to show slight under penetration or near optimum mixing. The calculated C value for equation 2.5 was between 3.2 and 3.4 in all of the tests. The optimum hole configuration for a J of 80 is 16 holes. The jets penetrate to approximately 27 mm in the 18 hole case, reaching near optimum penetration. The 12 hole configuration should show substantial over penetration. The data in Figure 40 do in fact show over penetration for the 12 hole case. The jets penetrate to a radius of approximately 22 mm, past the area half-radius of 28.2 mm. The area half-radius is the penetration desired for optimum mixing. There was not a substantial difference seen in penetration with an increase in pressure. The NASA design method was used to design the quick-mix modules. Since there was not a difference in jet penetration with increasing pressure and the predicted jet penetration levels were evident in the results, the NASA design method is applicable at elevated pressure conditions.

#### *Mixing Equilibrium-Plane 5*

In plane 5 the mixing is expected to be complete. The progression to equilibrium can be explained by the smoother contours and lower gradients found in plane 5, compared to plane 4 (see Figure 41). The over penetration is still apparent in this plane for the 12 hole cases shown in Figure 42. From the inner to outer radius there is a gradient of approximately 250°F for both pressures. The standard deviation in the 12 hole case at 1 atm was 67°F and 79°F at 6 atm. The 12 hole case shows nearly identical planes. The 18 hole case has a temperature gradient from the inner to outer radius of 50°F and 75°F with much wider bands of constant temperature. The standard deviation in the plane at 1 atm was 19°F and 37°F at 6 atm. As the jet penetration gets

closer to optimum the lower the temperature gradient is at plane 5. For over penetrating jets, the mixing could be improved by operating at a higher  $J$ , which would reduce the jet penetration.

**Figure 39 Plane 1 (X/R=-0.3) Non-Reacting Temperature Data**

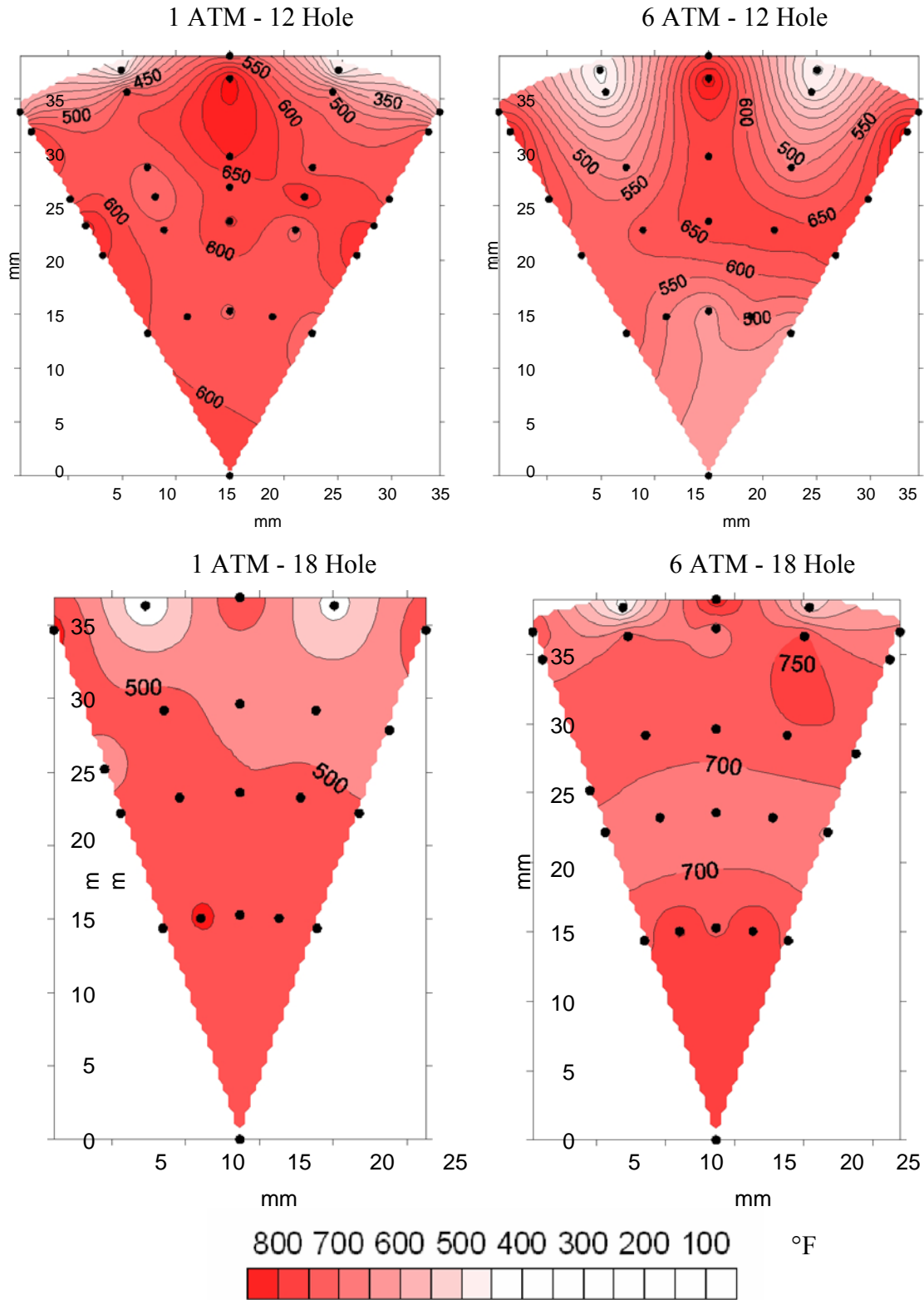


Figure 40 Plane 3 ( $x/R=0.275$  for 12 Hole,  $x/R=0.225$  for 18 Hole Modules) Temperature Data

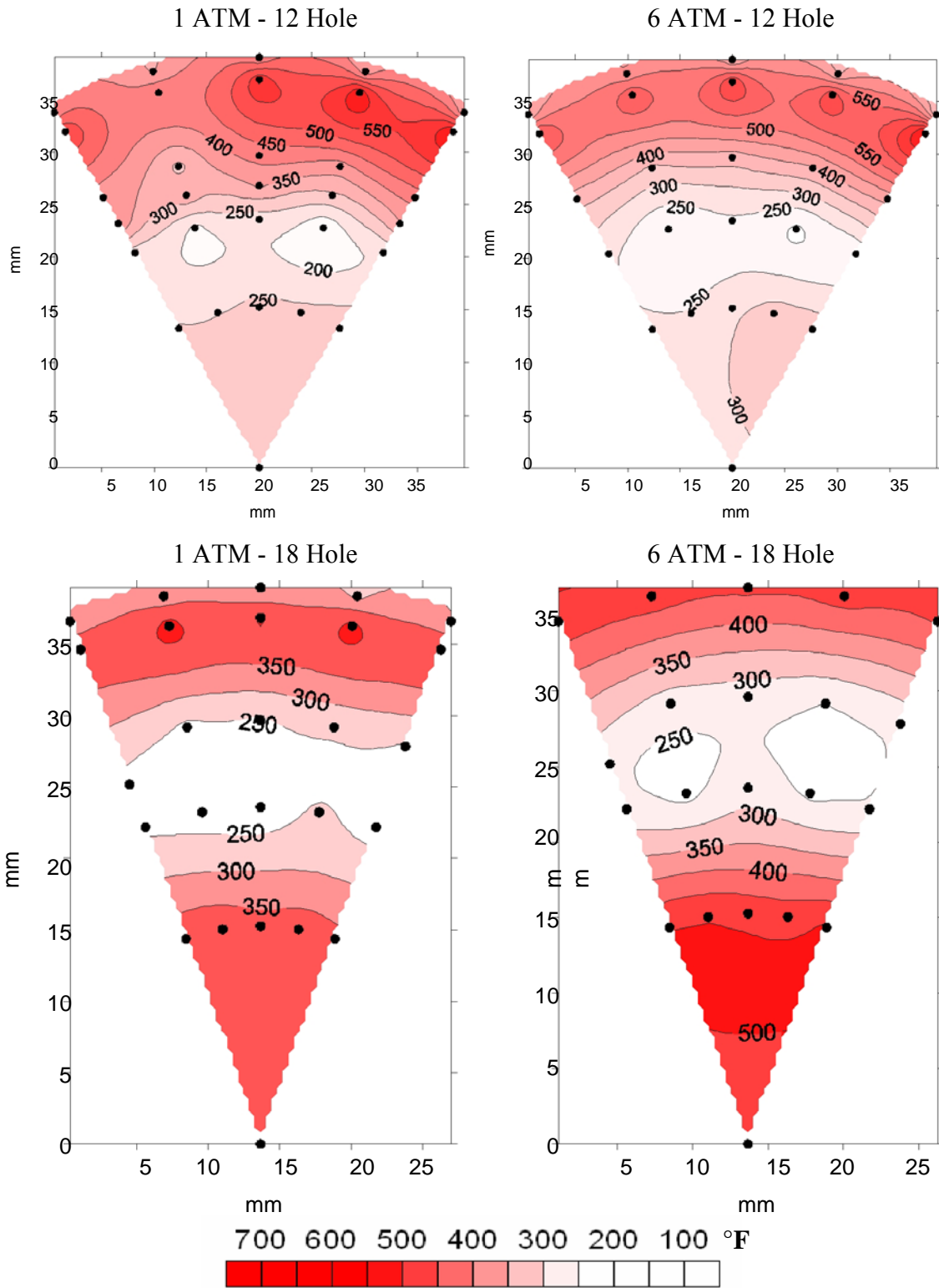


Figure 41 Plane 4 ( $x/R=1$ ) Non-Reacting Temperature Data

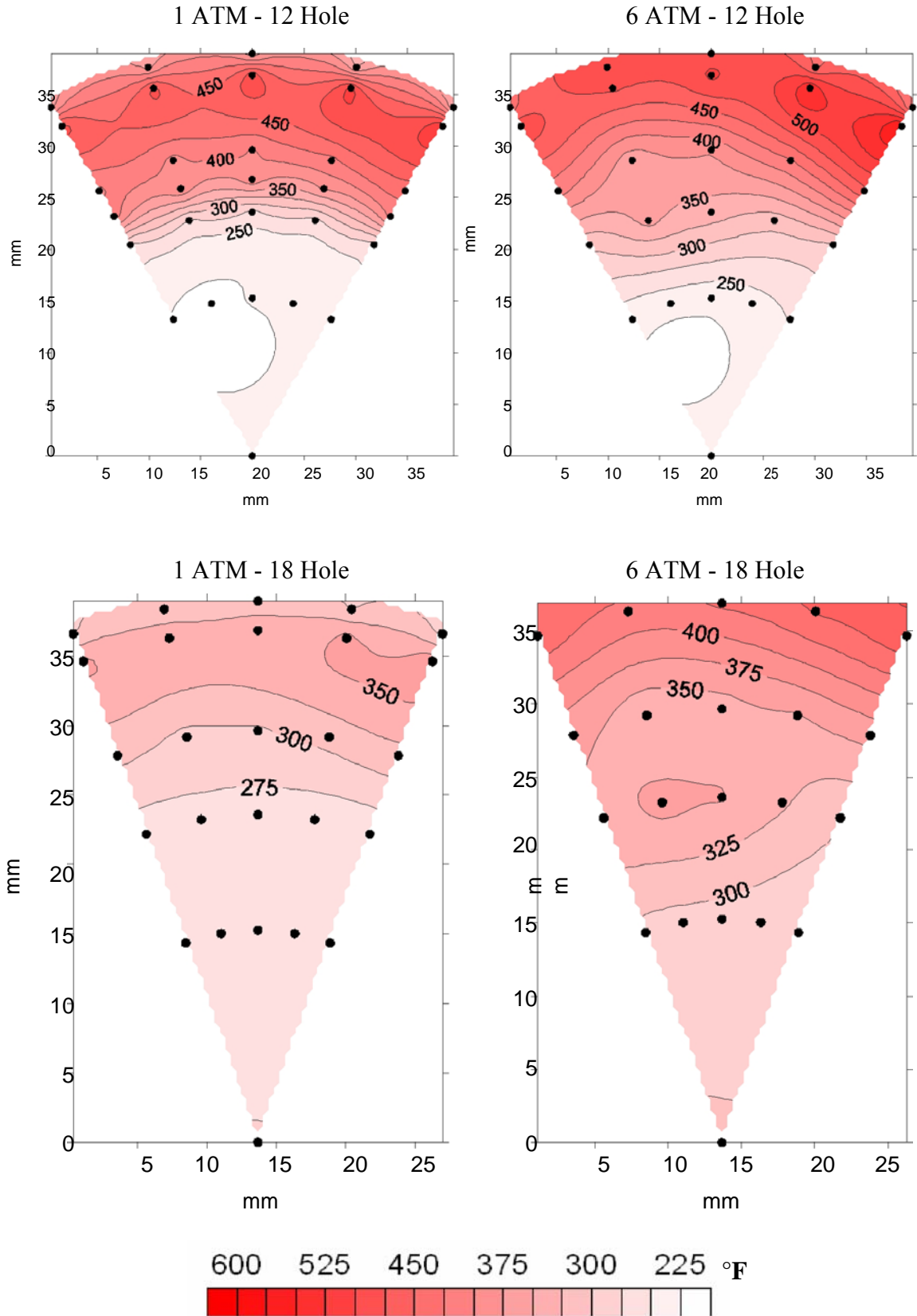
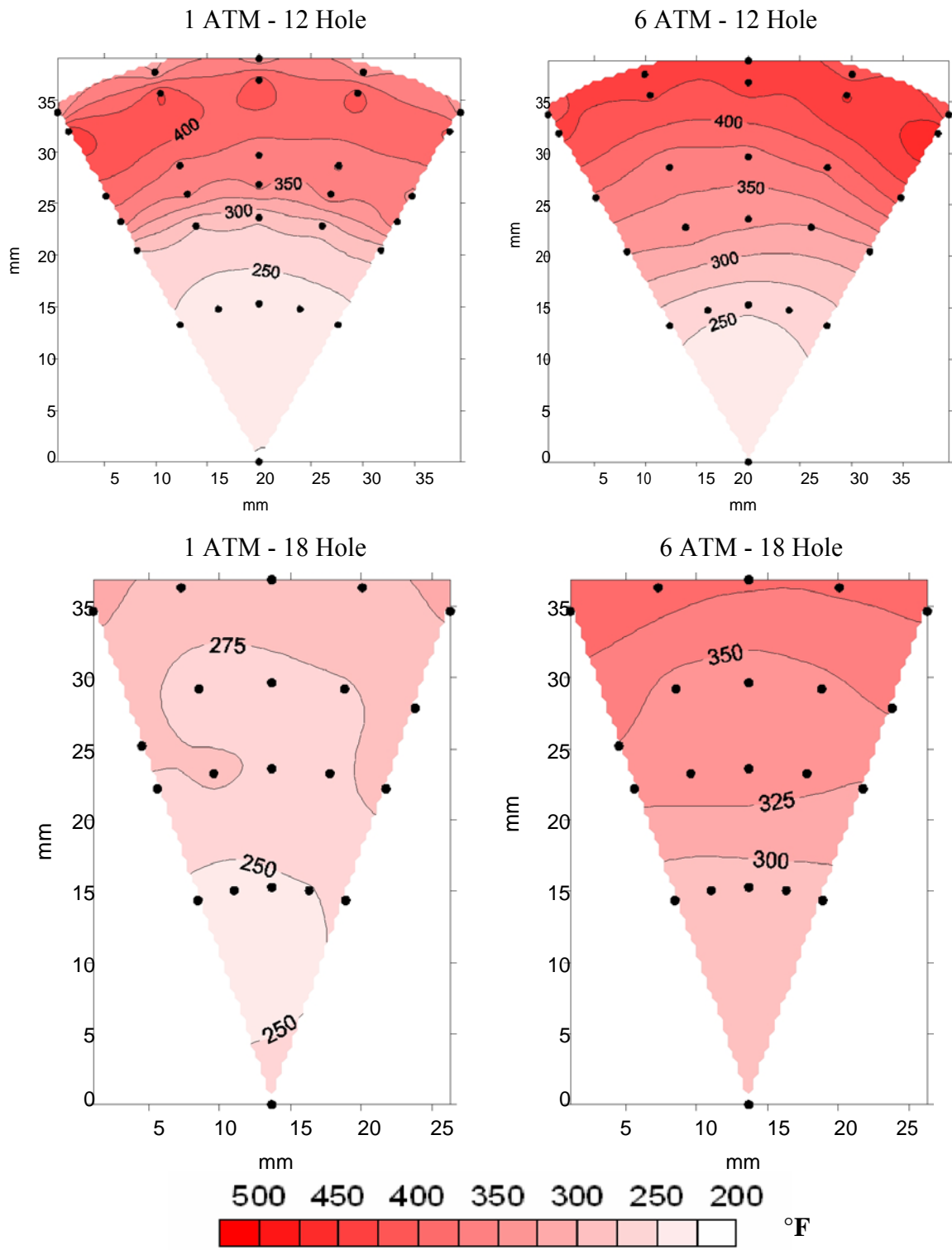


Figure 42 Plane 5 (X/R=2) Non-Reacting Temperature Data



### 3.2.2 Elevated Pressure Reacting Mixing Experiment

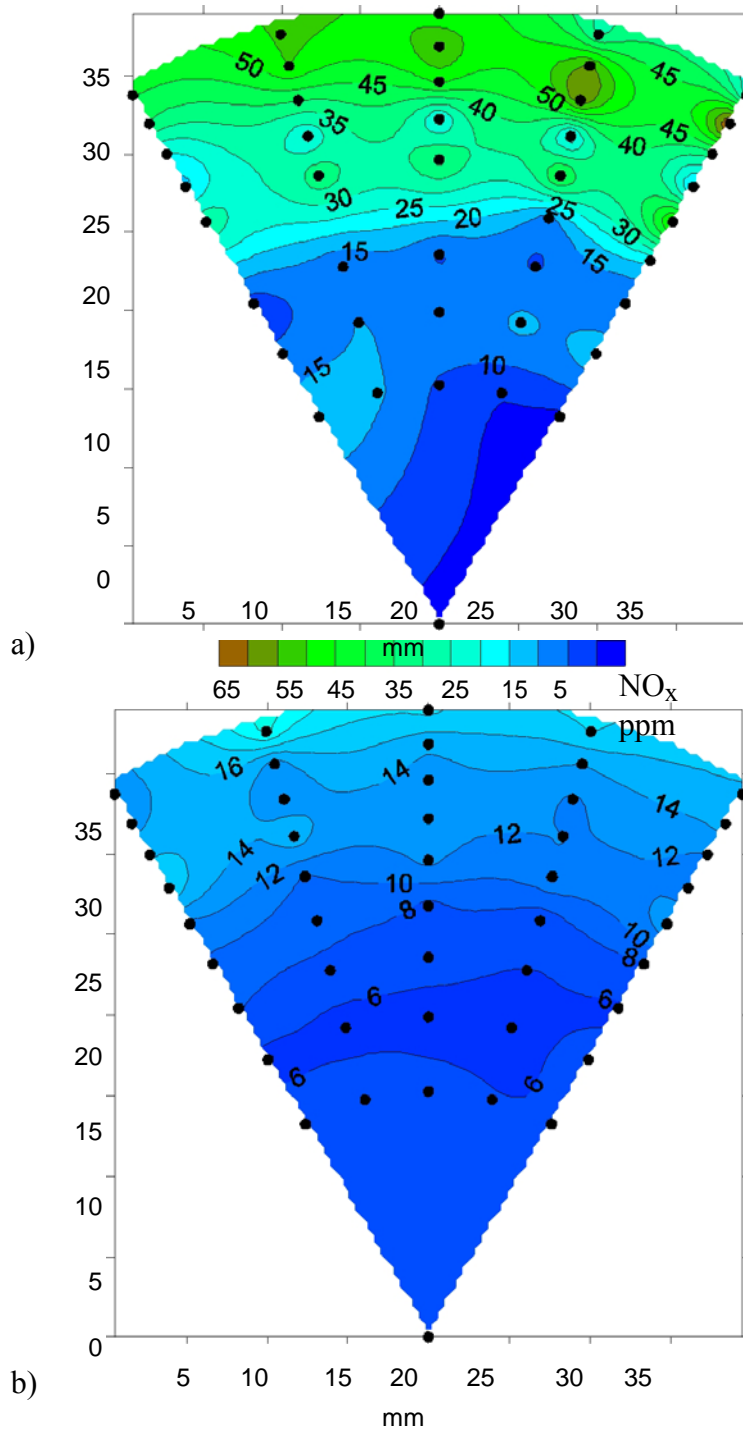
The reacting mixing experiment results showed that elevated pressure caused a substantial increase in  $\text{NO}_x$ . The  $\text{NO}_x$  rose from 10.4 to 27.2 ppm when the pressure was increase from one to six atmospheres.

The atmospheric reacting mixing experiment running on natural gas was repeated at an elevated pressure of six atmospheres. Emissions measurement of  $\text{NO}_x$ , CO,  $\text{CO}_2$ , HCs, and  $\text{O}_2$  were made on plane 5, two duct radii downstream of the leading edge of the jet holes. This experiment served as a straightforward method to investigate the effect of temperature on  $\text{NO}_x$  emissions. This experiment successfully demonstrated the ability to conduct future elevated pressure experiments safely and reliably. The operating conditions of the experiment were the same as the atmospheric reacting mixing tests. The momentum-ratio was maintained at 57 and MR was 2.5. The fuel rich equivalence ratio was 1.66 and the overall equivalence ratio was 0.45. The main air preheat temperature was 533 K (500°F) and the jet air preheat temperature 380 K (225°F).

The measured  $\text{NO}_x$  data at atmospheric and elevated pressures are presented in the contour plots in Figure 43. The non-reacting experiments showed that the mixing trends should not change with an increase in pressure. So similar mixing is expected in both the cases plotted. The  $\text{NO}_x$  levels near the core of the combustor are lower than the near the walls in both cases. The  $\text{NO}_x$  levels near the core of the combustor are twice as high in the elevated pressure case compared to the atmospheric case. This could be a result of the higher temperature in the fuel rich product in the high pressure case.

At the wall of the combustor, where the jet wakes produce high levels of  $\text{NO}_x$  due to near stoichiometric vortices, the  $\text{NO}_x$  levels are very high for both cases. The  $\text{NO}_x$  level is close to three times higher in the high pressure case. Since mixing is the same and the only condition that was varied was the pressure, the increase in  $\text{NO}_x$  is a result of the elevated pressure. Since the velocities, temperature, and area of the duct are the same. The pressure is the only effect on the system. The thermal  $\text{NO}_x$  formation in the jet wakes is the cause of this increase. In the jet wakes high residence times and near-stoichiometric, high temperature, and high thermal  $\text{NO}_x$  producing pockets of air and fuel are present. Through equilibrium calculations, we found, that pressure causes an increase in  $\text{NO}_x$  formation for methane at equivalence ratios between 0.7 and 0.9. It is reasonable to assume that the near stoichiometric pockets at higher pressures caused the increase in  $\text{NO}_x$ . Further study of different mixing condition, for example, jet over penetrating and under penetrating cases, would garner insight into the effects of mixing on  $\text{NO}_x$  at elevated pressures as well.

Figure 43 Plane 5 (X/R=2) No<sub>x</sub> Data From the Natural Gas Tests at Different Pressures a) Six Atmospheres and b) One Atmosphere.



### 3.2.3 Elevated Pressure Parametric Test Matrix Development

The development of the experimental combustor, reacting stability test, and atmospheric mixing tests allowed the test ranges for next phase of testing to be finalized. The test ranges for future elevated pressure mixing tests are presented in Table 10. These tests will be conducted using natural gas as the fuel. The elevated pressure test matrix was not implemented during the course of the project because of unforeseen issues regarding the use of the RQL facility used by Leong, et al. (1999) and Vardakas, et al. (1999).

The focus of the test matrix is on the parameters of rich equivalence ratio, operating pressure, momentum-flux ratio, number of jet mixing holes, and the preheat temperature. The preheat temperature range is 500°F to 850°F. 500°F has been selected as the minimum temperature because it corresponds to the preheating used in the previous atmospheric tests. 850 °F is the highest preheat temperature that the facility can reach with confidence and repeatability as demonstrated in the previous testing.

The operating pressure range is 2 atm to 6 atm. During atmospheric mixing tests (at a pressure of one atm), the sampling lines in the PG-250 had a low enough flow rate and a small leak that the pump sucked extra air into the emissions system. Therefore, the low end of range of pressure was changed from one atm to 2 atm. The 2 atm pressure condition will avoid having the emissions system suck air into the sampling lines by having a larger backpressure behind it. From the experience during non-reacting mixing tests, it became evident that the probe must be above the holes at a distance where the spokes will not interfere with jet air. Hence, the upstream condition measurement of the rich burn products has been moved farther upstream to an axial location of -1.

**Table 10 Proposed Parameter Ranges**

<b>Parameter</b>	<b>Ranges</b>
Overall $\Phi$	0.45
Rich $\Phi$	1.66, 1.95
Operating Pressure (atm)	2, 6
Momentum-Flux Ratio	45, 70
Mass-Flow Ratio	2.5
Number of Jet Mixing Holes	12, 18
Preheat Temperatures (°F)	500, 850
Axial Sampling Planes z/R	-1, 1, 2
Radial Sampling	9 Equal area annuli & centerline
Angular sampling	Five angles spanning two centerlines of jet holes

Chemkin Equil modeling showed that the minimum TFN levels for natural gas are different than the minima for propane. The 6 atmosphere with 500°F preheat main air case has a

minimum TFN value at an equivalence ratio of 1.66. The minimum changes as pressure and preheat temperature are changed. The equivalence ratio for minimum TFN for the atmospheric cases and the 6 atmospheres with 900°F preheat case varied from 1.85 to 2.05. The equivalence ratio of 1.95 is chosen for Phase II testing because for each of those cases the TFN value is not more than one ppm higher than the minimum for each specific case.

The number of jet holes and momentum-flux ratio ranges are related to each other. The NASA Design Method (see equation 2.3) incorporates both of these parameters to design the quick-mix section of the RQL experimental combustor. For a J equal to 45 the optimum number of jet holes is 12. The jets will over penetrate if the J is increased while the 12 holes remain constant. The opposite is expected when the J remains constant and hole number is increased to 18. The jets will under penetrate in this case. At a J of 70 the optimum number of jet mixing holes is 15. This means that for a constant J of 70, the 12 holes will cause the jets to over penetrate and the 18 holes will cause under penetration. The test ranges will allow for different levels of jet penetration to be analyzed and insight will be gained into the role of jet penetration in the production of NO<sub>x</sub> in the quick-mix section.

A statistically designed experiment test matrix will be implemented in future testing. A full two-level factorial of the statistically designed experiment would total 32 experiments, 2<sup>5</sup>. The five parameters in this study tested at every combination of high and low values of the test ranges (two-level) make up the full two-level factorial. A subset or fraction of the full test matrix will be conducted initially. This is because it is not a wise allocation of all the testing resources to conduct 32 experiments when 16 would produce the same results. The fractional test matrix will consist of 16 experiments and still have the capability to statistically show the effect of each parameter. The results will then be evaluated and used to identify a second series of tests to address any remaining questions. This could include additional measurements at other axial planes and/or additional conditions. Table 11 summarizes the proposed fractionalized test matrix. In bold are the center-points of the test matrix, which help identify systematic error.

**Table 11 Fractional Test Matrix**

Test	Equivalence Ratio, $\Phi$	Pressure, atm	Momentum-Flux Ratio, J	# Holes	Inlet Temp, °F
1	1.66	2	45	12	850
2	1.95	2	45	12	500
3	1.66	6	45	12	500
4	1.95	6	45	12	850
5	1.66	2	70	12	500
6	1.95	2	70	12	850
7	1.66	6	70	12	850
8	1.95	6	70	12	500
9	1.66	2	45	18	500
10	1.95	2	45	18	850
11	1.66	6	45	18	850
12	1.95	6	45	18	500
13	1.66	2	70	18	850
14	1.95	2	70	18	500
15	1.66	6	70	18	500
16	1.95	6	70	18	850
17	1.80	4	57.5	12	675
18	1.80	4	57.5	18	675

### 3.3 Summary

A high pressure experimental facility has been designed and successfully demonstrated in non-reacting and reacting operating conditions, with both natural gas and propane, for the study of jet mixing in a RQL experimental combustor. Atmospheric performance testing of the rich product generator characterized the recirculation zone with DPIV and high-speed video imaging. Atmospheric performance testing also characterized the stability of the reaction. Testing of the rich product generator at elevated pressures and preheat temperatures proved to be stable at the desired operating conditions, using both natural gas and propane.

In the reacting atmospheric mixing experiments conducted to commission the facility, it was possible to safely and repeatedly operate the facility. Emissions measurements were made to characterize the quick-mix section. For a set momentum-flux ratio of 57, mass-flow ratio of 2.5, and a 12 hole quick-mix section module it was found:

- The propane atmospheric tests conducted by Vardakas, et al. (1999) were successfully repeated. At one duct radius downstream of the leading edge of the jet holes the  $\text{NO}_x$  results were about 25percent lower, while the CO results were four times lower.
- The jet mixing in the propane atmospheric tests resulted in mixing to the centerline of

the quick-mix section and with a wide jet mixing range from the centerline to a radius of 25 mm, which was not apparent in the tests conducted by Vardakas, et al. (1999).

- The plane two duct radii downstream (plane 5) of the leading edge of the jet holes proved to be an important plane to measure as the mixing and reaction in the quick-mix section are closer to completion compared to the plane one duct radii downstream of the leading edge of the jet holes (plane 4).
- The high levels of NO<sub>x</sub> near the walls of the combustor were indicative of the jet wakes in the quick-mix section.
- 10 sampling points provided better resolution than the four sampling points used by Vardakas, et al. (1999), and as a result, provided significant information about the emissions levels in each plane.
- The natural gas produced lower NO<sub>x</sub> and CO than propane.
- The elevated pressure experiment with natural gas showed that NO<sub>x</sub> increased with pressure in the quick-mix section of the RQL experimental combustor from 10.4 ppm at one atmosphere to 27.2 ppm at six atmospheres.

In the systematic non-reacting atmospheric mixing studies it was possible to determine the jet trajectory using an intrusive sampling probe. For a set momentum-flux ratio of 80 and a mass-flow ratio of 2.5 it was found:

- The low temperature regions in plane 3 (one jet hole diameter past the leading edge of the jet holes) were used to identify the region of jet penetration.
- The 12 hole and 18 hole quick-mix sections both resulted in jet penetration past the area half-radius of the duct.
- The 18 hole module provided better mixing than 12 hole module because of the lower jet penetration.
- As the number of jet holes was increased the jet penetration decreased at atmospheric and at elevated pressures.
- Elevated pressures did not change the jet penetration and overall mixing.

The kinetics modeling of the RQL experimental combustor was used to help understand the means by which NO<sub>x</sub> and CO are produced in the mixing section and were an important complement to the mixing studies.

- The rich products of the RQL combustor are more accurately modeled with equilibrium

results compared to using a PSR or plug flow reactor.

- NO<sub>x</sub> (and TFN) production decreased with increasing pressure in the fuel rich PSRs, decreased with residence time, and increased with preheat temperature.

# CHAPTER 4:

## Conclusions and Recommendations

### 4.1 Conclusions

The conclusions that relate to the project objectives are:

- The experimental results show that an increase in the air temperature entering the rich reactor, resulting in higher reaction temperatures, increases the production and emission of  $\text{NO}_x$ , and thereby validates prior reports that the rich reactor air preheat temperature is a major driver for overall  $\text{NO}_x$  production in RQL combustion.
- The natural gas atmospheric test results showed lower  $\text{NO}_x$  and CO levels compared to the propane tests, suggesting that stationary and aerospace gas turbines that utilize the RQL combustion concept can achieve lower  $\text{NO}_x$  and CO when using natural gas as a fuel instead of propane.
- Elevated pressures do not change the level of jet penetration and overall mixing. As a result, the NASA design method developed to optimize jet mixing performance at atmospheric pressure is valid as a tool under elevated pressure conditions for the design of the quick-mixing section.
- Based on kinetics modeling, an increase in pressure decreases the production of  $\text{NO}_x$  and TFN in the fuel rich reactor as a result of elevated pressure inhibiting the rate limiting steps of the thermal and prompt mechanisms.
- Elevated pressure increases the  $\text{NO}_x$  produced in the quick-mix section of the RQL combustor due to the increase in thermal  $\text{NO}_x$  formed in the jet wakes near the wall of the combustor.

The broader conclusions resulting from this study are:

- The high pressure test rig developed in the present study provides uniform and axis-symmetric temperature and species to the quick-mix section while stabilizing rich reactions up to an equivalence ratio of 2.3 at elevated pressure. The jet mixing studies conducted with the test rig were able to confirm previous results, which proves that the facility is commissioned for future jet mixing studies.
- The Ballal and Lefebvre correlation for weak extinction limits applies to the rich product generator geometry and suggests, as a result, that the correlation can be used to scale the stability to other conditions.

## 4.2 Recommendations

The results from the experimental and modeling studies suggest that further insight into RQL combustion can be revealed by:

- Applying the test plan presented in section 5.2.2 to answer questions regarding jet mixing effects on NO<sub>x</sub> production at elevated pressure.
- Measuring the hydrocarbon emission in the quick-mix section.
- Using a high CO analyzer to measure the CO entering quick-mix section.
- Using an 8-hole quick-mix section module to simulate jet penetration levels that the 12-hole and 18-hole sections cannot provide.
- Continue refining the kinetics model using multiple reactors in series to analyze NO<sub>x</sub> formation in the jet mixing section.
- Sensitivity analysis would be useful in identifying detailed kinetics effects on the fuel rich side of the model.

## 4.3 Benefits to California

The PIER goal of improving the energy cost and value of California's electricity is met by this project. The development and research in RQL combustion technology has the potential to provide power generation with high combustion stability that will meet the accordance with the strictest air quality standards in the nation. The research in this project showed that the use of natural gas has a better potential than propane in meeting air quality standards in stationary gas turbines. This is important for manufacturers and designers of RQL combustors. In addition, the project outcomes showed that elevated pressures did not change the jet penetration and mixing in the RQL experimental combustor. The designers of RQL combustors can use this knowledge to model prototype combustors in atmospheric reacting and non-reacting conditions. The new RQL high pressure test rig at UCICL is an asset to the research facilities in CA, as it can provide the opportunity for elevated pressure research in fundamental mixing studies in RQL, fuel rich combustion, and emissions production from different fuels. The high pressure test rig can be used to repeat experiments conducted by industry to verify their findings.

## CHAPTER 5: Glossary

$A_{eff}$	Effective Area of the Jets
$B_a$	Aerodynamic Blockage
C	Geometric Blockage
$C_d$	Experimentally Derived Constant
D	Duct Diameter
$d_{bb}$	Jet Hole Diameter
$d_j$	Discharge Coefficient
H	Duct Height
J	Jet-to-Mainstream Momentum-Flux Ratio
K	Constant of Proportionality
$m$	Mass Flow Rate
MR	Jet-to-Mainstream Mass-Flow Ratio
n	Number of Jet Holes
NETL	National Energy Technology Laboratory
P	Pressure
ppm	Parts Per Million by Volume
R	Duct Radius
RQL	Rich-Burn, Quick-Mix, Lean-Burn
S	Orifice Spacing
T	Temperature
U	Velocity
UTRC	United Technologies Research Center
$\theta$	Angle
$\rho$	Density
$\Phi$	Equivalence Ratio

## CHAPTER 6: References

- Bain, D. B., Smith, C.E., and Holdeman, J.D. (1993). CFD Mixing Analysis of Axially Opposed Rows of Jets Injected Into Confined Crossflow. NASA TM 106179 (also see AIAA 93-2044).
- Bain, D. B., Smith, C.E., and Holdeman, J.D. (1995). "Mixing Analysis of Axially Opposed Rows of Jets Injected into Confined Crossflow." Journal of Propulsion and Power Vol. 11(No. 5): pp. 885-893.
- Bain, D. B., Smith, C.E., Liscinsky, D.S., and Holdeman, J.D. (1999). "Flow Coupling Effects in Jet-in-Crossflow Flowfields." Journal of Propulsion and Power Vol. 15(No. 1): pp. 10 -16.
- Ballal, D. R., and Lefebvre, A.H. (1979). "Weak Extinction Limits of Turbulent Flowing Mixtures." Journal of Engineering for Power Vol. 101: pp. 343-348.
- Choi, G. M., and Katsuki, M. (2002). "Chemical Kinetic Study on the Reduction of Nitric Oxide in Highly Preheated Air Combustion." Proceedings of the Combustion Institute Vol. 29: pp. 1165-1171.
- Correa, S. M. (1992). "A Review of NO<sub>x</sub> Formation Under Gas-Turbine Combustion Conditions." Combustion Science and Technology Vol. 87: pp. 329-362.
- De Nevers, N. (2000). Air Pollution Control Engineering. Boston, McGraw-Hill.
- Demayo, T. N., Leong, M.Y., Samuelsen, G.S., and Holdeman, J.D. (2003). "Assessing Jet-Induced Spatial Mixing in a Rich, Reacting Crossflow." Journal of Propulsion and Power Vol. 19(No. 1): pp. 14-21.
- Diers, O., Koopman, J., Fishcer, M., and Hassa, C. (2002). "Investigation of Two Advanced Cooling Mixing Concepts for a Rich Quench Lean Combustor." Journal of Engineering for Gas Turbines and Power Vol. 124: pp. 1-8.
- Feitelberg, A. S. and Lacey, M.A. (1998). "The GE Rich-Quench-Lean Gas Turbine Combustor." Journal of Engineering for Gas Turbine and Power Vol. 120: pp. 502-508.
- Fric, T. F. (1993). "Effects of Fuel-Air Unmixedness on NO<sub>x</sub> Emissions." Journal of Propulsion and Power Vol. 9(No. 5): pp. 708-713.
- Golden Software, Surfer 8: Help Manual, 2002.
- Hatch, M. S., Sowa, W.A., Samuelsen, G.S., and Holdeman, J.D. (1992). Jet Mixing Into a Heated

Cross Flow in a Cylindrical Duct: Influence of Geometry and Flow Variations. NASA TM 105390 (also see AIAA 92-0773).

Hatch, M. S., Sowa, W.A., Samuelsen, G.S., and Holdeman, J.D. (1995). "Geometry and Flow Influences on Jet Mixing in a Cylindrical Duct." Journal of Propulsion and Power Vol. 11(No. 3): pp. 393-402.

Hatch, M. S., Sowa, W.A., Samuelsen, G.S., and Holdeman, J.D. (1995). Influence of Geometry and Flow Variation on NO Formation in the Quick Mixer of a Staged Combustor. NASA TM 105639.

Hayashi, S., Yamada, H., and Makida, M. (2000). "Short-Flame/Quick-Quench: A Unique Ultralow Emissions Combustion Concept for Gas Turbine Combustors." Proceedings of the Combustion Institute Vol. 28: pp. 1273-1280.

Hendricks, R. C., Shouse, D.T., Roquemore, W.M., Burrus, D.L., Duncan, B.S., Ryder, R.C., Brankovic, A., Liu, N.S., Gallagher, J.R., and Hendricks, J.A. (2004). Experimental and Computational Study of Trapped Vortex Combustor Sector Rig with Tri-Pass Diffuser. NASA TM 2004-212507.

Holdeman, J. D., Liscinsky, D.S., Oeschle, V.L., Samuelsen, G.S., and Smith, C.E. (1996). Mixing of Multiple Jets with a Confined Subsonic Crossflow in a Cylindrical Duct. NASA TM 107185 (also see ASME 96-GT-482).

Holdeman, J. D., Reynolds, R., and White, C. (1987). A Numerical Study of the Effects of Curvature and Convergence on Dilution Jet Mixing. AIAA/SAE/ASME/ASEE 23rd Joint Propulsion Conference, San Diego, CA.

Holman, J. P. (1978). Experimental Methods for Engineers. New York, McGraw-Hill.

Konnov, A. A., Dyakov, I.V., and de Ruyck, J. (2002). "Nitric Oxide Formation in Premixed Flames of H<sub>2</sub> + CO + CO<sub>2</sub> and Air." Proceedings of the Combustion Institute 29: pp. 2171-2177.

Kroll, J. T., Sowa, W.A., Samuelsen, G.S., and Holdeman, J.D. (1993). Optimization of Circular Orifice Jets Mixing Into a Heated Cross Flow in a Cylindrical Duct. NASA TM 105984 (also see AIAA 93-0249).

Lefebvre, A. H. (1983). Gas Turbine Combustion. London, Taylor & Francis.

Lefebvre, A. H. (1999). Gas Turbine Combustion. London, Taylor & Francis.

Leong, M. Y. and Samuelsen, G.S. (1996). Quick-Mixing Studies Under Reacting Conditions. NASA CR 195375.

Leong, M. Y., Samuelsen, G.S, and Holdeman, J.D. (1999). "Mixing of Jet Air with a Fuel-Rich, Reacting Crossflow." Journal of Propulsion and Power Vol. 15(No. 5): pp. 617-622.

Leong, M. Y., Samuelsen, G.S., and Holdeman, J.D. (1997). Optimization of Jet Mixing Into a Rich, Reacting Crossflow. NASA TM 97-206294 (also see AIAA 98-0156).

Liscinsky, D. S., True, B., and Holdeman, J.D. (1995). Crossflow Mixing of Noncircular Jets. NASA TM 106865 (also see AIAA 95-0732).

Liscinsky, D. S., True, B., Vranos, A., and Holdeman, J.D. (1992). Experimental Study of Cross-Stream Mixing in a Rectangular Duct. NASA TM 105694 (also see AIAA 92-3090).

Liscinsky, D. S., True, B., Vranos, A., and Holdeman, J.D. (1993). Experimental Investigation of Crossflow Jet Mixing in a Rectangular Duct. NASA TM 106152 (also see AIAA 93-2037).

Lyons, V. J. (1982). "Fuel/Air Nonuniformity- Effect on Nitric Oxide Emissions." AIAA Vol. 20(No. 5): pp. 660-665.

Margason, R. J. (1993). Fifty Years of Jet in Crossflow Research. Computational and Experimental Assessment of Jets in Cross Flow, AGARD CP 534 ID 94N28004.

McDonell, V. G., and Samuelsen, G.S. (2000). "Measurement of Fuel Mixing and Transport Processes in Gas Turbines." Measurement Science Technology Vol. 11: pp 870-886.

Meisl, J., Koch, R., Kneer, R., and Wittig, S. (1994). "Study of NO<sub>x</sub> Emission Characteristics in Pressurized Staged Combustor Concepts." Proceedings of the Combustion Institute Vol. 25: pp. 1043-1049.

Nicol, D. G., Steele, R. C., Marinov, N. M., and Malte, P. C. (1995). "The Importance of the Nitrous Oxide Pathway to NO<sub>x</sub> in Lean-Premixed Combustion." Journal of Engineering for Gas Turbine and Power Vol. 117: pp. 100-111.

Oechsle, V. L., and Holdeman, J.D. (1995). Numerical Mixing Calculations of Confined Reacting Jet Flows in a Cylindrical Duct. NASA TM 106736 (also see AIAA 95-0733).

Oechsle, V. L., Mongia, H.C., and Holdeman, J.D. (1994). Comparison of Mixing Calculations for Reacting and Non-reacting Flows in a Cylindrical Duct. NASA TM 106435 (also see AIAA 94-0865).

Petersen, C. O., Sowa, W.A., and Samuelsen, G.S. (2002). Performance of a Model Rich Burn-Quick Mix-Lean Burn Combustor at Elevated Temperature and Pressure. NASA CR-2002-211192.

Reaction Design. (2005). Theory Manual 4.0.2.

Rosfjord, T. J., and Padget, F.C. (2001). Experimental Assessment of the Emissions Control Potential of a Rich/Quench/Lean Combustor for High Speed Civil Transport Aircraft Engines. NASA CR 2001-210613.

Rutar, T., and Malte, P.C. (2002). "NO<sub>x</sub> Formation in High-Pressure Jet-Stirred Reactors with Significance to Lean-Premixed Combustion Turbines." Journal of Engineering for Gas Turbines and Power Vol. 124: pp. 776-783.

Rutar, T., Malte, P.C., and Kramlich, J.C. (2000). "Investigation of NO<sub>x</sub> and CO Formation in Lean-Premixed, Methane/Air, High-Intensity, Confined Flames at Elevated Pressures." Proceedings of the Combustion Institute Vol. 28: pp 2435-2441.

Sepman, A., Mokhov, A.V., Levinsky, H.B. (2002). "A Laser-Induced Fluorescence and Coherent Anti-Stokes Raman Scattering Study of NO Formation in Preheated, Laminar, Rich Premixed, Methane/Air Flames." Proceedings of the Combustion Institute Vol. 29: pp. 2187-2194.

Smith, C. E., Talpallikar, M.V., and Holdeman, J.D. (1991). A CFD Study of Jet Mixing in Reduced Flow Areas for Lower Combustor Emissions. NASA TM 104411 (also see AIAA 90-2460).

Straub, D. L., Casleton, K.H., Lewis, R.E., Sidwell, T.G., Maloney, D.J., and Richards, G.A. (2005). "Assessment of Rich-Burn, Quick-Mix, Lean-Burn Trapped Vortex Combustor for Stationary Gas Turbines." Journal of Engineering for Gas Turbines and Power Vol. 127: pp. 36-41.

Talpallikar, M. V., Smith, C.E., Lai, M.C., and Holdeman, J.D. (1991). CFD Analysis of Jet Mixing in Low NO<sub>x</sub> Flametube Combustors. NASA TM 104466 (also see ASME 91-GT-217).

Turns, S. R. (2000). Introduction to Combustion. Boston, McGraw-Hill.

Vardakas, M. A., Leong, M.Y., Brouwer, J., and Samuelson, G.S. (1999). The Effect of Air Preheat at Atmospheric Pressure on the Formation of NO<sub>x</sub> in the Quick-Mix Section of an Axially Staged Combustor. NASA TM 1999-209431.

## APPENDIX A:

### Non-Reacting Jet In Crossflow Experiments

Crossflow mixing is inherently important in RQL combustion systems. Crossflow mixing in RQL combustors is a control mechanism that is used to reduce pollution. The goal of crossflow mixing is to obtain a homogenous mixture of the mainstream and jet injection rapidly. Non-reacting mixing experiments were first used to verify the correlations in designing an optimum mixer. Rapid mixing was necessary to minimize the time at high NO<sub>x</sub> producing conditions in the mixing region (Liscinsky, et al. 1995). Liscinsky, et al. (1993), experimentally derived that the constant C in the equation

$$C = \left( \frac{s}{H} \right) \sqrt{J} \quad (2.7),$$

is equal to 2.5 for optimum jet mixing effectiveness for opposed inline round holes in a rectangular duct.

In another study, Liscinsky, et al. (1992), used spatial concentration measurements to quantify the mixing of jets in a crossflow. The measurements taken in non-reacting cross-flow experiments were used to characterize the level of unmixedness. The experimental studies also included varying geometry, different orifice spacing, and size as variables. The use of slots was studied along with the conventional circular geometry. The research concluded that the mixing rate increases with increasing momentum-flux ratio and is also more dependent on orifice geometry than mass-flow ratio. Depending on the specific design of the quick-mix section, orifices operating at a higher momentum-flux ratio, (while maintaining optimum jet penetration) are advantageous (Liscinsky, et al. 1993).

The study by Hatch, et al. (1995), explored the use of slots and round orifices in non-reacting mixing tests. Data were taken at five different planar locations after the leading edge of the jet holes and were presented using 3-D plots. Hatch observed that under penetration created an unmixed core that persisted downstream of the jets, while over penetration created an unmixed circumference especially near the walls in both slots and round holes. The research also showed that the aspect ratio of slanted or angled slots was a major factor in the level of jet penetration. As the aspect ratio was increased the level of jet penetration decreased (Hatch, et al. 1995). Hatch also conducted non-reacting mixing tests to study the effect of circular orifices on jet penetration and the optimization of mixing. Hatch concluded that the mean trajectory of the jet should be close to the modules half area radius for uniform mixing one-duct radii downstream (Hatch, et al. 1992).

## Non-Reacting Jet In Crossflow Modeling

Non-reacting models (computational fluid dynamic, CFD) of jet mixing in a crossflow were developed to complement the experimental research. In typical gas turbine combustion applications, jet mixing has played a vital role in the dilution zone of the combustor. The purpose of the dilution zone jets is to mix with the primary zone combustion products. The mixing aid in reduction of pollutant emissions and the design of dilution jets is motivated by the need to reduce hot spots to avoid destroying the turbine blades. But the design of the jet mixing section is motivated by the need to initiate rapid mixing to reduce emissions. The difference between conventional combustor concepts using jet mixing and the RQL combustor is that the jet-to- mainstream mass-flow ratio, MR, is much higher for an RQL combustor than the dilution zone of a typical combustor. The mass flow ratio for the RQL combustor is approximately 2.0 compared to 0.25-0.50 of a typical combustor.

CFD analysis was used to verify that the jet mixing design principles were similar at different range of MR. The study by Bain, Smith, and Holdeman (1995) modeled a rectangular duct with rectangular slots. The CFD results showed that a non-reacting opposed row of jets has similar mixing result at high MR levels indicating the applicability of these design principles to RQL combustors (Bain, et al. 1993). The study also concluded that the two factors, jet-to-mainstream momentum-flux ratio and the orifice spacing-to-duct height ratio (S/H), are coupled. Therefore, the aforementioned equation 2.5 is another form of the optimum mixing equation and can be restated as

$$C = \left( \frac{\pi}{n} \right) \sqrt{2J} \quad (2.8).$$

Calculating C can be useful in real experiments to ascertain the level of jet penetration. If C is close to 2.5 then optimum mixing has been achieved. If C is larger than 2.5 the jets over penetrate and if it is less than 2.5 the jets under penetrate (Holdeman, et al. 1996).

Using equation 2.8, Bain, et al. (1995) studied the effect of jets with the centerlines inline and staggered jets on mixing performance with MR in the range closer to a practical RQL combustor. The study showed that for a given J, inline jets have a unique spacing for optimum mixing but with staggered jets there are two different spacing configurations that give optimum mixing. As the spacing progresses from low to high the jets initially under penetrate and then hit optimum before over penetrating for a given J. Inline configurations also differ from staggered configurations in respect to the downstream mixing. Inline configurations have better initial mixing which is important from a practical standpoint because it would help reduce combustor size (Bain, 1993). Typically inline jets are used but it has been suggested that staggered jets that penetrate past each other may provide better mixing. Staggered jets show better downstream mixing while inline jets have better initial mixing (Bain, et al. 1995). Another advantage of in-line holes is that they are smaller for the same total area. There are four times as many holes for an optimum in-line configuration than for an optimum staggered configuration, so the hole diameter must be doubled for the staggered configuration. Note that the jets from opposite sides must pass each other in an optimum staggered configuration. If the spacing is

too small, staggered configurations will not work.

CFD analysis by Talpallikar, et al. (1991), suggested that for slots conventional methods for designing jet mixing orifices might not be applicable. The analysis showed that as the momentum-flux ratio was increased the jets began to over penetrate. After reaching an optimum mixing state, a transition to over penetration occurs. In general, under penetrating jets exhibit worse mixing effectiveness than over penetrating jets. Talpallikar used these observations in the non-reacting model and applied a reacting mathematical model to match the condition of the non-reacting model. Talpallikar then coupled the reacting model to a  $\text{NO}_x$  formation model, which was used to evaluate the influence of mixing on  $\text{NO}_x$  formation. The  $\text{NO}_x$  emissions were shown to be highly sensitive to variations in  $J$  and the mixing performance (Talpallikar, et al. 1991).

## Reacting Jet In Crossflow Models

The non-reacting experiment and modeling led to the need to study jet mixing with reacting models. For instance, Oeschle, Mongia, and Holdeman (1994), studied the mixing in non-reacting and reacting flows using a numerical model. Researchers in the past have used non-reacting mixing results of planar concentrations and temperatures to deduce the reacting flow field. This results in uncertainty in the use of non-reacting mixer designs for optimizing reacting mixer geometry. The results showed that non-reacting temperature profiles are valid when used to predict the reacting flow equivalence ratio distribution. Oeschle also showed that the rich reacting flow fields induce better mixing because of an apparent reaction delay. The reaction delay allows more time for mixing to take place, which would then simultaneously decrease the formation of pollutants in localized high temperature pockets created by jet wakes (Oechsle, et al. 1994).

Another CFD model was used to assess the use of reduced flow areas or neck down of the mixing section of the RQL combustor for further reduction  $\text{NO}_x$  and optimization of mixing. Neck down showed a significant reduction in  $\text{NO}_x$ . This was attributed to the reduction of the residence time of species in high reaction temperature regions, causing a reduction in thermal  $\text{NO}_x$  formation. Neck down did not show any improvement in the mixing (Smith, Talpallikar, and Holdeman, 1991).

Numerical modeling has been significant in moving RQL research forward. The validation of non-reacting model has led to research in to reacting models using to predict  $\text{NO}_x$  and mixing behavior in practical combustion operating conditions. Oeschle and Holdeman (1995) studied the effect of jet penetration in relation to  $\text{NO}_x$  production. A 3-D model of the RQL combustor was used in the study with orifice size, shape, and momentum-flux ratio as the varying parameters. The study showed that if the jets under penetrate the  $\text{NO}_x$  production is initially low but after one-duct radii downstream the unmixed jets eventually mix with the hot mainstream flow in the centerline and produce thermal  $\text{NO}_x$ . The  $\text{NO}_x$  production when the jets over penetrate into the duct using with round orifices was attributed to the production of large wakes created by the jets. Despite all these observation the model did not show that

optimization of mixing would in turn lead to the lowest overall NO<sub>x</sub> production (Oechsle and Holdeman, 1995). This is a gap in jet mixing and RQL research that has yet to be filled.

The study by Bain, et al. (1999), used CFD to study the flow coupling effects in jet mixing. The study showed that the thinner the liner walls the more penetration achieved by the jets. The CFD results also showed a strong coupling between the jet and mainstream flow because of the high velocity profile at the exit of the orifices. The models used plenums to feed the jet air to more accurately predict the flow fields in the different mixing cases (Bain, et al. 1999).

## Reacting Jet In Crossflow Experiments

Non-reacting experiments, along with modeling research, served as a stepping-stone to reacting experiments. The influence of mixing on emissions was the driver of this research. Hatch conducted a study to analyze NO formation in the quick-mixing section. NO measurements are hard to obtain in the high temperature reacting flow field of the mixing section. Instead of measuring the NO, the data were obtained by analytically applying non-reacting mixing results to reacting conditions. This is a valid technique since non-reacting and reacting mixing flow fields are known to be similar (Oeschle, et al. 1994). The results suggested that the best mixer is not necessarily the best in terms of NO emissions. In addition, it may not be possible to come up with a rule of thumb to design a good mixer that produces low emissions (Hatch, et al. 1995).

Vardakas, et al. (1999), conducted a reacting experiment that included measurements of the NO<sub>x</sub> output of the experimental combustor. The research focused on the effect of air preheat temperatures on the formation of NO<sub>x</sub>. The study showed that the main air preheat temperature had a large effect on NO<sub>x</sub> formation. In addition, the study highlighted that a quick-mix configuration produces most of the NO in the wake of the jets because of increased residence time. The preheat temperature of the jets showed a minimal effect on the overall production of NO<sub>x</sub> despite jet air flow constituting about 70 percent of the total air entering the combustor. This finding is suspicious because jet preheat temperature would intuitively increase thermal NO<sub>x</sub> (Vardakas, et al. 1999).

In Europe, because of concerns regarding NO<sub>x</sub> production in aviation, research has been conducted through the LOWNOX program. Early research tested the extent to which RQL could respond to different fuels, specifically fuels with high fuel bound nitrogen and/or low heating values. The research at German Aerospace Center aimed to find how readily the RQL combustor could be cooled at high pressures and temperatures. Two advanced cooling concepts, impingement and effusion, were tested on a rectangular sector combustor. The research used observations from atmospheric tests to predict the response at high pressure. It also used TFN minimization during the rich stage to reduce overall NO<sub>x</sub> production. TFN stands for the total fixed nitrogen species which include: NO, NO<sub>2</sub>, N<sub>2</sub>O, HCN, and NH<sub>3</sub>. The rich primary zone of the combustor had a low residence time of 5 ms and was ignited at equivalence ratios up to 2.2. The effusion cooling concept resulted in incomplete combustion and the impingement cooling resulted in non-uniform mixing. The research showed pockets of high TFN production with over penetration and stated that with a modified mixing concept the NO<sub>x</sub> production could be reduced (Diers, et al. 2002).

There has been limited research with the goal of characterizing the mixing section in reacting flows compared to non-reacting flows. Leong, et al. (1999), were able to take extensive concentration measurements during reaction while studying the mixing of an RQL experimental combustor. Leong in her reacting flow research used species concentration, temperature, and unmixedness to evaluate mixing of the jets into the crossflow. Leong also measured uniformity with spatial unmixedness parameter,  $U_s$  by using carbon as a conserved

scalar. The bulk of the mixing takes place in the first duct radii downstream of the leading edge of the jets. Under penetration of the jets resulted in allowing copious amounts of mainstream flow to pass through the core of the mixing section without reacting. A momentum-flux ratio of 57 was used to study the mixing modules. A ratio of 60 is typical for an aircraft gas turbine engines. The fuel used in the study was propane. The research also showed that reaction in the quick-mix section is nearly complete at two duct radii downstream of the jet holes (Leong, et al. 1999). The mixing section of the RQL combustor not only needs to reduce  $\text{NO}_x$  formation but it also must successfully oxidize CO from the rich burn section. In under penetrating mixing cases the CO may not oxidize as well because the jets do not reach the centerline of the combustor. Demayo expanded upon the research of Leong to conclude that carbon, oxygen, and helium could all be used as tracers to determine reaction and mixing characteristics (Demayo, et al. 2003).

Elevated pressure studies of an RQL combustor are limited. A study by Petersen, Sowa, and Samuelsen (2002) tested a model RQL combustor at elevated pressures and temperatures. The study operated the main air inlet temperature in the range 367 K (201 °F) to 700 K (800 °F), pressures up to 1000 kPa (9.9 atm), and up to a rich burn equivalence ratio of 1.5. The  $\text{NO}_x$  emissions output increased to the 0.4 power with pressure, which is lower than typical non staged combustors (Petersen and Samuelsen, 2002). The study did not study the jet mixing; however, one of the conclusions was that only 16 percent of total  $\text{NO}_x$  is formed in the rich zone. This shows that most of the  $\text{NO}_x$  emissions are formed in the quick-mix and lean zones of the combustor.

Meisl, et al. (1994) conducted an elevated pressure study of the RQL staged combustion concept. The study showed a dependence on pressure for the  $\text{NO}_x$  formation in the experimental combustor. The TFN minima level in the initial rich condition was critical in adjusting the operating conditions of the combustor during experiments. An important conclusion made by Meisl is that even though there is a pressure dependence on  $\text{NO}_x$ , the mixing is the critical point design of the RQL combustor to reduce overall emissions. The study therefore shows that a mixing experiment at elevated pressures with the design parameters of hole size, hole number, and jet-to-mainstream of momentum-flux ratio being optimized would be highly valuable (Meisl, et al. 1994).

Another elevated pressure study up to 1013 kPa (10 atm) was conducted using an RQL prototype combustor. The objective of the study was to quantify the ability of the RQL combustor in reducing  $\text{NO}_x$  emissions from systems running on low heating value and high fuel bound nitrogen containing fuels. The RQL combustor had an 8 percent overall conversion of  $\text{NH}_3$  to NO that was nearly a factor of four lower than conventional lower heating value combustors (Feitelberg and Lacey, 1998). Feitelberg also modeled the  $\text{NO}_x$  emissions using sequentially linked ideal chemical reactors and compared the results of the model to measured data. The rich reactor was modeled with a perfectly stirred reactor, PSR, linked to a plug flow reactor, PFR. A second PSR, linked to the PFR, was used to model the quick-mixing section. A second PFR, the final reactor, was used to simulate the lean burn section. The modeling and measured data showed excellent agreement and proved that modeling approach is reasonable (Feitelberg and Lacey, 1998). A PSR is used to model systems that are uniformly mixed, where the effect of the chemical reaction kinetics are isolated in the conversion of reactants to

products. A PFR is used to simulate the flow through a tube where there is no mixing axially but perfect mixing in the crossflow direction, thereby maximizing the reactant conversion. (Reaction Design, 2005)

Research at UTRC (United Technology Research Center) was conducted at pressure up to 1034 kPa (10.2 atm) and demonstrated that the RQL combustor can achieve stable, robust, and efficient combustion at all operating conditions representative of a high speed civil transport engine cycle (Rosfjord and Padget, 2001). The research also concluded that the rich  $\text{NO}_x$  was negligible because of dominance of  $\text{NO}_x$  formed in the quick-mix section. In addition, the study showed that the equilibrium computations reasonably represent the composition of rich products. The high pressure reacting studies mentioned did not concentrate on the effects of mixing on  $\text{NO}_x$  emission.